

THE FREQUENCY OF GROWING SEASON FROST IN THE SUBALPINE
ENVIRONMENT (MEDICINE BOW MOUNTAINS, SOUTHEASTERN WYOMING),
THE INTERACTION OF LEAF MORPHOLOGY AND INFRARED RADIATIONAL
COOLING, AND THE EFFECTS OF FREEZING ON NATIVE VEGETATION

by
Dean. N. Jordan

RECEIVED
JUL 22 1997
OSTI

A dissertation submitted to the Department of Botany and the
Graduate school of the University of Wyoming in partial
fulfillment of the requirements for the degree of

DOCTOR OF PHILOSOPHY

in

BOTANY

MASTER

DISTRIBUTION OF THIS DOCUMENT IS UNLIMITED

Laramie, Wyoming

May, 1995


19980416 032

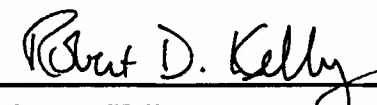
DISCLAIMER

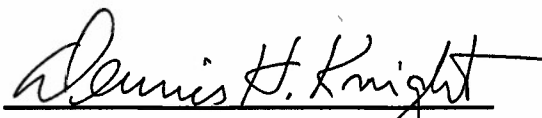
This report was prepared as an account of work sponsored by an agency of the United States Government. Neither the United States Government nor any agency thereof, nor any of their employees, makes any warranty, express or implied, or assumes any legal liability or responsibility for the accuracy, completeness, or usefulness of any information, apparatus, product, or process disclosed, or represents that its use would not infringe privately owned rights. Reference herein to any specific commercial product, process, or service by trade name, trademark, manufacturer, or otherwise does not necessarily constitute or imply its endorsement, recommendation, or favoring by the United States Government or any agency thereof. The views and opinions of authors expressed herein do not necessarily state or reflect those of the United States Government or any agency thereof.


TO THE GRADUATE SCHOOL:

The members of the Committee approve the dissertation of Dean N. Jordan
presented on December 20, 1994.


William K. Smith, Chairman

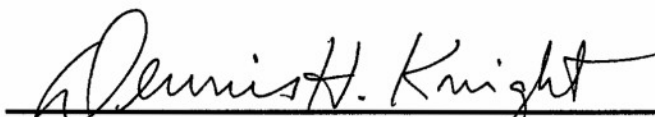

Robert D. Kelly


Dennis H. Knight


Richard A. Marston


William A. Reiners

APPROVED:


Dennis H. Knight, Head, Department of Botany

Thomas G. Dunn, Dean, The Graduate School

GRADUATION/TITLE FORM

This form is for graduate students intending on graduating. This form, completed, must be submitted to the Graduate School (Room 109 Knight Hall) no later than the deadline date (usually a week before midterm) for the semester in which graduation is anticipated (please check in the Graduate School for specific dates each semester). If graduation does not occur during the projected semester, the student must resubmit a new form no later than the deadline date for the new final semester.

Please note: Your program of study and committee must be approved and on file in the Graduate School before you can be placed on the graduation list.

Please Type

Semester of Graduation: Spring, 1995

PII Redacted

Name Dean Nichols Jordan

City

State

Zip

Degree Sought Ph.D. Area Botany Plan A Plan B

Thesis (Plan A) and Dissertation Students:

Official title to appear on thesis/dissertation: The frequency of growing season frost in the subalpine environment (Medicine Bow Mountains, southeastern Wyoming), the interaction of leaf morphology and infrared radiational cooling, and the effects of freezing on native vegetation

This title is: X new changed unchanged from previously submitted title

Signatures:

[Signature]
Major Professor/Chairperson

Date

[Signature]
Department/Division Chairperson

12-6-94
Date

Received in Graduate School:

12/1/94
Date

[Initials]
Initials

Yellow/Pink/Graduate School

Green/Registration and Records

Gold/Student

Blue/Department

Jordan, Dean N., The Frequency of Growing Season Frost in the Subalpine Environment (Medicine Bow Mountains, Southeastern Wyoming), the Interaction of Leaf Morphology and Infrared Radiational Cooling, and the Effects of Freezing on Native Vegetation, Ph.D., Department of Botany, May, 1995.

The subalpine environment is characterized by the possibility of frost throughout the summer. The frequency and severity of summertime frost episodes appeared particularly dependent on net losses of infrared energy to a cold night sky (radiation frost), as well as air temperature and wind speed. Longwave radiation minima from the night sky were strongly correlated with the occurrence of leaf temperature minima. Leaf temperatures were modelled using an energy balance simulation that quantified the specific effects of ambient air temperature, wind speed, sky infrared radiation, and sky exposure characteristic of this high-elevation environment. Plants growing in exposed and sheltered habitats have characteristic leaf structures (smaller, thicker leaves in more exposed locations) that have been traditionally associated with the total amount of incident sunlight. However, smaller leaves also appear adaptive for reducing the susceptibility to radiation frosts. Larger, more exposed leaves resulted in colder nocturnal leaf temperatures and greater frost frequencies. Microsite sky radiation, microtopography, plant habit and leaf structure all have important implications for estimating growing season length and plant distribution patterns, especially at higher elevations where summer frosts are common.

Radiational frosts at night are typically followed by clear skies and full-sun exposure the next morning. The combination of low temperature stress followed by high

light exposure can result in strong photoinhibition of photosynthesis. The morphology of a variety of conifer needles as well as of a broadleaf was modelled to evaluate the effect on incident sunlight intensity. Conifer leaf morphology was found to be particularly adaptive for avoiding high incident light conditions compared to broadleaves. Thus, broadleaf plants were chosen to investigate the photosynthetic response to freezing and high light, both in the field and in growth chambers using native subalpine plants (*Rumex densiflorus* and *Arnica cordifolia*) and a crop plant (*Lycopersicon esculentum*). Plants were frozen with temperature regimes experienced during the growing season in the local mountains under high and low light environments.

Acknowledgments

Support was provided by grant #NAGU-2808 of the Innovative Research Program of NASA awarded to W. K. Smith and a Graduate Fellowship for Global Change awarded to D. N. Jordan by the Oak Ridge Institute for Science and Education, U.S. Department of Energy. The efforts of my Committee members (Dr. Robert D. Kelly, Dr. Dennis H. Knight, Dr. Richard A. Marston and Dr. William A. Reinert) and advisor (Dr. William K. Smith) in editing and reading this document are greatly appreciated. Valuable field assistance was provided by Mike Bynum and Kristen Mitchell. Mark Hemmerlein helped carry equipment to the field which more than offset the damage caused by his dog. Mark also removed numerous ancient trees with great enthusiasm, leading us to suspect that he might seek employment in the U.S. Forest Service. This was confirmed when we began finding his empty soda cans left on site. John Zuver helped more than anyone in getting field work done, even though he hates entering data. He accompanied me on more late night trips than all others combined. Dave Myers provided valuable assistance in the operation of, and interpretation of results from, the PAM fluorometer. I would also like to acknowledge Carol Brewer, whose frequent attempts to get others to do her work and to trade cookies for data motivated me to greater efforts.

Table of Contents

Chapter 1:	Energy balance analysis of nighttime leaf temperatures and frost formation in a subalpine environment	1
	Introduction	1
	Methods and materials	2
	General methodology	2
	Microclimate and leaf temperatures	2
	Energy balance equations	4
	Micrometeorological conditions	6
	Model validation	8
	Simulations	8
	Results and discussion	10
	Field measurements and model validation	10
	Simulations	14
	Air temperature	14
	Wind speed	14
	$R_{l,\downarrow}$	14
	Sky exposure	18
	Previous research	18
	Conclusions	20
Chapter 2:	Radiation frost susceptibility and the association between sky exposure and leaf size	22
	Introduction	22
	Materials and methods	22
	Site description	23
	Elevation effects on sky IR	23

Sky exposure, sky IR and incident sunlight	24
Leaf size	25
Results	25
Elevation effects on sky IR	25
Sky exposure, sky IR, and leaf size	27
Discussion	32
Conclusions	35
Chapter 3: Microclimate influences on the frequency and duration of growth season frost for subalpine plants	36
Introduction	36
Methods	37
Study site and species	37
Microclimate, air and plant temperatures	38
Results	40
Frequency, duration and intensity of freezing temperatures	40
Nocturnal microclimate and leaf temperatures	45
Long term air temperature records	50
Discussion	53
Frequency, duration and intensity of freezing temperatures	53
Nocturnal microclimate and leaf temperatures	55
Long-term air temperature records	55
Conclusions	56
Chapter 4: Simulated influence of leaf geometry on sunlight interception and photosynthesis in conifer needles	57
Introduction	57
Methods and materials	58

Results	62
Light interception	62
Simulated carbon gain	65
Discussion	68
Chapter 5: Changes in chlorophyll fluorescence and photosynthetic gas exchange following summertime frost in the field and laboratory	74
Introduction	74
Methods and materials	75
Growth chamber experiment	77
Field experiment	81
Results	84
Growth chamber experiment	84
Field experiment	86
Discussion	85
Growth chamber experiment	91
Field experiment	94
Conclusions	95
Summary	97
Literature Cited	99

List of Tables

Table 1.1: Conditions of energy balance simulations. In all cases, elevation was fixed at 3230 m, relative humidity at 90%, leaf height above ground at 5 cm, and $R_{l,\uparrow}$ at 330 W m ⁻² . The leaf temperatures were calculated using air temperature extrapolated downward to this height. In the figures, temperature depressions ($T_{\text{air}} - T_{\text{leaf}}$) were expressed relative to a reference air temperature at 35 cm.	9
Table 3.1: The number of frost events and total hours of frost for 1992 and 1993 <i>Erigeron peregrinus</i> , and 1993 air temperature across a gradient of sky exposure. The height of the 1992 T_{air} measurement was 35 cm, while in 1993 all T_{air} measurements were made at 8 cm. This prohibits direct comparison, but provides evidence of the impact of T_{air} inversions. The 1992 growth season comprised 71 days (July 9 - Sept. 18). The 1993 season was limited to 61 days (July 22 - Sept. 23).	44
Table 3.2: Statistical analysis of leaf (3-7 cm height) and flower temperatures (15-25 cm height) of <i>Polygonum bistortoides</i> and <i>Erigeron peregrinus</i> during a radiation frost event. The 2-tailed critical t for 94 degrees of freedom at $p=0.05$ is $t_{94,0.05}=1.99$	48
Table 4.1: The surface area and volume and surface:volume ratio for a unit length of simulated leaf, along with the corresponding mean photosynthetic photon flux density (PPFD) and estimated integrated photosynthetic carbon gain expressed on a surface and volume basis.	60
Table 5.1: Statistical tests of freezing effects on fluorescence parameters of <i>Arnica cordifolia</i> in high- and low-light chambers (high-light $n = 37$, low-light $n = 41$), and <i>Lycopersicon esculentum</i> (high-light $n = 51$, low-light $n = 52$). The mean parameter values prior to freezing and the change	

resulting from the freeze are reported. Significant changes ($p < 0.05$) in
parameters are indicated by * and highly significant changes ($p < 0.01$)
are indicated by **. 86

List of Figures

- Figure 1.1: Measured vertical air temperature gradient on calm, clear nights (July 21-24, 1992) in the open at Brooklyn Lake site, Medicine Bow National Forest, WY (3230 m). Horizontal bars indicate one standard deviation. The dotted lines indicate the conditions at the air temperature thermocouple used in the validation observations. 7
- Figure 1.2: Measured relationship between sky% and $R_{l,\downarrow}$ at 3000 m on a clear night (June 16, 1993). 11
- Figure 1.3: Air temperature, leaf temperature, $R_{l,\downarrow}$, and wind speed from 2100-0500 h on representative radiation frost nights during the 1992 growing season. X-axis tic marks are positioned at midnight. 12
- Figure 1.4: Comparison of air temperatures (—), observed *Erigeron peregrinus* leaf temperatures (●: leaf size \approx 2 cm), and energy balance predicted leaf temperatures for a leaf with a characteristic dimension of 2 cm (---). 13
- Figure 1.5: Energy balance simulation results: Ambient air temperature versus leaf temperature depression for 2, 5, and 10 cm leaves. Elevation is 3230 m ... 15
- Figure 1.6: Energy balance simulation results: Wind speed versus leaf temperature depression for 2, 5, and 10 cm leaves. Elevation is 3230 m 16
- Figure 1.7: Energy balance simulation results: $R_{l,\downarrow}$ versus leaf temperature depression for 2, 5, and 10 cm leaves. Elevation is 3230 m 17
- Figure 1.8: Energy balance simulation results: Sky exposure versus leaf temperature depression for 2, 5, and 10 cm leaves. Elevation is 3230 m ... 19
- Figure 2.1 Changes in sky IR with elevation measured on three nights under clear skies. All transects were measured on both the outgoing and return trips from the mountains of southeastern Wyoming to the plains of

western Nebraska. The starting point for each transect was Laramie, Wyoming at an elevation of 2205 m. The best fit linear equations of the data were: June sky IR = $-27.9 * \text{elevation} + 344$ ($r^2 = 0.88$): August sky IR = $-33.3 * \text{elevation} + 376$ ($r^2 = 0.90$): October sky IR = $-26.2 * \text{elevation} + 335$ ($r^2 = 0.60$).	26
Figure 2.2 A: Sky IR predictions from Idso (1981) shown plotted against measurements from Fig. 2.1 ($r^2 = 0.52$). B: Sky IR predictions from Idso (1981) with a linear correction for elevation of $-0.014 \text{ W m}^{-2} \text{ m}^{-1}$ plotted against measurements ($r^2 = 0.71$).	28
Figure 2.3 Determination of sky exposure at a representative meadow site at an elevation of 3230 m near Brooklyn Lake in the Medicine Bow National Forest of southeastern Wyoming. Circle symbols are centered on sampling locations and their diameters are scaled to indicate the values measured. A: Percentage of sky exposure. B: Upper hemisphere energy incident on a radiometer at the top of the herbaceous plant canopy during a radiation frost on the night of July 21, 1993.	29
Figure 2.4 Relationship between sky% and sky IR at the microsites indicated in Fig. 2.3. Sky IR = $-1.02 * \text{sky}\% + 366$ ($r^2 = 0.98$).	30
Figure 2.5 A: Changes in leaf width (■) in <i>Taraxacum officinale</i> across a gradient in elevation and sky IR. B: Changes in leaf width (■) and leaf length (○) of <i>Erigeron peregrinus</i> with sky IR measured from randomly selected leaves within 0.5 m of the points shown in Fig. 2.3. Best fit linear regressions were: <i>T. officinale</i> leaf width = $0.029 * \text{sky IR} - 3.1$ ($r^2 = 0.85$), <i>E. peregrinus</i> leaf width = $0.010 * \text{sky IR} - 1.25$ ($r^2 = 0.36$) and <i>E. peregrinus</i> leaf length = $0.027 * \text{sky IR} - 0.96$ ($r^2 = 0.13$).	31

- Figure 3.1: A: Time distribution of nightly T_{air} (8 cm height) minima. B: Time distribution of nightly *Erigeron peregrinus* T_{leaf} minima during the 1993 growing season (61 nights) at the center of the research site. Temperature minima $< 0^{\circ}\text{C}$ are represented by ■, and temperature minima $> 0^{\circ}\text{C}$ are depicted by □). Each night is represented on the histogram at the time of occurrence of the lowest temperature (of air or leaf). 41
- Figure 3.2: Time series of T_{air} (8 cm height at clearing center) (dashed line) and *Erigeron peregrinus* T_{leaf} on July 27-28, 1993 (solid line). The open arrow marks the minima of T_{air} and the solid arrow marks the minima of T_{leaf} 42
- Figure 3.3: Maximum, minimum, and mean temperature record of air, *Erigeron peregrinus* leaves, and *Abies lasiocarpa* needles at the clearing center during 1993. The sensors were located within 2 m of each other at heights of 8, 3 and 27 cm respectively. 43
- Figure 3.4: Frequency and duration of temperatures below 0°C for T_{air} (8 cm height), *Abies lasiocarpa* (27 cm height), and *Erigeron peregrinus* (approx. 3 cm height) during 1993. Each column indicates a frost event, and height of columns indicates the duration. The top three graphs represent observations from the clearing center with 96% sky exposure. The lower three graphs represent a gradient of upper hemisphere exposure with 96, 87 and 29% sky exposure, respectively, due to shelter by a spruce-fir forest canopy. Horizontal axis tic marks are positioned at midnight. 46
- Figure 3.5: Vertical profile of air temperature on the night of Aug. 25, 1993 between 0000 and 0500. The five sampling points between 10 and 200

cm were located on an instrument stand within the clearing. The horizontal bars indicate the range of the temperature observations. The sampling points are connected through the observation means. The 8 cm measurements were recorded as 15 min means from the central air temperature sensor at the study site. The 10 m values were hourly means of 10 s observations provided by a USFS from a weather station 1 km SE of the site. As such, the lowest and highest points on the graph were not taken at exactly the same location or at the same time frequency as the intermediate points, but are included in order to extend the vertical profile, and demonstrate comparability with nearby measurements. The horizontal dashed lines represent the heights of measured *Erigeron peregrinus* leaves and flowers, and the measured *Abies lasiocarpa* needle. 47

Figure 3.6: A (upper left axis): Sky radiation measurements for a consecutive 9-day period (Aug. 26-Sept. 3, 1993). Vertical bars topped with arrows indicate the time of occurrence and $R_{l,\downarrow}$ measured at the time of nightly *Erigeron peregrinus* temperature minima. B: The T_{air} (open bars) and *E. peregrinus* temperature minima (striped bars) are indicated in the lower graph (right axis). The corresponding wind speed (solid bars) during the nightly leaf temperature minima is indicated on the lower left axis. Horizontal axis tic marks are positioned at midnight. 49

Figure 3.7: Mean $R_{l,\downarrow}$ versus *Erigeron peregrinus* leaf temperature depression ($\Delta T = T_{air} - T_{leaf}$) for nights with subfreezing T_{leaf} (1993). The number of nights are indicated along with corresponding percentages of all frost nights (parentheses). Nights with ΔT between 4 and 5 were averaged to produce the upper left-most point, nights with ΔT between 3 and 4

produced the point below, etc. Horizontal error bars represent the coefficient of variation of sky infrared radiation and vertical error bars represent the standard deviations of ΔT values. The equation for the least-squares linear fit was: $\Delta T = -0.072 * R_{i,\downarrow} + 22.7$ ($r^2 = 0.96$).	51
Figure 3.8: Daily growing season T_{air} extremes for 5 years from a U. S. Forest Service 10 m meteorological tower (1989-1993). Horizontal bars to the right of each series indicate seasonal mean T_{air} maxima (open bars) and minima (striped bars). Horizontal error bars indicate \pm one standard deviation.	52
Figure 4.1: Cross sections of modelled leaves used in computing light interception and photosynthetic CO_2 assimilation.	59
Figure 4.2: Idealized photosynthetic response to light of conifer leaves that was used to estimate carbon gain based on intercepted light.....	61
Figure 4.3: Graphical representation of the computation of light interception and CO_2 uptake on an <i>Abies nordmanniana</i> needle with incident light at 30°	63
Figure 4.4: Distribution of PFD ($\mu mol\ m^{-2}\ s^{-1}$) on modelled leaves at selected angles of incident light.....	64
Figure 4.5: Calculated mean PFD intercepted per unit surface area as a function of incident light angle and leaf shape (●: <i>Pinus monophylla</i> ; ○: <i>Pinus sylvestris</i> ; ▼: <i>Pinus cembra</i> ; ■: <i>Abies nordmanniana</i> ; ◇: <i>Picea asperata</i> ; —: Flat leaf section).	66
Figure 4.6: Calculated mean CO_2 uptake per unit surface area as a function of incident light angle and leaf shape (Symbols are consistent with Figure 4.5).	67

- Figure 4.7: Calculated mean CO₂ uptake per unit volume as a function of incident light angle and leaf shape (Symbols are consistent with Figure 4.5). 69
- Figure 5.1: Light (left axis) and air temperature (right axis) in the high-light growth chamber. The lines represent observations made by a 21X datalogger (Campbell Scientific) with a LI-190SB quantum sensor (LI-COR Inc.) and a 0.2 mm copper-constantan thermocouple (Omega Engineering Inc.) at 1 min intervals over 24 h. The low-light chamber temperature conditions were similar but the light intensity was reduced by half..... 79
- Figure 5.2: Typical freezing treatment of *Arnica cordifolia* leaves measured with a 0.2 mm copper-constantan thermocouple (Omega Engineering Inc.). Pots were moved from the growth chambers during the dark period at 5 °C to the refrigerator on a cart under an inverted cooler. The transport time from chamber to refrigerator was approximately 1 min and leaf temperatures were not monitored during this interval. 80
- Figure 5.3: Nighttime leaf temperatures of *Rumex densiflorus* in four sheltered (solid line) and four exposed (dashed line) plants. The temperature record extends from midnight to after the shelters were removed at 0600. The vertical error bars represent \pm one standard deviation. 82
- Figure 5.4: Photosynthetically active radiation (■) and *Rumex densiflorus* leaf temperatures (Δ) measured during gas exchange observations beginning at first direct sun following a frost event. 83
- Figure 5.5: Ratio of light-adapted variable fluorescence to maximal fluorescence (F_v/F_m) in *Rumex densiflorus* over the hours following a frost event. The dashed and solid lines represent the linear regression versus time of leaves from sheltered (■) and exposed (○) plants. 87

- Figure 5.6: A: Trend in non-photochemical quenching over time following a frost event in *Rumex densiflorus*. The two populations were best represented by a single quadratic equation. B: Trend in photochemical quenching in the same *R. densiflorus* leaves. Two separate quadratic equations were used to describe the observations. The dashed and solid lines represent the means of leaves from sheltered (■) and exposed (○) plants. 88
- Figure 5.7: Quantum yield of *Rumex densiflorus* following a freeze event. The dashed and solid lines represent the means of leaves from sheltered (■) and exposed (○) plants. 89
- Figure 5.8: A: Stomatal conductance of eight *Rumex densiflorus* leaves in direct sunlight following a frost event. The line through the data is a least squares fit of a natural log function. B: Rate of vapor loss by leaves. A linear regression was fit to the data. C: Rate of net carbon assimilation. The curve fit is a natural log function. Each graph is the summary of individual leaves from 8 different clones of *R. densiflorus* measured repeatedly over time. 90
- Figure 5.9: Mean instantaneous fluorescence (F_t) measured at 20 s intervals in *Arnica cordifolia* averaged across all treatments except freezing. Solid line: Unfrozen (—), Frozen (— — —). All observations after 20 s were highly significantly different ($p < 0.01$)..... 93

Chapter 1: Energy balance analysis of nighttime leaf temperatures and frost formation in a subalpine environment

Introduction

Plant temperatures at night are important for native and agricultural plant species because of rate limitations to nocturnal respiration as well as the potential influence of frost and dew formation on growth and reproduction (Arny and Upper 1973; Holopainen 1990; Lu et al. 1992; Rejman 1977; Smith and McClean 1989). Although the seasonal occurrence of frost is used commonly to estimate the length of the growing season of agricultural species, only a few studies have evaluated the effects of frost on growth and distribution of native plants (Paton 1988; Raitio 1987; Silberbauer-Gottsberger et al. 1977). Nighttime frost can lead to a significant reduction in carbon assimilation over several subsequent days (Dang et al. 1992; Lundmark and Hällgren 1987; Lundmark et al. 1988), while dew formation on leaves has been shown to inhibit photosynthetic CO₂ uptake because of a water film that may develop on the leaf surface (Smith and McClean 1989). In the subalpine environment, frost and dew formation on leaves can occur during the entire summer growing period.

My goal was to develop energy balance equations to predict nocturnal plant temperatures and the occurrence of leaf frost in a high elevation environment. At night, the energy balance of a leaf is dominated by longwave radiation exchange and convective heat exchange. Of special interest was the influence of longwave radiation from the cold night sky as a major determinant of leaf frost, as well as being an effective integrative measure of atmospheric temperature. The energy balance equations predicting leaf temperature were validated by measuring micrometeorological conditions adjacent to natural leaves and then comparing computed with measured leaf temperatures. After validation, the equations were used to simulate the independent influences of longwave

radiation from the sky, wind speed, and leaf dimension to quantitatively determine the sensitivity of leaf temperature and frost occurrence to each of these factors.

Methods and materials

General methodology

In order to validate a leaf energy balance model and to establish representative values of subalpine micrometeorological factors, a forest clearing at an elevation of 3230 m was selected near Brooklyn Lake in the Medicine Bow National Forest of southeastern Wyoming, USA (41° 22' 25" N. Longitude, 106° 14' E. Latitude). This area is dominated by open meadows interspersed with spruce-fir forest that forms ribbon-like islands of trees. The tree islands may be over 1000 m² in size with meadow areas twice as large. The forest canopy height is typically about 15 m (Billings 1969), while the herbaceous vegetation height is rarely over 0.3 m. In wind-swept areas, cushion-like plants with small leaves dominate. The flora of the mountain range encompassing the meadow was listed by Nelson (1984).

Microclimate and leaf temperatures

Erigeron peregrinus (Banks ex Pursh) Greene (Subalpine Daisy) was selected as a representative herbaceous species in the subalpine environment that would be expected to show leaf temperature depressions ($\Delta T = T_{\text{air}} - T_{\text{leaf}}$) due to radiational cooling if the leaves were exposed to the sky. The leaves originate from a basal rosette and tend to have petioles and blades angled at 30 to 60 degrees from the horizontal. The leaf blade is usually about 2 cm wide and 5 to 8 cm in length. Leaf heights were approximately 5 to 10 cm above ground level. The leaves were considered to have a characteristic dimension (short axis) of 2 cm. Leaf dimensions can be substantially larger in the more sheltered locations under the forest edge.

Air temperature was monitored using type T, 0.2 mm copper-constantan thermocouples (Omega Engineering Inc., Stamford, CT) mounted adjacent to other

micrometeorological instruments on a stand at a height of 35 cm. This height was selected as representative of leaf heights across the site. A thermocouple reference junction built into a 21X datalogger (Campbell Scientific Instruments, Logan, UT) was used for temperature reference. Wind speed was monitored adjacent to the air temperature thermocouple using a thermistor anemometer modified from a design described by Bergen (1971). Resistors appropriate for a 12 V source were substituted for those in the original design. Thermistor anemometers produce a voltage output that is logarithmically proportional to the wind speed. These devices are extremely sensitive to wind speeds below 2 m s^{-1} , relatively insensitive above 5 m s^{-1} , and well suited to studies involving low wind speeds. A temperature correction was required to obtain accurate measurements under field conditions. Calibration of the anemometers was performed in a wind tunnel with a reference speed provided by a commercial air flow meter (Kurz Instruments Inc., Monterey, CA). Calibration temperatures in the wind tunnel were varied between -5 and $+24$ °C.

A total hemispherical radiometer (REBS, Inc., Seattle, WA) was used to measure upward ($R_{l,\uparrow}$) and downward ($R_{l,\downarrow}$) infrared radiation. The radiometer measures incident energy in all wavelengths from both the upper and lower hemispheres. Dew formation on the upper sensor dome was a major measurement problem and caused observations from numerous nights to be discarded. Only data from nights when the radiometer remained above dewpoint were used in the current study, although dew and frost formation did occur on leaves. Relative humidity was monitored at 35 cm with a HX 92V Relative Humidity Transmitter (Omega Engineering Inc.).

Leaf temperatures were also monitored with the fine wire thermocouples. Approximately 1.5 cm of Teflon insulation was removed from thermocouple wire (Omega Engineering Inc.) and the two strands were twisted together and soldered with 60/40 solder to maintain a reliable and durable contact junction. A thermocouple was

inserted in a leaf by carefully stitching the thermocouple junction through the center of the leaf, maintaining multiple contact points with the leaf. Only the first junction of this construction operates, but the thermal conductivity of the wire maintains this junction near the mean leaf temperature. All microclimate and leaf temperature data were collected on a 21X datalogger. Sensors were sampled every minute, and averages were computed and recorded every 15 minutes.

Simulation modelling of percent sky exposure (sky%) required observations of the relationship between sky% and $R_{l,\downarrow}$. This relationship is of interest in studies of the spatial distribution of plants at the microsite level because of the differing freezing potential with changes in location within a clearing, as well as the effects of neighboring vegetation or forest canopy (Freeburg 1972; Lundmark and Hällgren 1987; Nunez and Bowman 1988). Sky view was photographed at leaf level in the field using a fish-eye lens, and sky% was calculated using software described in Chazdon and Field (1987). A geometric approach to addressing sky exposure has been described by Unsworth (1975).

Energy balance equations

The energy balance approach to predicting nighttime leaf temperature was modified from a model previously validated by Foster and Smith (1986) and used to predict daytime leaf temperatures of subalpine plants at a nearby research site. The leaf temperature was iteratively solved for the temperature at which the net energy flux of the leaf was zero, expressed as

$$\alpha(R_{l,\downarrow} + R_{l,\uparrow}) - \epsilon\sigma T_{\text{leaf}}^4 - H = 0 \quad [\text{Eqn. 1.1}]$$

Here, $R_{l,\downarrow}$ and $R_{l,\uparrow}$ are the upper and lower hemisphere longwave radiation flux densities. H represents the convective heat loss and incorporates both leaf temperature (T_{leaf}) and air temperature. The longwave absorptivity (α) and emissivity of the leaf (ϵ) were set to 0.97 (Gates 1980). Latent heat exchange due to nocturnal transpiration was considered negligible (Gates 1980).

The convection parameters were expressed in terms of dimensionless numbers, namely the Reynolds (Re), Grashof (Gr), and Nusselt (Nu) numbers (Campbell 1977; Nobel 1983). The Reynolds number incorporates leaf dimension (d), as well as velocity (u) and kinematic viscosity of the air (ν), into a term that both indicates the condition (laminar or turbulent convection) of the boundary layer,

$$Re = ud/\nu \quad [\text{Eqn. 1.2}]$$

and is used in the calculation of energy and mass exchange between air and leaf.

Convective parameters were adapted from engineering equations for heat exchange of a horizontal flat plate, although Grace (1978) urges caution in applying such a simplification to leaves in a turbulent environment. When $Re > Re_{\text{critical}}$ ($Re_{\text{critical}} = 4000$), the boundary layer convection is dominated by turbulent exchange. However, during frost events observed in the field, Re was never found to exceed this value of Re_{critical} .

The Grashof number depends upon the kinematic viscosity of the air, along with leaf size and air and leaf temperature (Campbell 1977):

$$Gr = agd^3(T_{\text{leaf}} - T_{\text{air}} - T_v)/\nu^2 \quad [\text{Eqn. 1.3}]$$

where a is a thermal expansion coefficient, and g is the gravitational acceleration constant. The kinematic viscosity of air and the virtual temperature correction term T_v were taken from Campbell (1977). T_v adjusts for air density changes due to moisture content. The ambient vapor density of air, the saturated vapor density of the leaf, and the boundary layer density were also taken from Campbell (1977).

The Nusselt number (see Thorpe and Butler 1977 for a discussion of Nu) was calculated from Re and Gr, as well as the Prandtl number (Pr) which was set to 0.7 for this study (Gates 1980). In theory, Nu has both forced and free components. The forced convection component, due to large-scale air movements, was taken to be

$$Nu_{\text{Forced}} = 0.64 * Re^{0.44} * Pr^{0.33} \quad [\text{Eqn. 1.4}]$$

The free convection component of Nu was calculated differently for upper and lower surfaces of a leaf cooler than the air:

$$\text{Nu}_{\text{Top Free}} = 0.29 * (\text{Gr} * \text{Pr})^{0.25} \quad [\text{Eqn. 1.5}]$$

$$\text{and } \text{Nu}_{\text{Bottom Free}} = 0.51 * (\text{Gr} * \text{Pr})^{0.25} \quad [\text{Eqn. 1.6}]$$

due to the tendency of cooled air to settle. A combined Nu was calculated for each leaf surface by a non-linear combination of the forced and free components as in Foster and Smith (1986):

$$\text{Nu}_{\text{Top/Bottom}} = \left(\text{Nu}_{\text{Forced}}^{3.55} + \text{Nu}_{\text{Top Free/Bottom Free}}^{3.55} \right)^{0.28} \quad [\text{Eqn. 1.7}]$$

Convective heat exchange was calculated from the combined Nu value, molecular diffusion coefficient of heat in air (D_H), heat capacity of air (c_p), dry air density (ρ_a), and leaf dimension:

$$H_{\text{Top/Bottom}} = \rho_a c_p (T_{\text{leaf}} - T_{\text{air}}) / \left(d / [D_H * \text{Nu}_{\text{Top/Bottom}}] \right) \quad [\text{Eqn. 1.8}]$$

Throughout this analysis, the temperature gradient between the upper and lower surfaces was assumed to be zero, and the predicted leaf temperature is for the center of the leaf. No heat storage term was included because heat storage in thin leaves is extremely small and equilibrium leaf temperature would be reached before sizable changes in environmental conditions would be expected (Gates and Papian 1971; Gates 1980). No adjustment was made for the blanketing effect of the leaf and subsequent thermal emission of the ground beneath the leaf (Leuning 1988).

Micrometeorological conditions

During radiation frosts and low wind conditions such as those present during radiation frosts, vertical T_{air} gradients may develop due to convective exchange between the air and surfaces cooled by exposure to night sky. In addition, settling of denser cold air towards the ground may enhance vertical temperature profiles. Air temperatures were monitored at 3 different heights at the site, and an equation was developed to extrapolate T_{air} from a reference height of 35 cm down to plant heights (Fig. 1.1). The natural

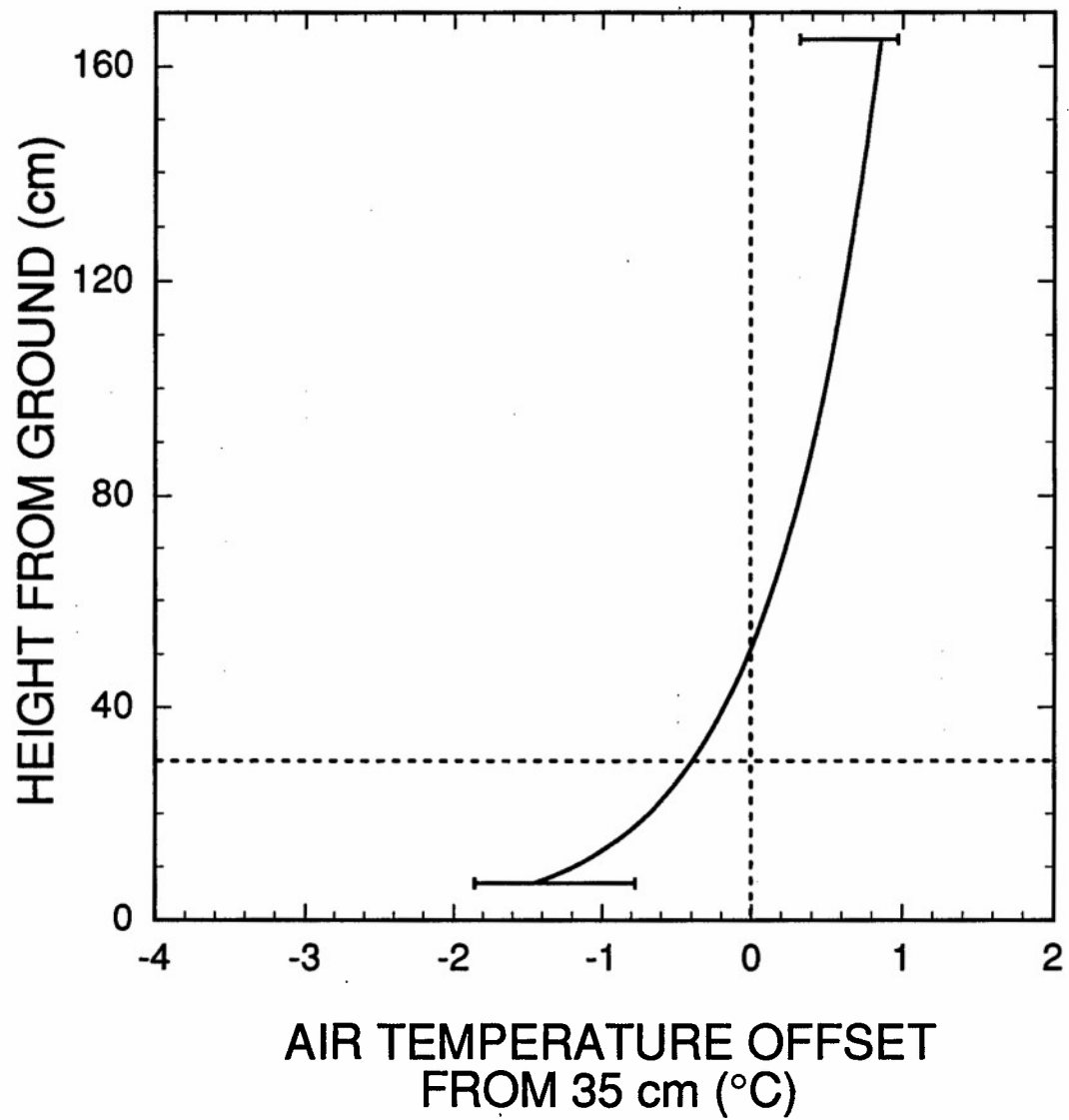


Figure 1.1: Measured vertical air temperature gradient on calm, clear nights (July 21-24, 1992) in the open at Brooklyn Lake site, Medicine Bow National Forest, WY (3230 m). Horizontal bars indicate one standard deviation. The dotted lines indicate the conditions at the air temperature thermocouple used in the validation observations.

logarithmic equation was based only on measurements from calm clear nights during frost or near-frost conditions, and represents a least-squares fit to the observed data.

Model validation

The leaf energy balance equations were validated using field data obtained in July, August and September of 1992. Fixed leaf parameters (size and height) were recorded at the time the leaf thermocouple was installed. For the purposes of modelling frost occurrence, only observations during the peak frost period (2100 through 0500) were utilized. Nights exhibiting meteorological conditions consistent with radiation frosts ($T_{\text{leaf}} < 0$, $T_{\text{air}} > 0$, low wind) were selected from the growing season record when all measurements were credible. Nights with visible dew formation on the radiometer surface were rejected because of interference with the $R_{\text{l},\downarrow}$ measurements.

Simulations

Using the validated energy balance equations described above, simulations were conducted by incrementing one variable while all others were kept constant. Simulations were run with environmental conditions typical of those observed during growing season frosts at a subalpine elevation (Table 1.1).

In simulations of the effect of ambient air temperature on leaf temperature, still wind conditions were established. $R_{\text{l},\downarrow}$ was set at a value characteristic of clear skies at 3000 m, and $R_{\text{l},\uparrow}$ was set at a radiation flux density produced by ground temperatures of approximately 5 °C (Table 1.1). The environmental conditions for the wind speed simulation were identical to those in the air temperature simulation, except that air temperature was fixed and wind speed was varied (Table 1.1). Similarly, the response of leaf temperature to $R_{\text{l},\downarrow}$ was simulated with fixed wind speed and air temperature (Table 1.1). This was approached from two perspectives: varying sky thermal emissions directly, and by varying exposure to a combination of forest canopy and open sky. In the direct $R_{\text{l},\downarrow}$ simulation, a range of thermal emissions was selected based on field

	<u>Parameter Values</u>		
	Air Temperature (°C)	Wind Speed (m s ⁻¹)	$R_{l,\downarrow}$ /Sky% (W m ⁻²)/%
Fig. 1.5: Air Temperature	0-8	0.2	230
Fig. 1.6: Wind Speed	4	0.0-1.5	230
Fig. 1.7: $R_{l,\downarrow}$ /Fig. 1.8: Sky%	4	0.2	220-300/0-100

Table 1.1: Conditions of energy balance simulations. In all cases, elevation was fixed at 3230 m, relative humidity at 90%, leaf height above ground at 5 cm, and $R_{l,\uparrow}$ at 330 W m⁻². The leaf temperatures were calculated using air temperature extrapolated downward to this height. In the figures, temperature depressions ($T_{\text{air}} - T_{\text{leaf}}$) were expressed relative to a reference air temperature at 35 cm.

observations. In the second approach, an assumption was made that the $R_{l,\downarrow}$ from an unobstructed upper hemisphere would be 220 W m^{-2} , with an increase of 0.86 W m^{-2} for each 1% increase in shelter by the forest canopy. This relationship was developed by measuring spatially distributed $R_{l,\downarrow}$ and calculating the sky% (Chazdon and Field 1987) at each observation (Fig. 1.2). It should be noted that no understory vegetation was observed at sky% < 20%, probably due to a limiting sunlight environment (unpublished data).

Results and discussion

Field measurements and model validation

Leaf temperature depressions of over 6°C occurred when wind speeds were less than about 0.5 m s^{-1} (Fig. 1.3). T_{leaf} and T_{air} tended to converge at higher wind speeds. However, on slightly windier nights that also had particularly cold night skies, similar leaf temperature depressions occurred (e.g., Aug. 27-28). The difference in temperature between two similar leaves separated by a few meters was as much as 4°C , but was more typically $\leq 2^\circ\text{C}$ (Fig. 1.3).

The predicted leaf temperatures for a 2 cm leaf agreed well with the observations on one of the *E. peregrinus* leaves (Fig. 1.4). In general, predicted leaf temperatures were within $\pm 0.5^\circ\text{C}$ of measured temperatures of *E. peregrinus*, and 95% were within $\pm 1.8^\circ\text{C}$. Differences between predicted and measured temperatures generated a root-mean-square error of 0.9°C , while the root-mean-square deviation between the air and leaf temperature observations was 3.9°C ($n = 461$). A portion of the higher predicted T_{leaf} resulted from the T_{air} gradient because the leaf temperature was measured at a lower height than the air temperature, while the remainder of the difference was caused by a negative leaf infrared flux. Microsite variations in air temperature and wind speed may be the cause of differences in temperatures of similar leaves separated by a few meters. Orientation of the wind direction relative to the leaf axis was not recorded, and could also

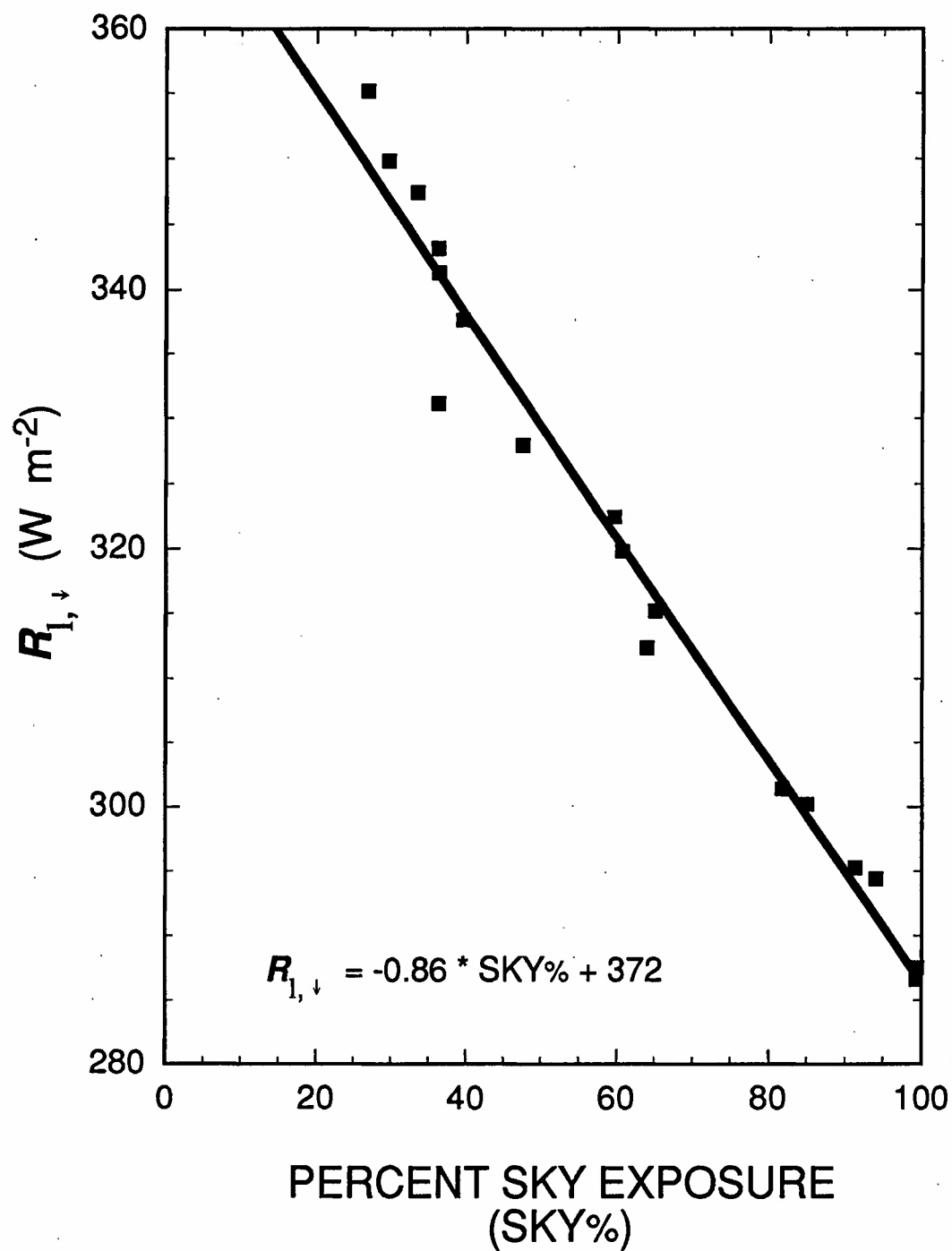


Figure 1.2: Measured relationship between sky% and $R_{l,↓}$ at 3000 m on a clear night (June 16, 1993).

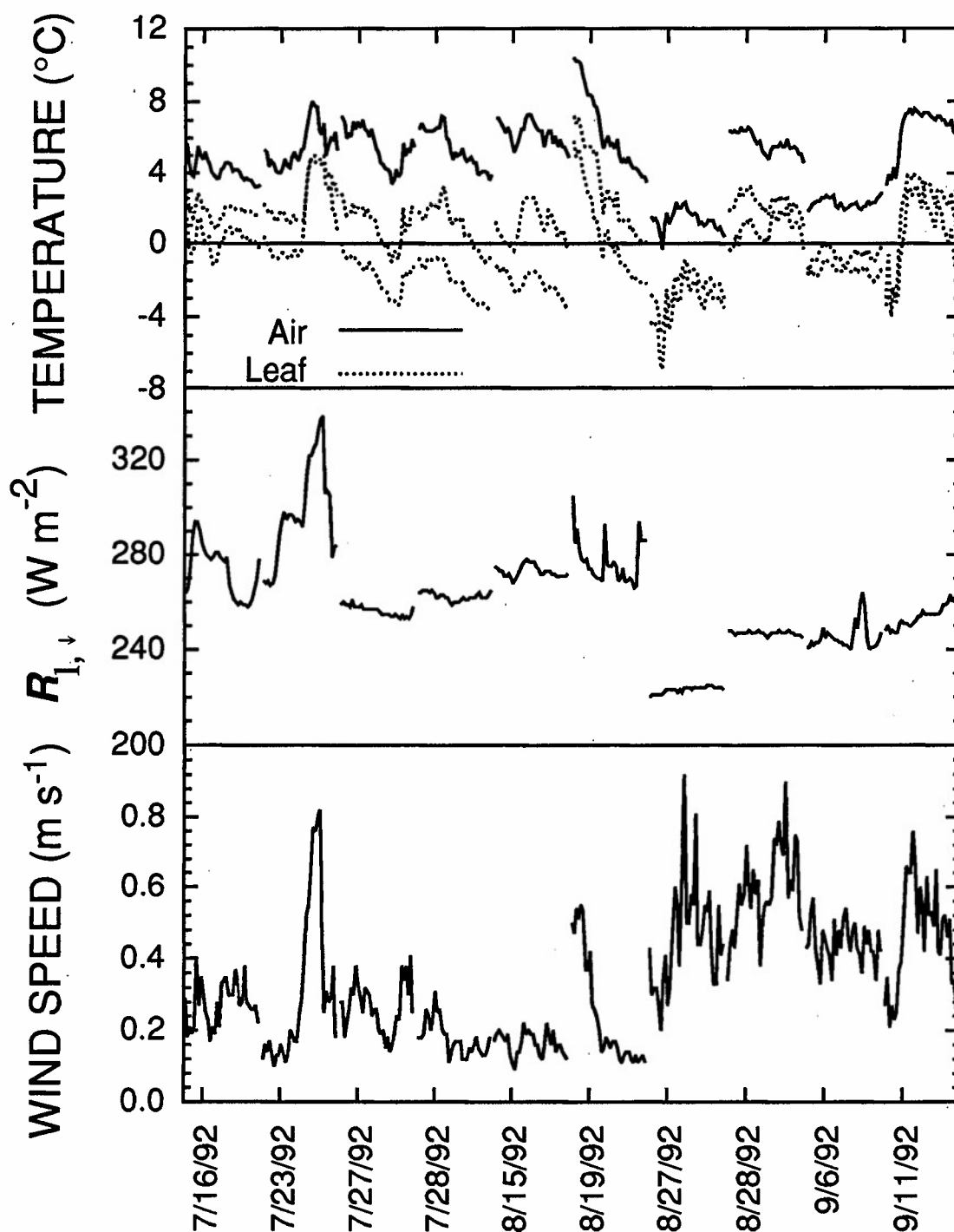


Figure 1.3: Air temperature, leaf temperature, $R_{L\downarrow}$, and wind speed from 2100-0500 h on representative radiation frost nights during the 1992 growing season. X-axis tic marks are positioned at midnight.

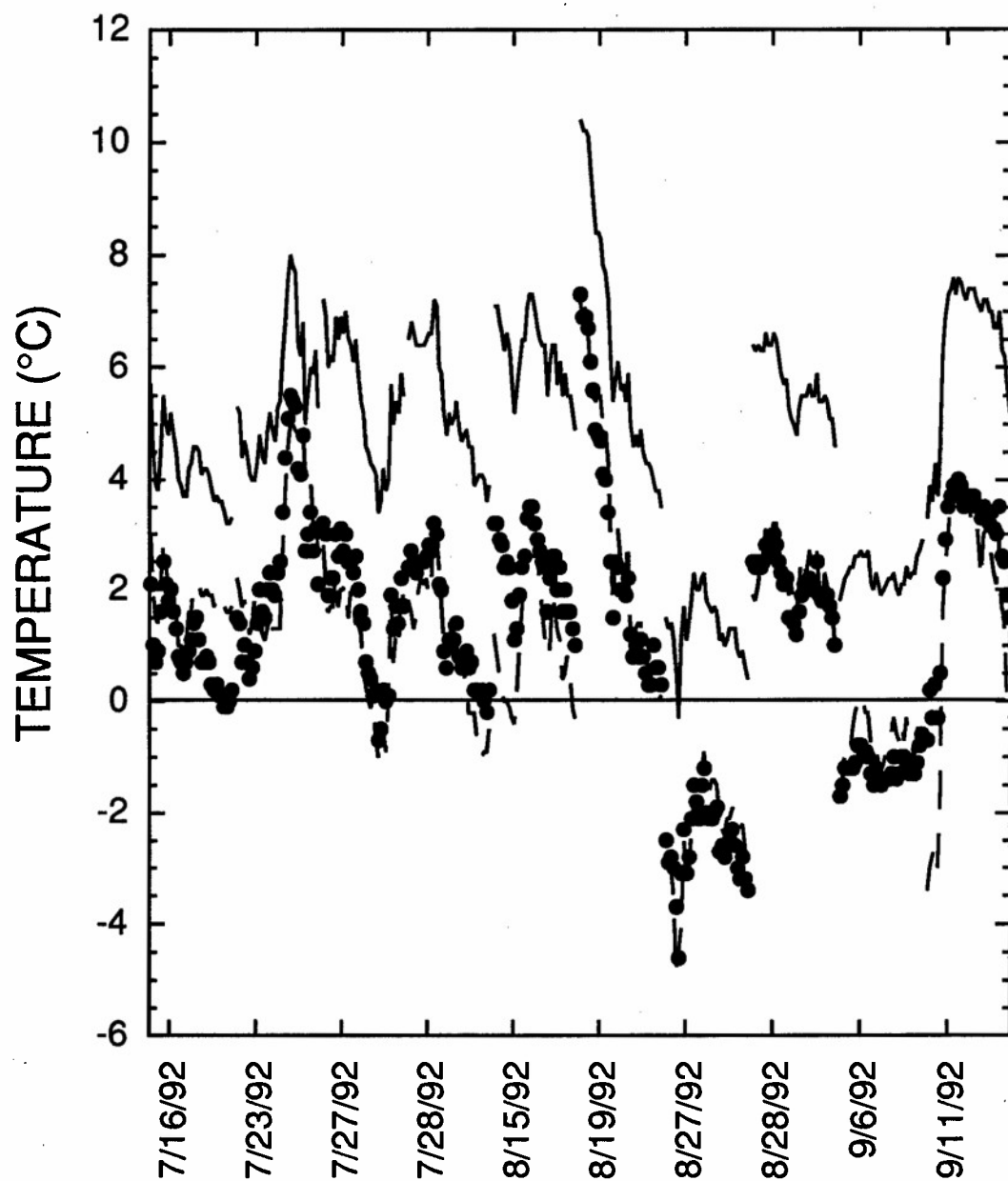


Figure 1.4: Comparison of air temperatures (—), observed *Erigeron peregrinus* leaf temperatures (●: leaf size \approx 2 cm), and energy balance predicted leaf temperatures for a leaf with a characteristic dimension of 2 cm (---).

account for differences between measured and predicted temperatures due to variation in the leaf characteristic dimension with wind direction

Simulations

Air temperature

Simulated increases in ambient air temperature resulted in a linear increase in the leaf temperature depression for all sizes of leaves, with a more sensitive response observed for leaves with a larger characteristic dimension (Fig. 1.5). At an air temperature of 0 °C, the 2 and 10 cm leaves had temperature differences of about 0.8 °C. This difference increased to over 1.8 °C at an air temperature of 8 °C. Thus, larger leaves will be cooler than smaller leaves and will experience freezing conditions at a higher ambient air temperature (1 to 2 °C) than smaller leaves.

Wind speed

Leaf temperature depressions increased rapidly at low wind speeds ($< 0.4 \text{ m s}^{-1}$) for all leaf sizes simulated (Fig. 1.6). Under the simulated conditions, the larger leaves experienced frost at all wind speeds less than 1.0 m s^{-1} , while the smaller leaves did not freeze until wind speeds dropped below 0.25 m s^{-1} . The wind speed range from 0.25 to 1.0 m s^{-1} is frequently observed in the field (Fig. 1.2), indicating the importance of the interaction between leaf size and wind speed to frost occurrence in subalpine plants.

$R_{l,\downarrow}$

Simulating the leaf temperature response to a range of $R_{l,\downarrow}$ values produced linear responses in leaves of different sizes, with a different slope for each leaf size (Fig. 1.7).

$R_{l,\downarrow}$ was varied from conditions ranging from clear, cold skies to overcast conditions (220 and 300 W m^{-2} represent blackbody equivalent sky temperatures of -23.5 and -3.5 °C, respectively). Clear, cold skies produced freezing leaf temperatures in all simulated leaf sizes. However, frost was predicted for 10 cm leaves at approximately 270 W m^{-2} , while the smaller, 2 cm leaves did not approach the frost point until $R_{l,\downarrow}$ was 240 W m^{-2} .

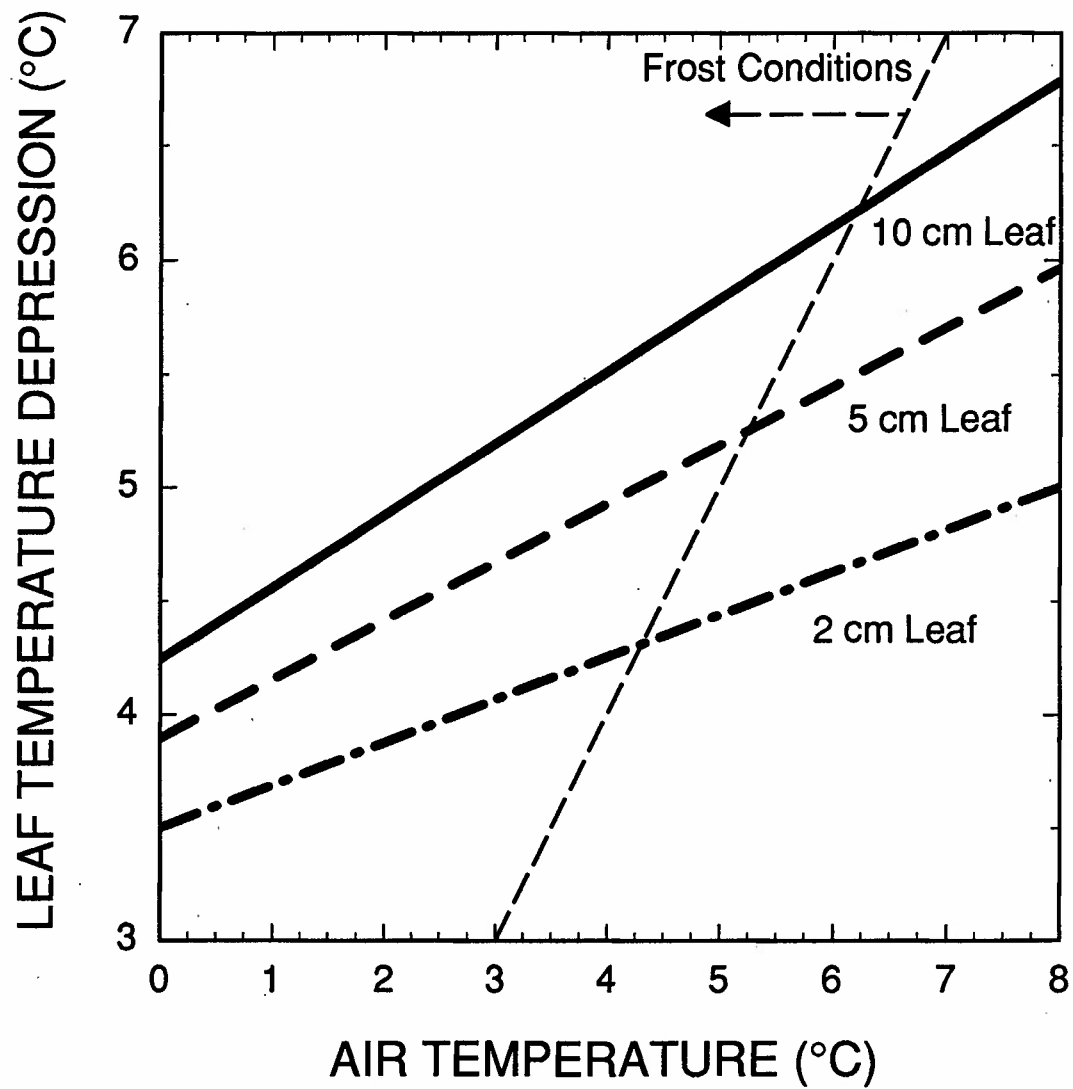


Figure 1.5: Energy balance simulation results: Ambient air temperature versus leaf temperature depression for 2, 5, and 10 cm leaves. Elevation is 3230 m; relative humidity is 90%; $R_{l,\uparrow}$ is 330 W m^{-2} ; $R_{l,\downarrow}$ is 230 W m^{-2} ; and wind speed is 20 cm s^{-1} . Freezing conditions in this and subsequent graphs are depicted by a dashed line with an arrow indicating colder leaf conditions. Line patterns are consistent with the indicated leaf sizes for Figures 1.5-1.8.

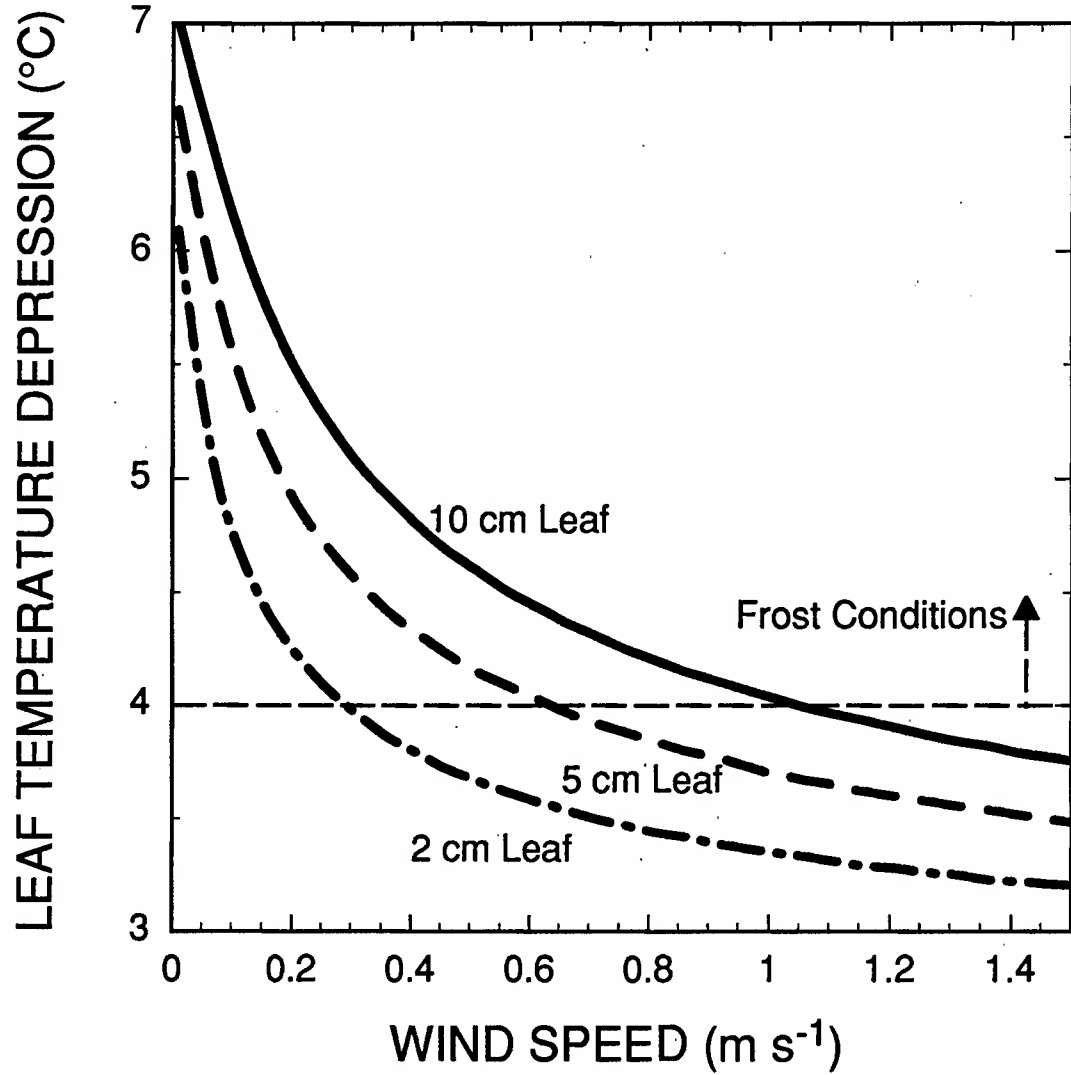


Figure 1.6: Energy balance simulation results: Wind speed versus leaf temperature depression for 2, 5, and 10 cm leaves. Elevation is 3230 m; relative humidity is 90%; $R_{l,\uparrow}$ is 330 W m^{-2} ; $R_{l,\downarrow}$ is 230 W m^{-2} ; and air temperature is 4°C .

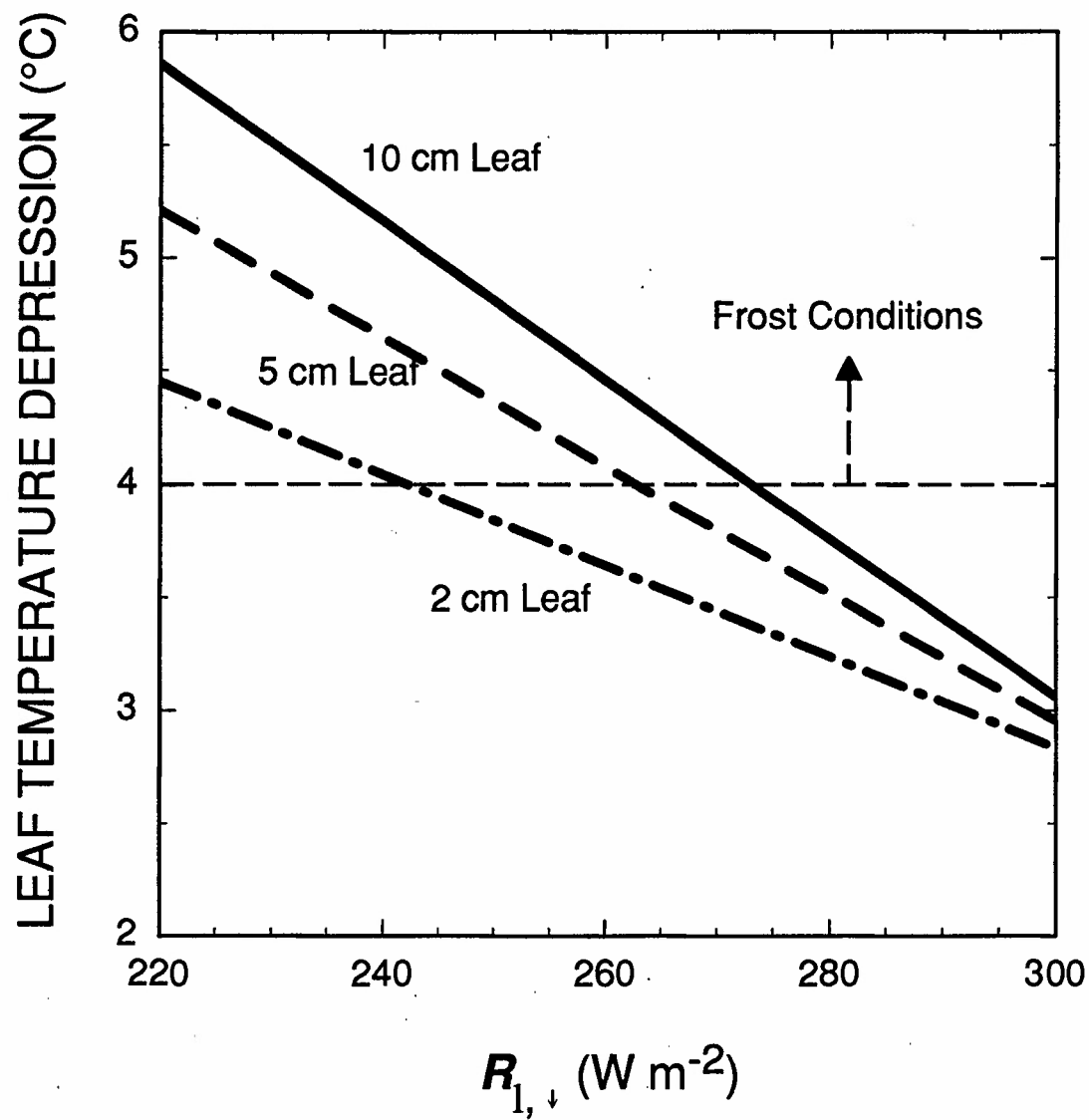


Figure 1.7: Energy balance simulation results: $R_{l,\downarrow}$ versus leaf temperature depression for 2, 5, and 10 cm leaves. Elevation is 3230 m; relative humidity is 90%; $R_{l,\uparrow}$ is 330 W m^{-2} ; wind speed is 20 cm s^{-1} ; and air temperature is 4°C .

This difference in sensitivity to $R_{l,\downarrow}$ could result in a dramatic change in the frequency of freezing episodes for larger leaves with a change in atmospheric emissions.

Sky exposure

The leaf temperature responses to varying sky% were also linear, with the larger leaves exhibiting a more sensitive response to sky% (Fig. 1.8). Under the conditions of the simulation, the smaller, 2 cm leaves reached the frost point at a sky% of 70%, while larger, 10 cm leaves approached 0 °C at a sky% of only 30%. On the basis of these simulations, sky% could limit establishment and growth of plants with larger leaves in subalpine meadows, favoring small broadleaf species, or other leaf configurations with smaller boundary layer resistances such as loosely packed conifer needles. The subalpine forests of the central Rocky Mountains are characterized by relatively widely spaced trees and a range of gap and clearing sizes. For 10 m tree heights, a minimum gap diameter of about 60 m would result in a sky% of roughly 70% for a plant located in the center of the gap, while a gap in a dense canopy of approximately 20 m diameter would reduce sky% to 30%. Relatively small gaps would benefit larger leafed plants, while larger gaps would favor smaller leaf dimensions. Previously, this association between leaf size and exposure has been based on the effects of sunlight exposure and temperature or water stress, not the potential effects of freezing.

Previous research

Energy balance concepts applied to biophysical parameters of leaves indicate that a leaf should lose heat by radiative transfer to a clear night sky, thus forcing the leaf temperature to drop below air temperature (Gardner et al. 1991; Leuning 1988; Leuning and Cremer 1988). Oke and Fuggle (1972) reported growing season $R_{l,\downarrow}$ measurements of similar magnitudes to those reported here (290 to 370 W m⁻²). Floor (1989) reported a grass temperature depression of 3.7 °C in the Netherlands. Leuning and Cremer (1988) observed depressions in *Eucalyptus* leaves of 1 to 3 °C, while Lu et al. (1992) reported

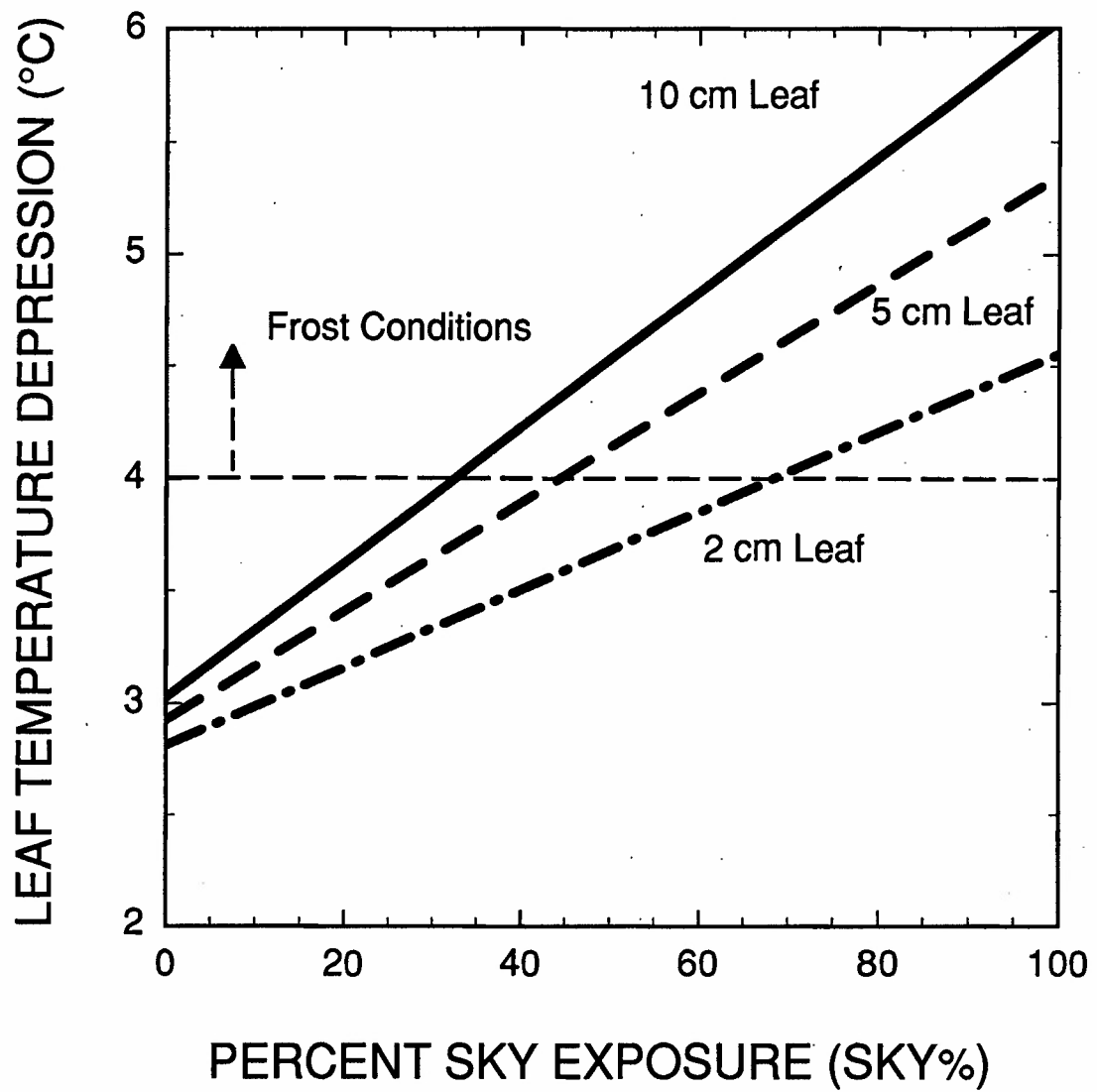


Figure 1.8: Energy balance simulation results: Sky exposure versus leaf temperature depression for 2, 5, and 10 cm leaves. Elevation is 3230 m; relative humidity is 90%; $R_{l,\uparrow}$ is 330 W m^{-2} ; wind speed is 20 cm s^{-1} ; and air temperature is 4°C .

peach flower depressions of 1.5 °C in Georgia. Some authors have observed a vertical gradient in T_{air} , particularly below 1 m (Leuning and Cremer 1988; Oke 1970), but only a few of the temperature depressions cited above indicate whether air and leaf or grass temperatures were taken at the same height (Leuning and Cremer 1988). Hadley and Smith (1987) reported leaf temperature depressions at night for conifer needles of up to 8.2 °C, with a mean depression of near 3 °C. This rather large depression for such a small leaf dimension was attributed to low wind speeds due to needle packing and a dense canopy configuration.

Radiative emission by the atmosphere is regulated by the temperature of the air column (Oke and Fuggle 1972) as well as the moisture content (Deacon 1970; Idso 1981) and factors such as particulate pollution (Nowak 1989). However, the most important single factor influencing upper hemisphere nocturnal longwave radiation is cloudiness (Floor 1989; Gardner et al. 1991; Kimball et al. 1982; Ramanathan et al. 1989). Clouds increase the input of heat energy from the night sky through thermal emission at the cloud base and back-scattering of thermal radiation emitted below the cloud layer, and therefore limit the potential cooling. Microsite variations in sky% may also strongly influence the impact of the sky thermal emissions (Freeburg 1972; Nunez and Bowman 1988).

Conclusions

Simulated results suggest that large leaves are most susceptible to freezing conditions in the subalpine environment. This may be a factor in selecting against large-leaved species in an environment with low nocturnal thermal fluxes from the upper hemisphere combined with low wind speed and air temperatures approaching freezing. In all broadleaf species, and even conifers with closely arranged needles, a combination of low wind speeds and cold skies can drive leaf temperatures well below ambient air temperatures. Increases in R_{\downarrow} would reduce both the frequency and severity of freezing events. This might result from a general warming of the atmosphere, an increase in

atmospheric dust, pollution, moisture content or cloud cover -- scenarios that have been postulated in conjunction with models of atmospheric change.

Environmentally mediated leaf size restrictions have traditionally been considered to be caused by sunlight interactions, with larger leaves favored in shaded situations where solar heating is less extreme. In environments where nocturnal $R_{l,d}$, wind, and air temperature regimes combine to create a possibility of growing season frost, it is likely that maximum leaf size restrictions in exposed sites are also established by temperature minima. Frost events during the growing season would tend to supplement the ecological effects of daytime temperature stress to favor smaller leaves in exposed conditions. It may even be possible that the detrimental effects of freezing are a stronger driving force limiting leaf size in high elevation microsites than those of daytime heating.

Chapter 2: Radiation frost susceptibility and the association between sky exposure and leaf size

Introduction

Nocturnal infrared radiation from the sky (sky IR) is important to the biophysics of plants because a net loss of radiant energy can lead to frost formation on leaves at night, even though air temperatures may remain well above freezing. Greater exposure to cold nighttime skies increases the susceptibility of leaves to radiation frost and, thus, is important to the growth and reproduction of agricultural species (Holopainen 1990; Lu et al. 1992) as well as native species (Raitio 1987; Sakai and Larcher 1987; Lundmark et al. 1988; Paton 1988).

One objective of the current study was to describe the variability of sky IR due to elevational effects and microsite exposure. Longwave radiant energy from the upper hemisphere at night has interested atmospheric scientists for a number of years, including studies that date back to the early part of this century (Ångström 1915; Brunt 1932). Later work focused on the development of equations that predict sky IR based on ground-level measurements of air humidity and temperature (Idso 1972, 1981; Brutsaert 1975; Aase and Idso 1978). In the present study, published empirical equations for predicting sky IR are compared to field measurements. A second objective was to evaluate the association between sky IR and leaf size at a particular microsite to test the hypothesis that decreases in leaf size, traditionally associated with greater sunlight exposure, may also be correlated with lower sky IR levels and conditions of increased frost susceptibility.

Materials and methods

The general approach was to measure actual changes in sky IR at different elevations and microsites and compare their relative effects on frost susceptibility. Also,

corresponding measurements of leaf size variation in two species were made to test the hypothesis that leaf size may be influenced by sky IR as well as by total solar irradiance.

Site description

The primary research site was a forest clearing at an elevation of 3230 m near Brooklyn Lake in the Medicine Bow National Forest of southeastern Wyoming where open subalpine meadows are interspersed with ribbon-like islands of spruce-fir (*Abies lasiocarpa* and *Picea engelmannii*). Typically, the tree islands were approximately 500 to 1000 m² in size with meadow areas over twice as large. Individual tree heights were about 15 m, while the height of the herbaceous meadow vegetation was usually less than 0.3 m. In more wind-swept areas, cushion-like plants with small leaves dominate. Billings (1969) described the vegetation of this area in detail and Nelson (1984) listed the flora.

Elevation effects on sky IR

Sky thermal changes across an elevational gradient were measured using a hemispherical, all-wave radiometer (REBS, Inc.) and 21X datalogger (Campbell Scientific Instruments). Calibration constants and calculations were incorporated into the datalogger software. Simultaneous air temperature measurements were made with a fine-wire thermocouple (type T, 0.2 mm copper-constantan, Omega Engineering Inc.) and a reference thermocouple junction built into the datalogger. Relative humidity was monitored with a HX 92V Relative Humidity Transmitter (Omega Engineering Inc.). All three sensors were mounted on a vehicle roof rack. Altitude measurements were made using an AlitiPlus S1 digital altimeter (Suunto USA, Carlsbad, CA). At the start of each sampling trip, the altimeter was set to the initial elevation of 2205 m (Laramie, WY, USA).

To minimize the potential influence of changing atmospheric conditions, each series of measurements was completed in as little time as reasonable. All measurements

were made while traveling between 90 and 130 km h⁻¹. Oke and Fuggle (1972) found that measurement variation due to velocity or other movement associated with an automobile-based instrument was negligible, and local tests confirmed this. Variation based on temporal differences between individual measurements was minimized by replicating all measurements on both the outgoing and return legs of each elevational transect.

Sky exposure, sky IR and incident sunlight

Eighteen microsites were subjectively located across a gradient in sky exposure (sky%) from the center to the edge of the subalpine forest/meadow boundary at the Brooklyn Lake site. The most sheltered of the microsites apparently did not permit sufficient sunlight penetration for understory plants to survive, as no appreciable understory was present. Fisheye photographs were taken at each microsite to evaluate the amount of forest canopy providing shelter from sky exposure. The lens adapter used produced a 176° field of view of the upper hemisphere, and each photograph was scanned digitally for calculation of sky% as in Chazdon and Field (1987).

To address the influence of microsite variations in sky exposure in the subalpine environment, total daily solar irradiance (DPAR, $\mu\text{mol m}^{-2}$) and sky IR were measured on clear days and nights. Sky IR was measured during a radiation frost at all 18 microsites using the same radiometer and datalogger as described above. The radiometer was moved to a microsite, leveled at approximate plant height (5 cm) and allowed to equilibrate. Ambient air temperatures averaged 1.8 ± 0.3 °C during the measurements and relative humidity was near 100%. During the measurement period, independent measurements of sky IR using permanent sensors at the center of the clearing did not change perceptibly. DPAR was also measured at three microsites near the forest edge and at the clearing center using LI-COR model 190 quantum sensors oriented horizontally.

Leaf size

Elevational and microsite differences in sky IR and DPAR were compared to corresponding measurements of leaf size in two species. *Erigeron peregrinus* is a common, broadly distributed meadow species of the central Rocky Mountains that grows from a basal rosette of leaves and produces a central flower stalk. Individual plants sprout from a perennial root system soon after snowmelt and persist through spring and early summer frosts until the occurrence of more severe frosts in the early autumn. Because this species has considerable variation in leaf size from sheltered locations to more exposed microsites, five fully developed leaves from sixteen different plants were randomly sampled at the end of the growing season (2 September 1993) from locations within 0.5 m of each sky IR microsite. Leaf width and length were recorded. At the two most sheltered microsites, no *E. peregrinus* leaves were available, and these locations were subsequently treated as missing from this phase of the analysis.

Leaf width (measured at the leaf midpoint) and DPAR were measured for *Taraxacum officinale* Webb at ten sites along the same elevational gradient as measured for sky IR. DPAR was determined by integrating measurements of instantaneous PAR throughout the day. Each sensor was oriented horizontally near the center and just above individual plants sampled. Measurements of incident sunlight were recorded every 5 min from 0700 to 1800 h.

Results

Elevation effects on sky IR

An elevational gradient of sky IR measurements made at > 90% sky exposure (Fig. 2.1) was compared to recent equations used for empirical predictions of sky IR. For example, Idso's (1981) estimate of sky IR is based on the computation of atmospheric emittance (ϵ_a) from measured vapor pressure (e_o) in kPa and surface air temperature (T_a) in K:

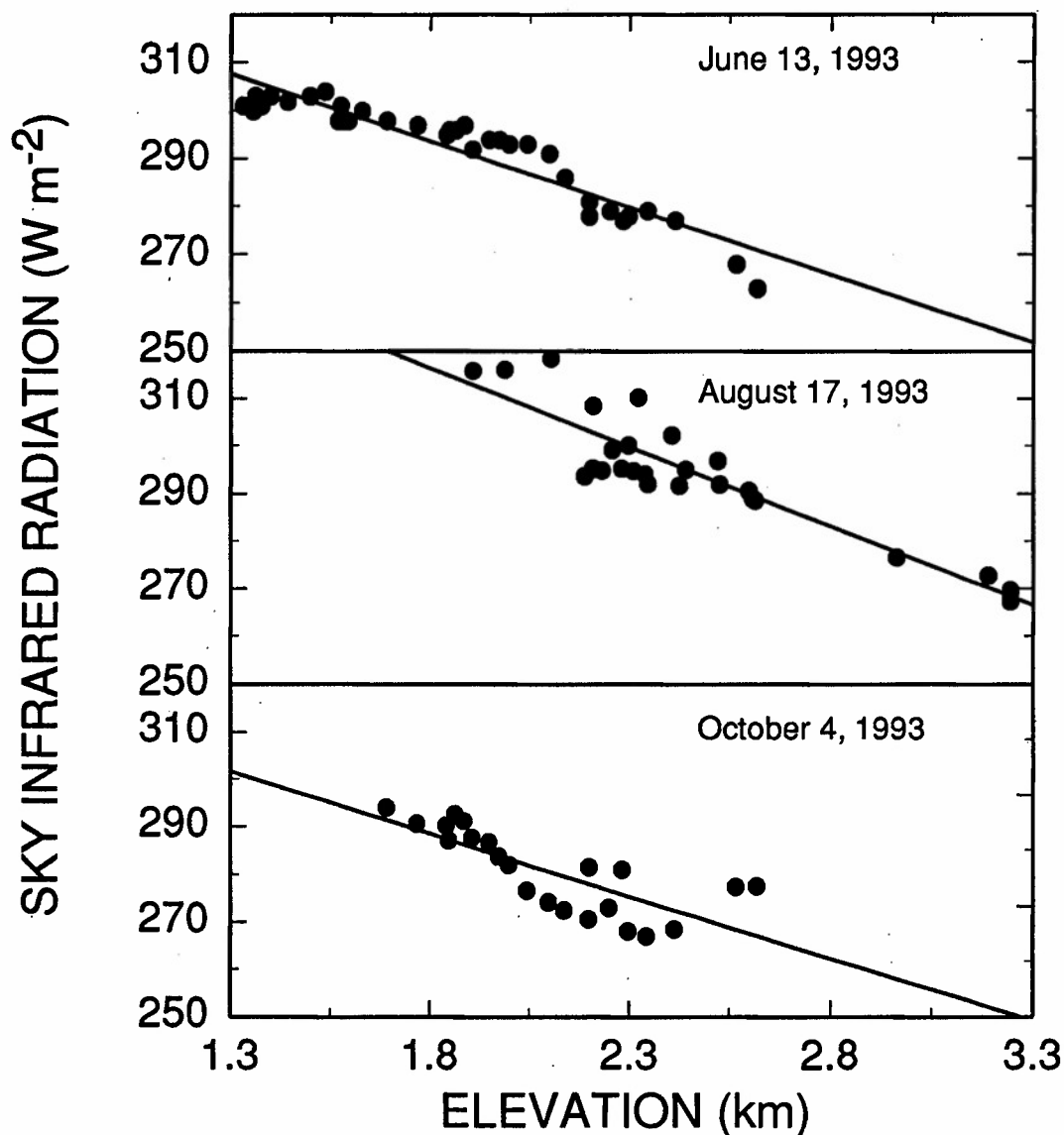


Figure 2.1

Changes in sky IR with elevation measured on three nights under clear skies. All transects were measured on both the outgoing and return trips from the mountains of southeastern Wyoming to the plains of western Nebraska. The starting point for each transect was Laramie, Wyoming at an elevation of 2205 m. The best fit linear equations of the data were: June sky IR = $-27.9 * \text{elevation} + 344$ ($r^2 = 0.88$): August sky IR = $-33.3 * \text{elevation} + 376$ ($r^2 = 0.90$): October sky IR = $-26.2 * \text{elevation} + 335$ ($r^2 = 0.60$).

$$\epsilon_a = 0.70 + 5.95 \times 10^{-4} e_o \exp(1500 / T_a). \quad [\text{Eqn. 2.1}]$$

The computed atmospheric emittance was then incorporated in the Stefan-Boltzmann equation:

$$R_{l,\downarrow} = \epsilon_a \sigma T_a^4, \quad [\text{Eqn. 2.2}]$$

where $R_{l,\downarrow}$ is sky IR and σ is the Stefan-Boltzmann constant. Idso's estimate of atmospheric emissivity, when compared, yielded an adjusted r^2 of 0.52 (Fig. 2.2A). A subsequent linear regression with elevation (coefficient of $-0.014 \text{ W m}^{-2} \text{ m}^{-1}$) improved the r^2 to a model-adjusted value of 0.71 (Fig. 2.2B). All model regression coefficients were statistically significant at $p < 0.0001$ (ANOVA).

Sky exposure, sky IR, and leaf size

Sky% ranged from 95% at the most exposed locations in the center of the research site to 25% at the most sheltered locations beneath ribbon-forest canopies (Fig. 2.3A). Measured values of sky IR ranged from over 340 W m^{-2} in the trees to less than 275 W m^{-2} at the clearing center. The influence of the forest canopy on sky IR appeared to extend only to about 10 m into the clearing (Fig. 2.3B). The association between sky% and sky IR was linear and inversely related (Fig. 2.3, 2.4). Under the clear sky conditions of 21 July 1993, the linear equation

$$\text{sky IR} = -1.02 * \text{sky\%} + 366, \quad [\text{Eqn. 2.3}]$$

produced an r^2 of 0.98. In comparison, there were relatively small decreases in DPAR (9-13%) from the clearing center to the forest edge. Also, these small differences in DPAR were generated primarily because of shading by adjacent trees in the early evening (1630 to 1900).

Significant decreases in leaf size of *T. officinale* were linearly related to decreases in sky IR with elevation (Fig. 2.5A). In contrast, no significant association was found between leaf size and DPAR. In *E. peregrinus*, leaf size was correlated with the sky IR of a given microsite. Regression analysis identified a significant relationship between

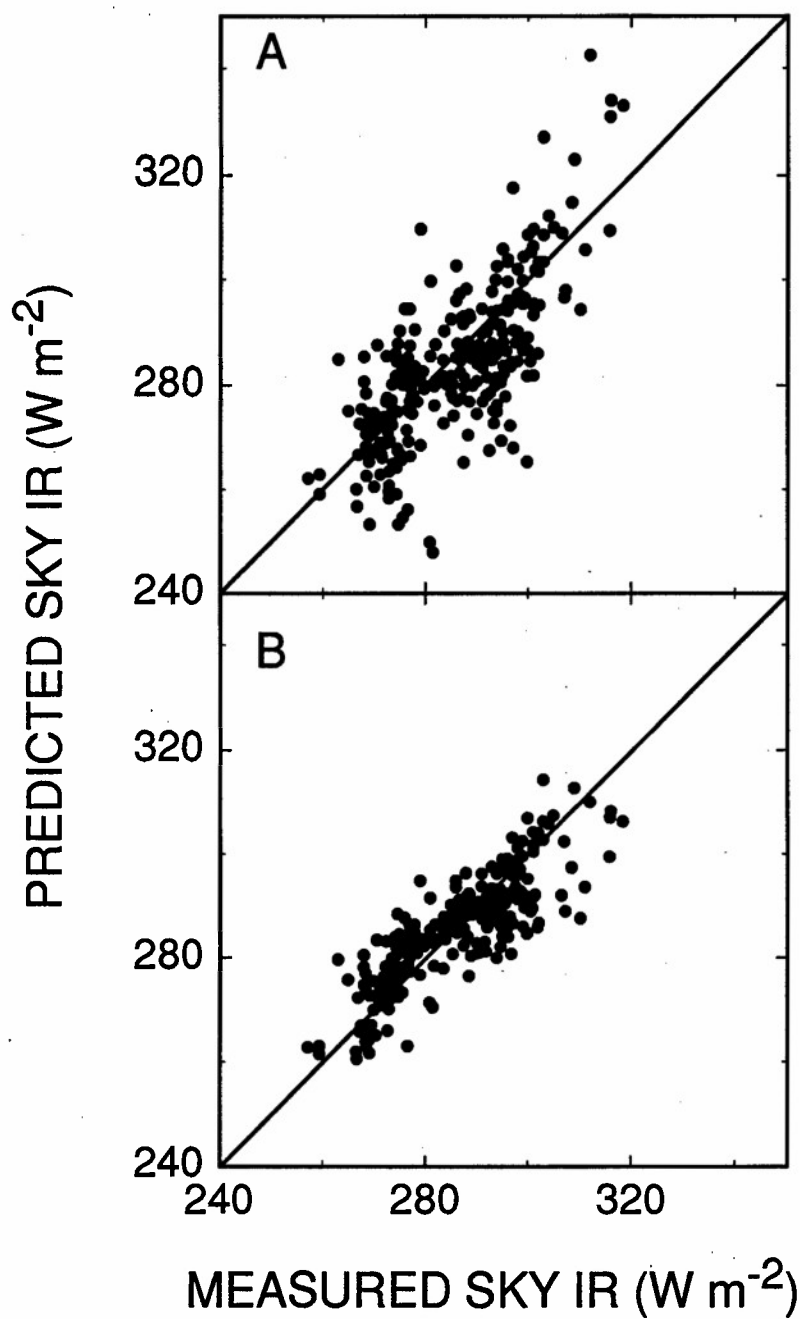


Figure 2.2 A: Sky IR predictions from Idso (1981) shown plotted against measurements from Fig. 2.1 ($r^2 = 0.52$). B: Sky IR predictions from Idso (1981) with a linear correction for elevation of $-0.014 \text{ W m}^{-2} \text{ m}^{-1}$ plotted against measurements ($r^2 = 0.71$).

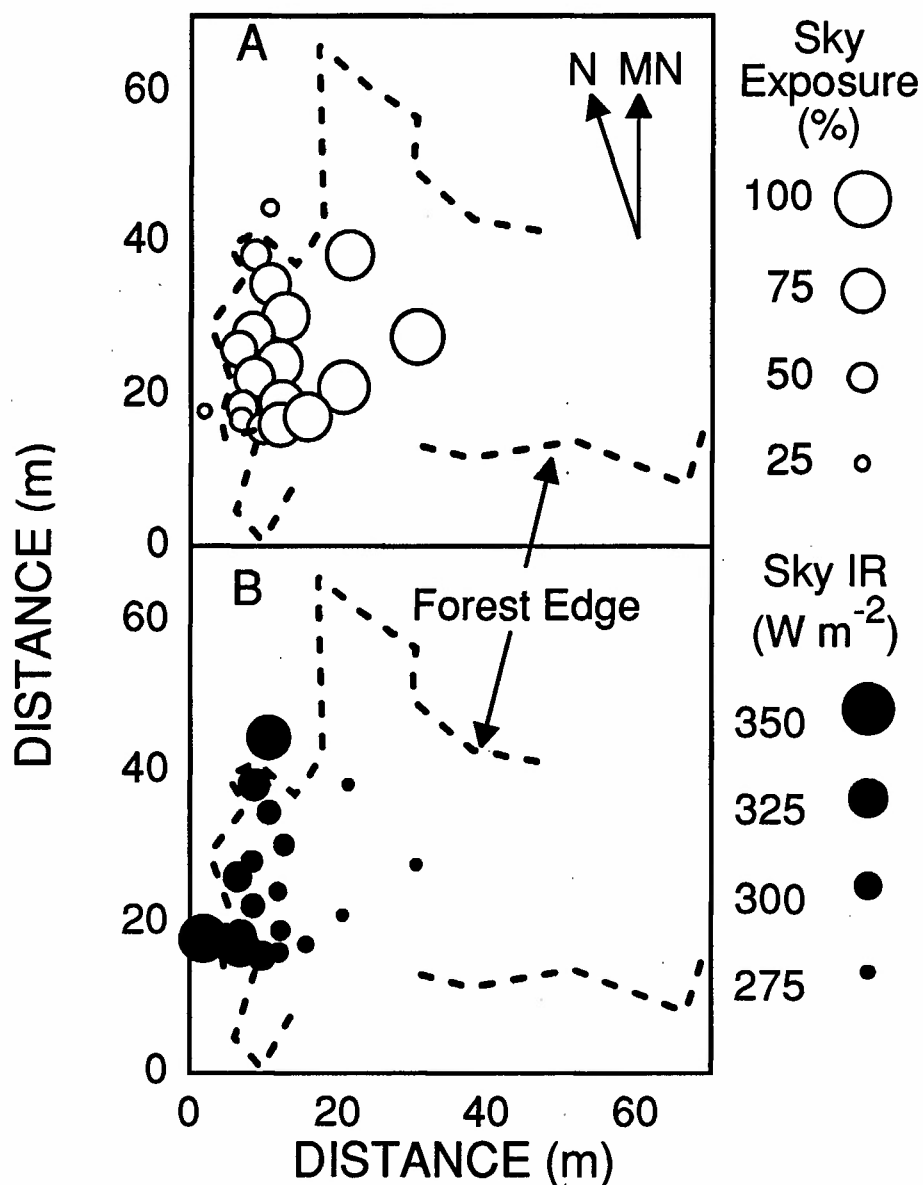


Figure 2.3 Determination of sky exposure at a representative meadow site at an elevation of 3230 m near Brooklyn Lake in the Medicine Bow National Forest of southeastern Wyoming. Circle symbols are centered on sampling locations and their diameters are scaled to indicate the values measured. A: Percentage of sky exposure. B: Upper hemisphere energy incident on a radiometer at the top of the herbaceous plant canopy during a radiation frost on the night of July 21, 1993.

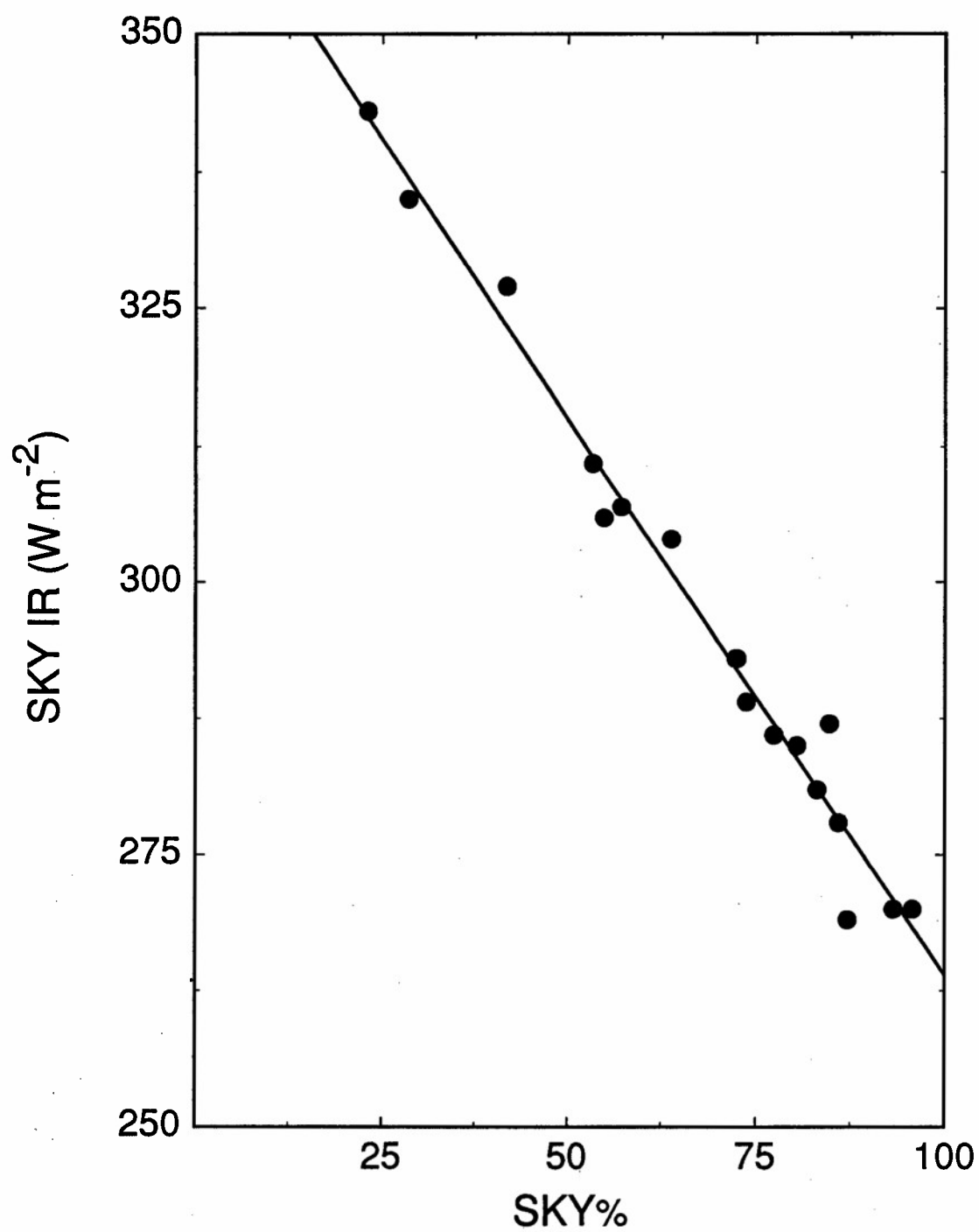


Figure 2.4 Relationship between sky% and sky IR at the microsites indicated in Fig. 2.3. Sky IR = $-1.02 * \text{sky}\% + 366$ ($r^2 = 0.98$).

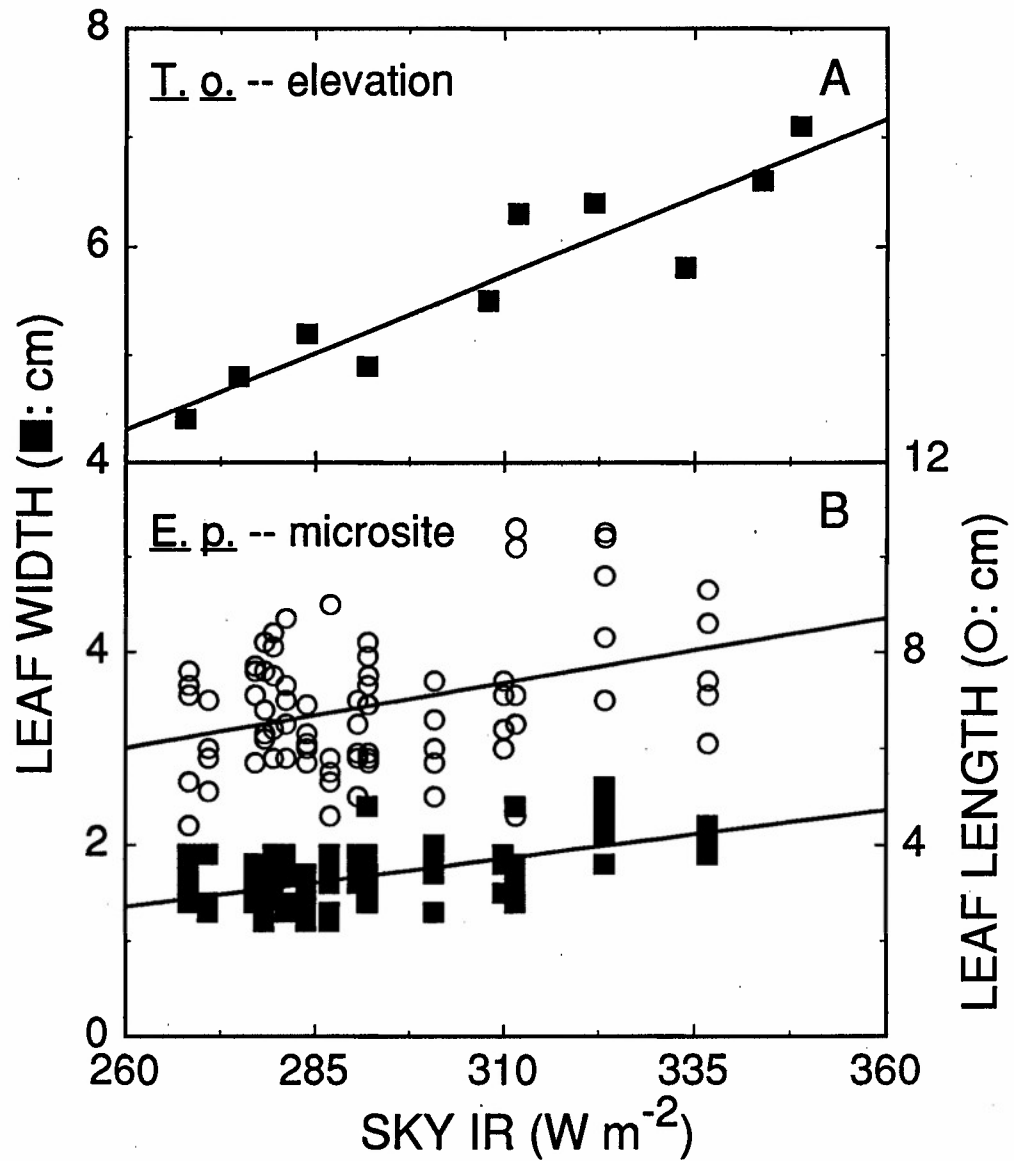


Figure 2.5 A: Changes in leaf width (■) in *Taraxacum officinale* across a gradient in elevation and sky IR. B: Changes in leaf width (■) and leaf length (○) of *Erigeron peregrinus* with increasing sky IR measured from randomly selected leaves within 0.5 m of the points shown in Fig. 2.3. Best fit linear regressions were: *T. officinale* leaf width = $0.029 * \text{sky IR} - 3.1$ ($r^2 = 0.85$), *E. peregrinus* leaf width = $0.010 * \text{sky IR} - 1.25$ ($r^2 = 0.36$) and *E. peregrinus* leaf length = $0.027 * \text{sky IR} - 0.96$ ($r^2 = 0.13$).

both leaf width and leaf length with sky IR (Fig. 2.5B). Although the r^2 for both regressions was low (< 0.4), a statistically significant ($p < 0.001$) trend of decreasing leaf size with increasing sky IR remained. Additionally, leaves from *E. peregrinus* plants growing beneath the south edges of saplings and fallen trees, thus experiencing only minor decreases in DPAR, were significantly larger than leaves measured during the random spatial sampling. Fifteen leaves from these sites, all well sheltered from radiative losses (sky% less than 30%), averaged $3.2 \text{ cm} \pm 0.7$ in width and $11.9 \text{ cm} \pm 2.0$ in length (\pm standard deviation), compared to means of $1.7 \text{ cm} \pm 0.3$ in width and 6.9 ± 1.4 in length measured for 80 leaves selected randomly.

Discussion

Early studies of longwave radiation from the sky tended to focus on the simplest case of uninterrupted exposure to a cloudless sky (Brutsaert 1975; Idso 1972, 1981). In modelling approaches to clear sky thermal emission, Idso (1981) applied a combination of empirical and theoretical approaches that included empirical estimates for sky emissivity and sky IR. Sky emissivity estimates were based on ground-level measurements of either atmospheric water vapor (Ångström 1915; Brunt 1932), air temperature (Swinbank 1963), or both (Idso 1981). Some more recent studies (Kimball et al. 1982; Ramanathan 1989; Ye et al. 1989) have also considered exposure to a sky partially obscured by clouds. Kimball et al. (1982) suggested that the increase in sky IR due to cloud cover was regulated by cloud base temperature, cloud emissivity, and the transmittance of the atmosphere between the observer and the cloud. They reported that cloud cover increased sky IR by an average of about 25%, but up to 40% over clear sky conditions. In this regard, it is well known that overstory vegetation can also generate microsites that are similarly protected from the cooling effects of exposure to the night sky (Percival et al. 1984; Eastham and Rose 1988).

Idso (1981) produced equations estimating sky IR based on ground-level measurements of water vapor and air temperature at a fixed site in Phoenix, Arizona. I found that his equations accurately predicted the same trends as my observations, but could not explain all the elevational variation. Higher elevation sites received less longwave radiation from the night sky than Idso's equations predicted. The reduced atmospheric density, or perhaps different vertical lapse rates in the upper atmosphere, might produce this result and be unaccounted for by Idso's (1981) equations. Addition of an elevation term to the equation dramatically improved the fit of the model. After accounting for differences in air temperature, water vapor content, and elevation, a small discrepancy still remained. This I attributed to slight differences in sky exposure and possible upper atmosphere differences on different days not perceptible from the ground except through the impact on sky IR. Idso (1972) suggested that atmospheric dust may generate differences in sky IR that are not predicted by changes in air temperature and water vapor content. Regardless of the mechanism, higher elevation locations should have a greater net loss of energy on clear nights. Reduced air density and thermal input from the sky at high elevation, combined with a potentially large lapse rate in air temperature, increases both the frequency and severity of frost episodes in plants of high elevation environments (Jordan and Smith 1994).

Because the conifer trees surrounding these meadow sites are rarely more than about 15 m in height, sky% and nocturnal radiational cooling increased rapidly with distance from the forest edge. Due to the low growth habit of herbaceous vegetation in this environment, the variation in sky% at plant leaf height was due solely to obstruction of the sky by the forest canopy. Over 80% of the total area of the forest clearing had greater than 80% sky exposure. The narrow band around the clearing periphery within about a tree height of the forest edge contains a strong gradient in sky%. However, this gradient in diffuse radiation is more broadly distributed than the gradient in PAR, which

is uniform across the site throughout the morning and early afternoon. As the sampling transect was on the northwestern edge of a clearing, the transect received direct sunlight for nearly the entire day until falling rapidly into the shadow in the late afternoon. The resulting decrease in DPAR near the edge of the clearing due to late afternoon canopy shading was between 9 and 13%, depending on the degree of cloud cover. Two of the sampling points were under sufficient canopy to be sheltered from most direct sunlight, and the understory vegetation at these points was correspondingly limited.

It has been suggested by Taylor (1975), Smith (1978), Gates (1980) and others that leaves tend to be smaller in exposed microsites because of the advantages of the increased convective heat exchange that would lower leaf temperatures and transpiration during the day. This idea has now become a somewhat traditional explanation for the adaptive significance of having smaller leaves in microsites with greater sun exposure. However, the correlation between leaf size and nocturnal sky exposure measured here could also be interpreted as an adaptation for reduced frost severity and frequency. Because all leaves were exposed to approximately the same duration and intensity of direct sunlight, but experienced corresponding gradients in nocturnal radiation and leaf dimension, I suggest that the nocturnal radiative environment may also be an important selective force influencing leaf size. Numerous other studies have alluded to the advantages of a smaller leaf dimension for raising leaf temperatures at night (e.g. Leuning 1988; Leuning and Cremer 1988; Jordan and Smith 1994), although no studies have associated changes in leaf size with nocturnal sky IR values. It appears possible that the well-documented advantages of a smaller leaf with greater sun exposure, as well as the avoidance of lower temperature minima at night, could both act as important selective forces favoring a smaller leaf dimension.

Conclusions

The influence of radiative energy exchange with the night sky on frost occurrence may be an important factor influencing plant growth and reproduction, as well as plant habit, structure, and spatial distribution. Larger leaves and greater sky exposure may result in the radiative cooling of these surfaces to well below ambient air temperature and, as a result, increases in the frequency, duration and intensity of frost episodes during the growth season. A smaller leaf size may be adaptive for limiting extremes not only of high temperatures during the day, but also minimum temperatures at night. Postulated warming of the atmosphere as a whole may increase the infrared output of the night sky, thereby influencing plant structural and distributional patterns on a global scale. More work is needed to clarify the importance of exposure to daytime sunlight with low nighttime sky IR and frost susceptibility to plant physiological ecology. The combination of these two stress factors may be particularly characteristic of plants in high elevation habitats.

Chapter 3: Microclimate influences on the frequency and duration of growth season frost for subalpine plants

Introduction

Plant temperatures at night are important to both native and agricultural plant species because of the potentially important influence of frost occurrence on growth and reproduction (Arny and Upper 1973; Sakai and Larcher 1987; Lu et al. 1992). Although the seasonal occurrence of frost is used commonly to estimate the length of the growing season of agricultural species (Suckling 1989), only a few studies have evaluated the effects of frost on growth and distribution of native plants (Silberbauer-Gottsberger et al. 1977; Paton 1988). In the subalpine environment, frost can occur during the entire summer growing period, leading to leaf damage and a substantial reduction in carbon assimilation for at least several days (Lundmark and Hällgren 1987; Lundmark et al. 1988; Dang et al. 1992). A recent, comprehensive treatment of the importance of frost tolerance to summer growth is provided by Havranek and Tranquillini (1994). Robberecht and Junttila (1992) suggested that plants growing in climates subject to growing season frost in the high Arctic must maintain a basal level of frost tolerance throughout the year to avoid damage or mortality.

Knowledge of the biophysical factors responsible for frost events may help in our understanding of the role of micrometeorological factors in limiting plant growth and distribution. The relative frequencies of advective frosts associated with cold air masses can be distinguished from frosts generated by radiation exchange with the cold night sky on both a meteorological and micrometeorological scale. This distinction may be especially important to plant/climate models that attempt linkages between atmospheric warming and the vegetative component. Radiational cooling was expected under clear skies when the net radiation flux to the ground was less than -6 W m^{-2} (André and Mahrt

1982). Negative net radiative fluxes were predicted to have a much greater impact on frost events for plants with larger, broadleaves growing in exposed microsites (Jordan and Smith 1994). Conversely, cold air settling into topographic depressions or moving along drainages can freeze plants (regardless of leaf morphology or sky exposure) due to the accumulation of cold air at plant level (Ball 1956; Oke 1970; Paton 1988).

The purpose of the present study was to evaluate the frequency, intensity and duration of frost episodes during the growing season in the subalpine environment. Also, the biophysical components of freezing were evaluated by measuring the convective and radiative microclimate across a gradient of sky exposure, along with accompanying leaf and flower temperatures of broadleaf and coniferous plants over an entire summer.

Methods

Study site and species

The primary research site was a subalpine meadow located near Brooklyn Lake in the Medicine Bow National Forest of southeastern Wyoming, USA. The meadow was at the top of a gentle ridge in an area where open meadows are generally larger than 2000 m² and are interspersed with spruce-fir forest. The height of the forest canopy surrounding these meadows is typically 10-15 m, while the herbaceous vegetation of the meadow is rarely over 0.3 m (Billings 1969; Nelson 1984). In the more wind-swept areas of the larger meadows, cushion-like plants with small leaves dominate. *Erigeron peregrinus* and *Polygonum bistortoides* Pursh were selected as representative of the broadleaf herbaceous species, and *Abies lasiocarpa* (Hook.) Nutt. was selected as representative of the needle-leaf conifers that dominate this area. Measured leaf blades of *E. peregrinus* were approximately 1.5 cm wide, 6.0 cm in length, and were located approximately 3-5 cm above the ground. One *E. peregrinus* leaf on each of three different plants was monitored across an exposure gradient (forest understory to clearing center), as well one needle on each of three nearby *A. lasiocarpa* saplings. The

dimension of the *A. lasiocarpa* needle in the clearing center was 1.8 cm in length and about 1 mm in width, and was located approximately 27 cm above the ground in the middle of a shoot on the upper side.

Microclimate, air and plant temperatures

Microclimate conditions were measured immediately adjacent to the leaves of *E. peregrinus* and the needle-like leaves of nearby *A. lasiocarpa* at 3 locations across a gradient of sky exposure (from the clearing center to nearby forest understory).

Temperatures, wind speeds and upper hemisphere radiation were continuously measured throughout the 1993 growing season to evaluate the occurrence of leaf frost events and the factors influencing those events. During the day, both solar and infrared components contributed to the radiation observations, while at night only the infrared component was present. Temperatures were monitored using type T, 0.2 mm diameter copper-constantan thermocouples (Omega Engineering Inc., Stamford, CT). The air temperature thermocouple was mounted on an instrument stand at approximate plant heights of 8-10 cm. Leaf thermocouples were stitched along the midvein at the center of the broadleaves or coiled around individual conifer needles. Leaf temperatures were monitored beginning approximately 10 days after initiation of annual growth, because of the need for sufficiently large leaves to support a thermocouple. Wind speed was monitored adjacent to the air temperature thermocouple using a thermistor anemometer modified from a design of Bergen (1971), as described in Jordan and Smith (1994).

The vertical air temperature profile was measured near the center of the clearing on the night of August 25, 1993. Thermocouples were positioned on the upwind side of an instrument tower at heights of 10, 20, 50, 100, and 200 cm. Instantaneous measurements were recorded every 10 s for 1.5 h using a 21X datalogger (Campbell Scientific Instruments, Logan, UT). The vertical profile of air temperatures was extended upwards by comparison to United States Forest Service data from a 10 m weather tower

at a site 1 km away (B. Connell, pers. commun., 1994). These data were also used to contrast our two-year dataset at ground level with a 5-year period. Air temperature observations from a 10 m tower should be relatively insensitive to radiative influences because the air and sensor were physically removed from surfaces where radiation exchange takes place. Also, air cooling by radiative processes at 10 m is overshadowed by turbulent transfer processes (André and Mahrt 1982).

During the nights of August 24 and 25, 1993, a hand-held infrared thermometer (C-600M, Linear Laboratories, Los Altos, CA) was used to measure paired leaf blade and flower bud temperatures of 27 *E. peregrinus* (entire flower disk) and 21 *P. bistortoides*. Both species have leaves of similar dimension growing from a basal rosette and have stalks lifting flower heads 15 to 25 cm above the meadow foliage. The calibration of the infrared thermometer was confirmed by comparison to simultaneous leaf temperature measurements using a thermocouple.

Total hemispherical all-wave radiometers (REBS, Inc.) were positioned next to individual leaves with thermocouples installed, and used to measure incident radiation from the lower and upper hemispheres. The radiometers were ventilated with fans (REBS, Inc.) to reduce dew formation on the upper dome that would tend to cause overestimation of infrared measurements from the upper hemisphere, especially on clear nights. At night the fans induced a continuous gentle air movement along the axis of the radiometer support arm and over the polyethylene domes. Microclimate and leaf temperature data were recorded every min on a 21X datalogger and 15 min means were computed. At each radiometer, a fisheye photograph (176° field of view) was also taken to compute the amount of sky exposure. These photographs were digitally scanned for calculation of the exposed portion of the upper hemisphere using procedures given in Chazdon and Field (1987).

Results

Frequency, duration and intensity of freezing temperatures

During the 1993 growing season (interval from the appearance of the first fully expanded leaf to leaf senescence in meadow broadleaf vegetation), T_{air} at a height of 8 cm at the clearing center was below 0 °C on 26 of 61 nights (Fig. 3.1A) while *E. peregrinus* leaf temperatures (T_{leaf}) were less than 0 °C on 38 occasions (Fig. 3.1B). Figure 3.2 shows a typical radiation frost night (July 27-28, 1993), with an above-freezing minima in T_{air} occurring at 0015, and a sub-freezing T_{leaf} minima occurring at 0245. Air temperature (T_{air}) minima occurred most frequently between 0600 and 0700 h, although T_{air} minima occasionally occurred shortly after sunrise or before midnight. Leaf temperature minima were more evenly distributed throughout the nighttime hours than T_{air} minima, with no dominant peak time. Only 43% of nightly T_{air} and T_{leaf} minima occurred at the same time, although 57% of T_{air} and T_{leaf} minima were within ± 15 min of each other.

Throughout the subalpine growing season, T_{leaf} of both the broadleaf and conifer species varied dramatically on a daily basis, and frequently was below-freezing at night, even though ideal photosynthetic temperatures occurred during the day (Fig. 3.2, 3.3). Due to reduced convective heating at night and decreased cooling during the day, leaves of *E. peregrinus* at the center of the clearing demonstrated a substantially greater diurnal temperature range (mean of daily maxima minus daily minima equals 25.4 °C) than nearby needles of *A. lasiocarpa* (seasonal mean range of 16.2 °C), which tended to track T_{air} (mean range of 16.7 °C) more closely (Fig. 3.3).

There was a strong inverse relationship between the amount of forest shelter and both the number of frost events and the total hours of frost for both broadleaf and ambient air temperatures (Table 3.1). Leaf frost events occurred on approximately 70% of days in both 1992 and 1993 in the meadow center, while occurring much less frequently in more

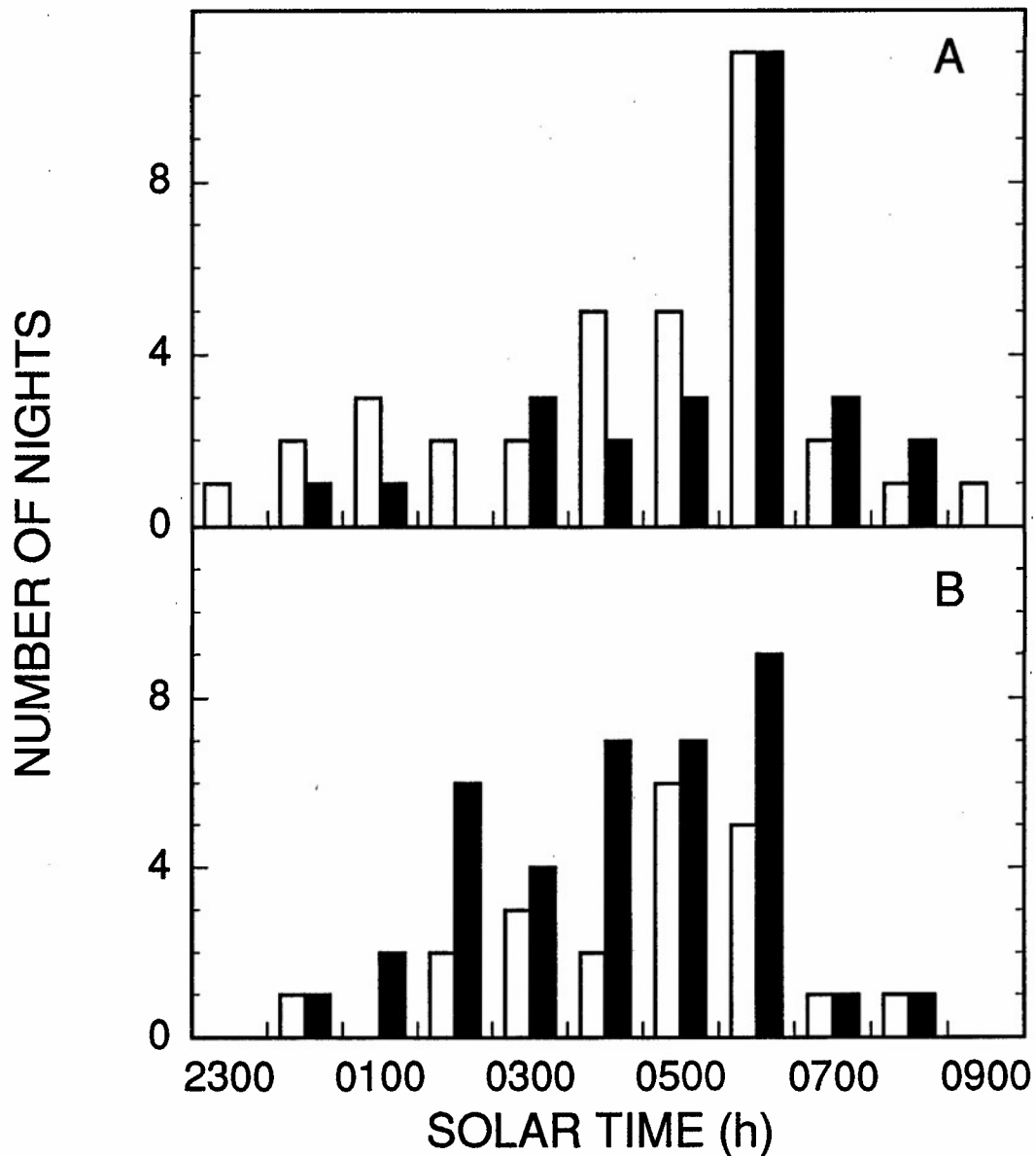


Figure 3.1: A: Time distribution of nightly T_{air} (8 cm height) minima. B: Time distribution of nightly *Erigeron peregrinus* T_{leaf} minima during the 1993 growing season (61 nights) at the center of the research site. Temperature minima $< 0^{\circ}\text{C}$ are represented by , and temperature minima $> 0^{\circ}\text{C}$ are depicted by . Each night is represented on the histogram at the time of occurrence of the lowest temperature (of air or leaf).

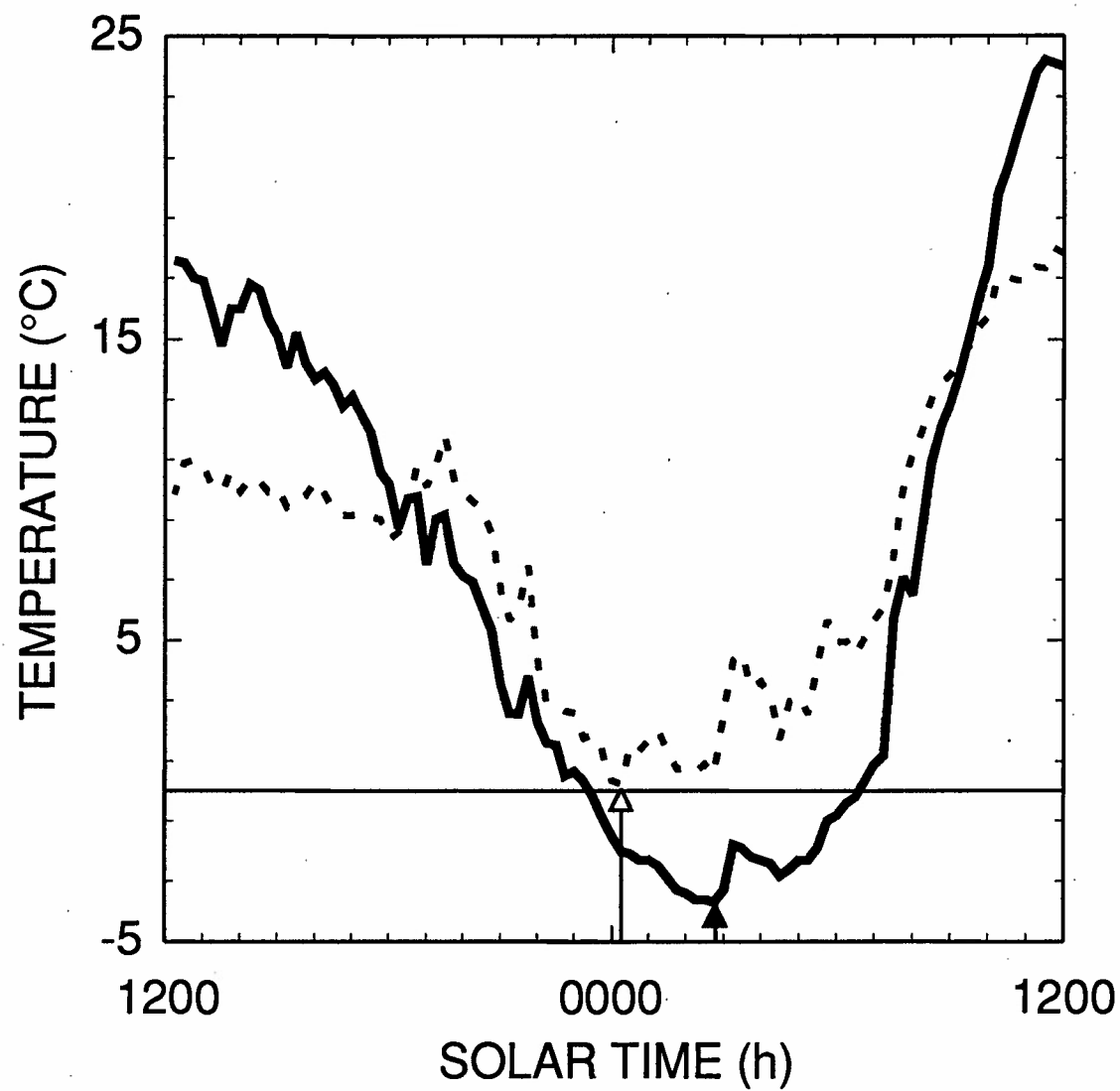


Figure 3.2: Time series of T_{air} (8 cm height at clearing center) (dashed line) and *Erigeron peregrinus* T_{leaf} on July 27-28, 1993 (solid line). The open arrow marks the minima of T_{air} and the solid arrow marks the minima of T_{leaf} .

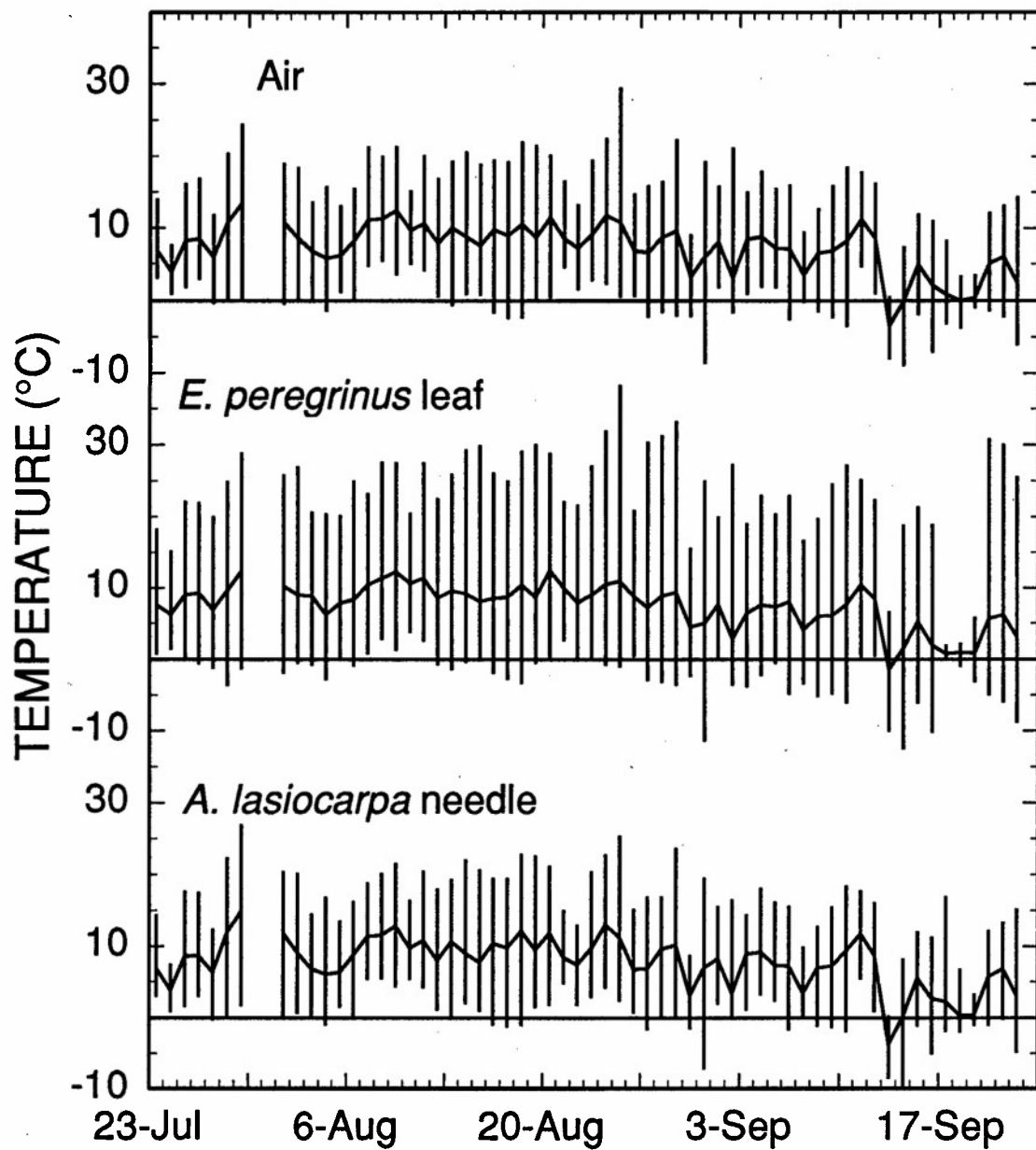


Figure 3.3: Maximum, minimum, and mean temperature record of air, *Erigeron peregrinus* leaves, and *Abies lasiocarpa* needles at the clearing center during 1993. The sensors were located within 2 m of each other at heights of 8, 3 and 27 cm respectively.

Sensor	Site	# of Frost Events		# of Frost Hours	
		1992	1993	1992	1993
<i>E. peregrinus</i> (≈ 3 cm)	Clearing center	55	41	241.5	226.00
	Clearing edge	38	33	154.5	151.25
	Forest understory	5	16	30.5	81.75
Air	Clearing center	-	26	-	137.50
	Clearing edge	7	25	15.5	125.25
	Forest understory	-	13	-	81.75

Table 3.1: The number of frost events and total hours of frost for 1992 and 1993 *Erigeron peregrinus*, and 1993 air temperature across a gradient of sky exposure. The height of the 1992 T_{air} measurement was 35 cm, while in 1993 all T_{air} measurements were made at 8 cm. This prohibits direct comparison, but provides evidence of the impact of T_{air} inversions. The 1992 growth season comprised 71 days (July 9 - Sept. 18). The 1993 season was limited to 61 days (July 22 - Sept. 23).

sheltered locations. The frequency of sub-freezing T_{air} events mirrored T_{leaf} frost events in the understory, but was much less frequent than leaf frost in the more exposed microsites (Table 3.1). The duration of *E. peregrinus* frost events is shown in Fig. 3.4 at three different levels of sky exposure, as well as for an exposed *A. lasiocarpa* sapling and an air temperature thermocouple. Both T_{air} measurements at the clearing center and T_{leaf} for *A. lasiocarpa* showed similar durations and frequencies of freezing events. On the other hand, exposed *E. peregrinus* leaves experienced frost much more frequently throughout the growing season, with only 5 consecutive days without a frost during the entire summer. Plants of *E. peregrinus* that were partially sheltered by forest overstory did not experience frost over two similar periods of 5 and 6 days, respectively, during mid-August. Sheltered plants in the forest understory (≈ 10 m NW of the forest edge microsite) experienced thirty-eight consecutive frost-free nights (Fig. 3.4).

Height above the ground had a major impact on plant temperatures due to the strong air temperature profile that developed (Fig. 3.5). Air closer to the ground was substantially cooler on clear, calm nights as temperature inversions developed near the ground. The measured vertical temperature gradient revealed a change in T_{air} of 4 to 6 $^{\circ}\text{C}$ over a short vertical distance through the plant canopy (below 1 m). Results of paired measurements of leaf and flower temperatures of *E. peregrinus* and *P. bistortoides* are shown in Table 3.2. Although analysis of variance of the temperature measurements yielded no significant differences between leaves and flowers between species, flowers were significantly warmer (≈ 2.0 $^{\circ}\text{C}$) than leaves (Table 3.2).

Nocturnal microclimate and leaf temperatures

On most nights, leaf temperature minima occurred during periods of combined low wind speeds and low nighttime sky infrared radiation ($R_{\text{I},\downarrow}$) (Figs. 3.6A, B). In addition, freezing nights were often followed by clear skies the following morning (i.e., Aug. 29, 31, Sept. 3). Although wind speed was variable, low speeds (< 0.75 m s^{-1})

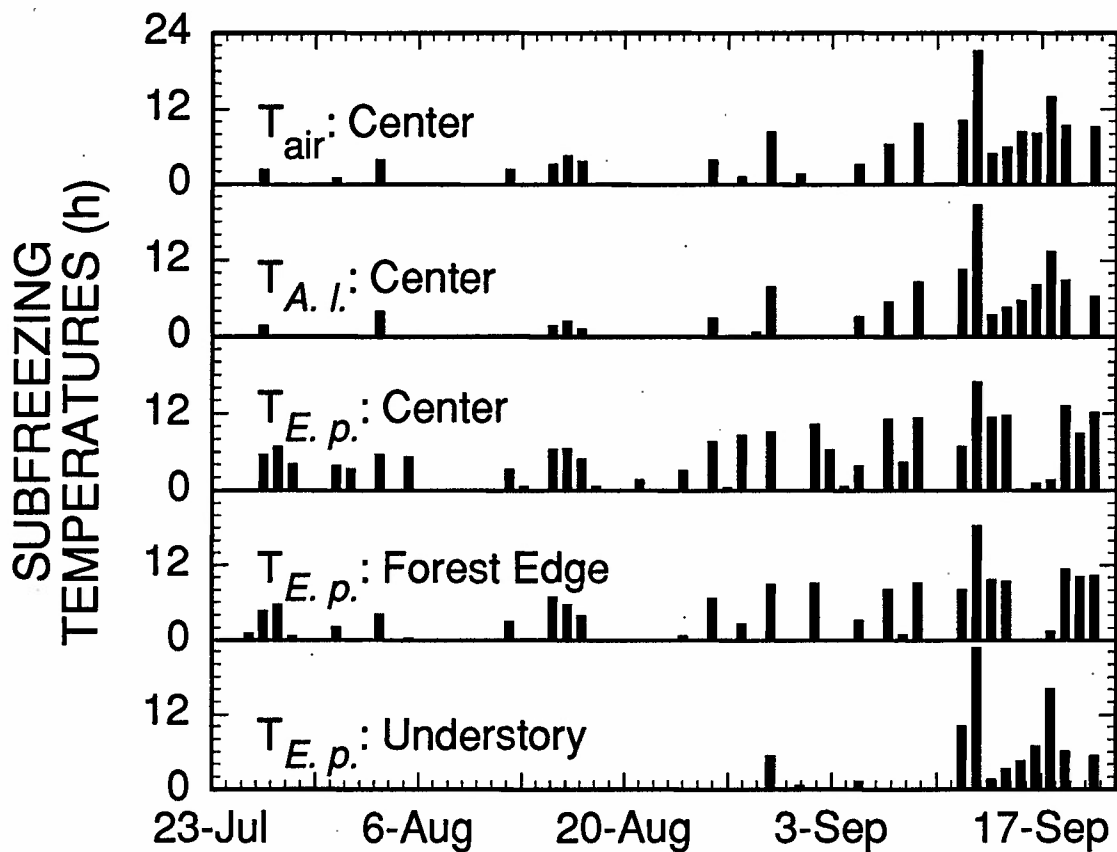


Figure 3.4: Frequency and duration of temperatures below 0 °C for T_{air} (8 cm height), *Abies lasiocarpa* (27 cm height), and *Erigeron peregrinus* (approx. 3 cm height) during 1993. Each column indicates a frost event, and height of columns indicates the duration. The top three graphs represent observations from the clearing center with 96% sky exposure. The lower three graphs represent a gradient of upper hemisphere exposure with 96, 87 and 29% sky exposure, respectively, due to shelter by a spruce-fir forest canopy. Horizontal axis tic marks are positioned at midnight.

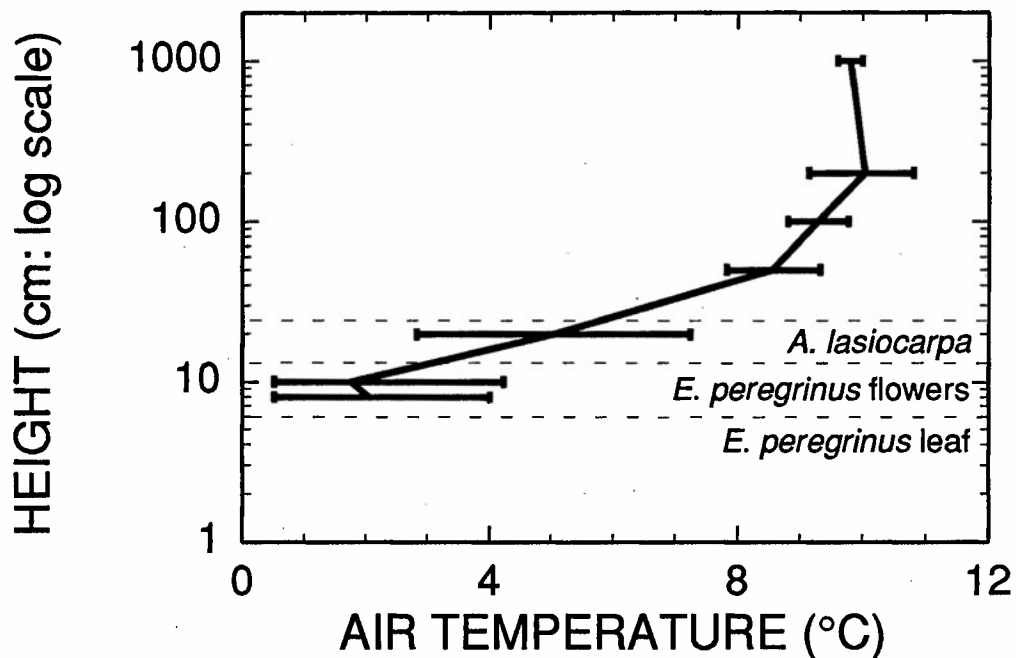


Figure 3.5: Vertical profile of air temperature on the night of Aug. 25, 1993 between 0000 and 0500. The five sampling points between 10 and 200 cm were located on an instrument stand within the clearing. The horizontal bars indicate the range of the temperature observations. The sampling points are connected through the observation means. The 8 cm measurements were recorded as 15 min means from the central air temperature sensor at the study site. The 10 m values were hourly means of 10 s observations provided by a USFS from a weather station 1 km SE of the site. As such, the lowest and highest points on the graph were not taken at exactly the same location or at the same time frequency as the intermediate points, but are included in order to extend the vertical profile, and demonstrate comparability with nearby measurements. The horizontal dashed lines represent the heights of measured *Erigeron peregrinus* leaves and flowers, and the measured *Abies lasiocarpa* needle.

Source	Mean	Variance	t	two-tailed p
Temperature				
<i>P. bistortoides</i>	2.8	6.7	0.05	0.95
<i>E. peregrinus</i>	2.8	6.4		
Flowers	3.8	4.6	4.12	< 0.001
Leaves	1.8	6.4		

Table 3.2: Statistical analysis of leaf (3-7 cm height) and flower temperatures (15-25 cm height) of *Polygonum bistortoides* and *Erigeron peregrinus* during a radiation frost event. The 2-tailed critical t for 94 degrees of freedom at $p=0.05$ is $t_{94,0.05}=1.99$.

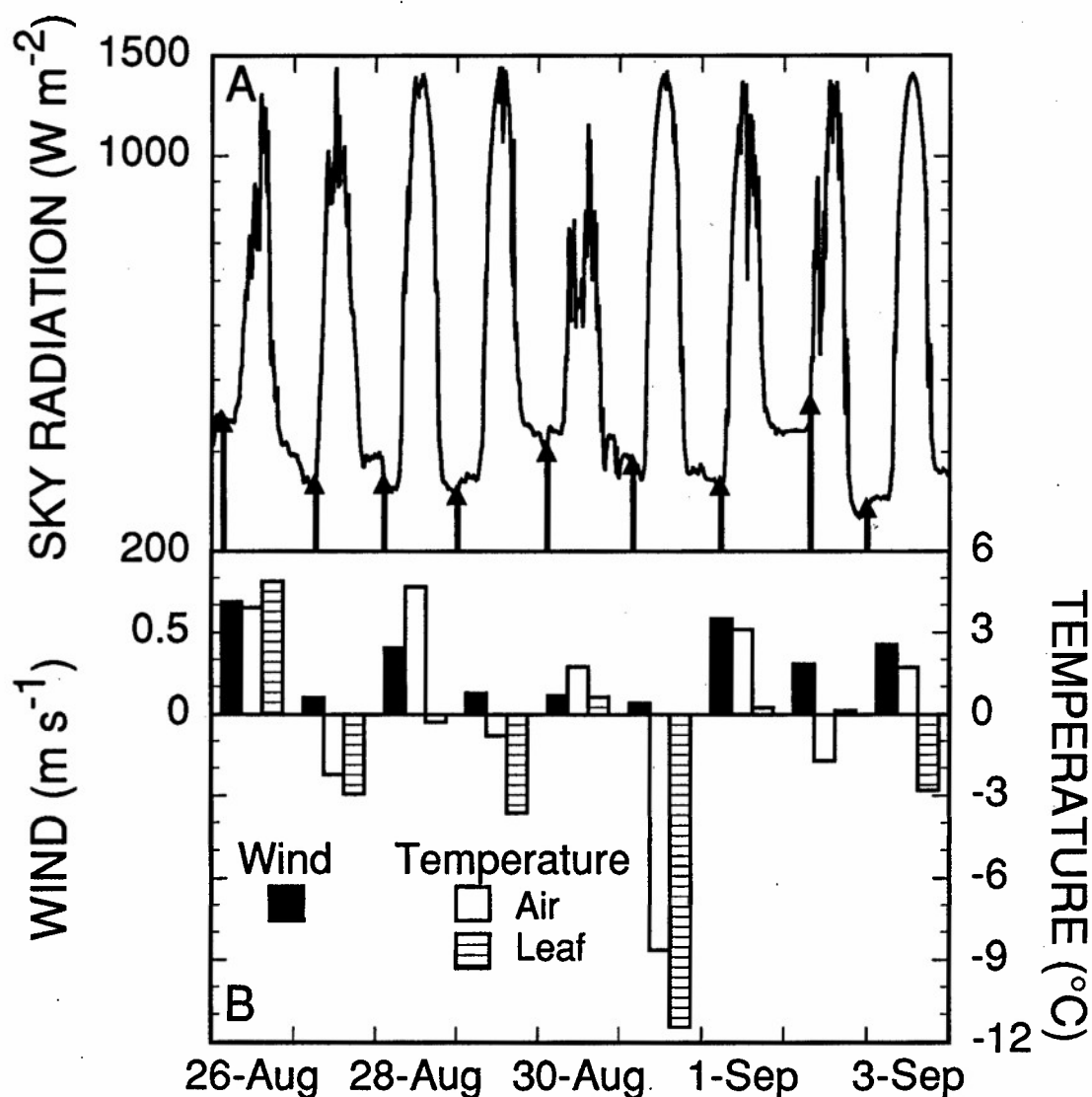


Figure 3.6: A (upper left axis): Sky radiation measurements for a consecutive 9-day period (Aug. 26-Sept. 3, 1993). Vertical bars topped with arrows indicate the time of occurrence and $R_{l,\downarrow}$ measured at the time of nightly *Erigeron peregrinus* temperature minima. B: The T_{air} (open bars) and $E.$ *peregrinus* temperature minima (striped bars) are indicated in the lower graph (right axis). The corresponding wind speed (solid bars) during the nightly leaf temperature minima is indicated on the lower left axis. Horizontal axis tic marks are positioned at midnight.

occurred at the time of leaf temperature minima (Fig. 3.6B). Likewise, while leaf temperatures varied continuously, they typically reached a temperature minima not greatly different from ambient T_{air} . During a representative period, the leaf temperature depression ($\Delta T = T_{\text{air}} - T_{\text{leaf}}$) ranged from -1.8 to 5.0 °C (Fig. 3.6B). Nighttime leaf temperatures above ambient T_{air} occurred when $R_{\text{l},\downarrow}$ was high enough to cause radiative heating (Fig. 3.6B).

On frost nights in the clearing center, there was a strong linear relationship between ΔT and $R_{\text{l},\downarrow}$ (Fig. 3.7). Leaf temperature depressions below T_{air} on frost nights were characterized by the amount of radiative cooling (i.e., $\Delta T \approx 4$ °C, $\Delta T \approx 3$ °C, etc.). Radiational cooling contributed to a substantial number of frost events, with thirty percent of 1993 frost events being directly attributable to, or enhanced by, radiative cooling of 3 °C or more (Fig. 3.7). The remainder of frost events were primarily advective in nature and were attributed to convective heat exchange with below-freezing T_{air} .

Long term air temperature records

To evaluate the normalcy of our 1992-1993 T_{air} data, a comparison was made between our measurements which were taken at plant level (8 cm) and measurements at 10 m on a nearby weather tower where a 5-year dataset was available (Fig. 3.8). The 10 m data were much further removed from radiative and convective heating and cooling effects at ground level. Although the 8 cm measurements had a greater diurnal range, there were consistent and predictable differences between the 8 cm and 10 m measurements, particularly during the day. At night, differences between T_{air} measurements at plant height and the weather tower were substantially greater, with plant-level temperatures cooler by more than 5 °C on clear nights, but there was still a correlation coefficient of 0.91 between the 8 cm and 10 m observations. Thus, the 10 m

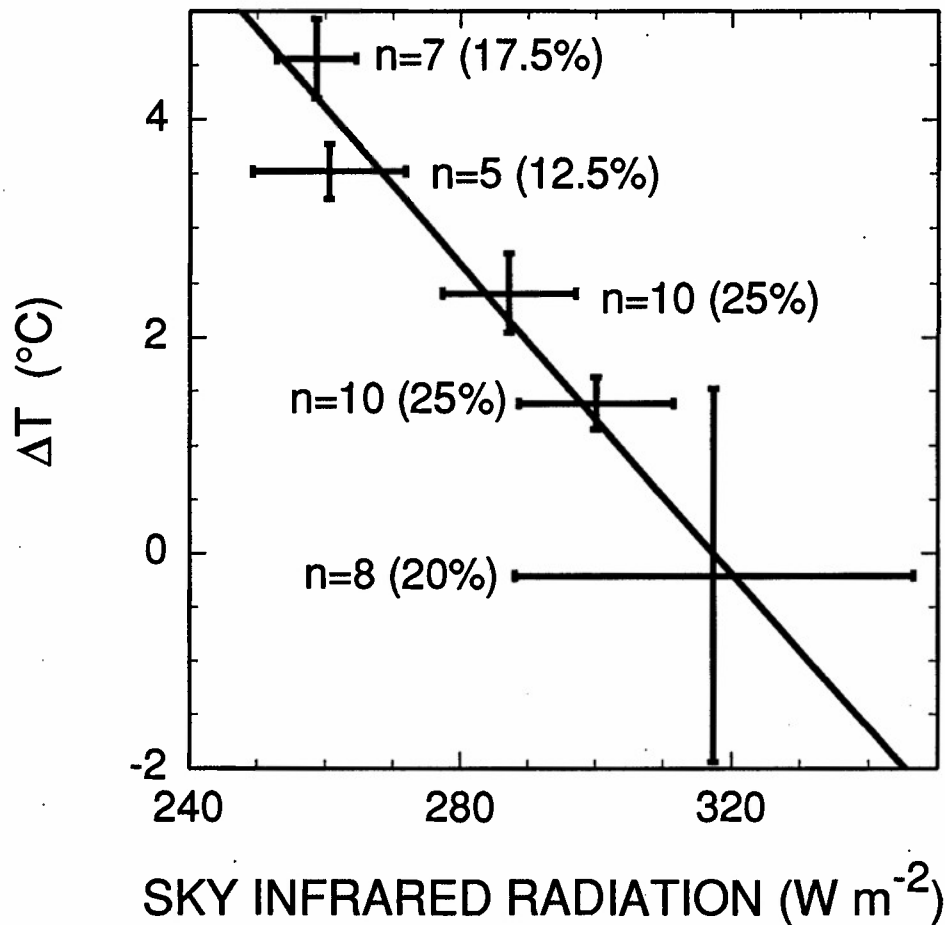


Figure 3.7: Mean $R_{l,\downarrow}$ versus *Erigeron peregrinus* leaf temperature depression ($\Delta T = T_{\text{air}} - T_{\text{leaf}}$) for nights with subfreezing T_{leaf} (1993). The number of nights are indicated along with corresponding percentages of all frost nights (parentheses). Nights with ΔT between 4 and 5 were averaged to produce the upper left-most point, nights with ΔT between 3 and 4 produced the point below, etc. Horizontal error bars represent the coefficient of variation of sky infrared radiation and vertical error bars represent the standard deviations of ΔT values. The equation for the least-squares linear fit was: $\Delta T = -0.072 * R_{l,\downarrow} + 22.7$ ($r^2 = 0.96$).

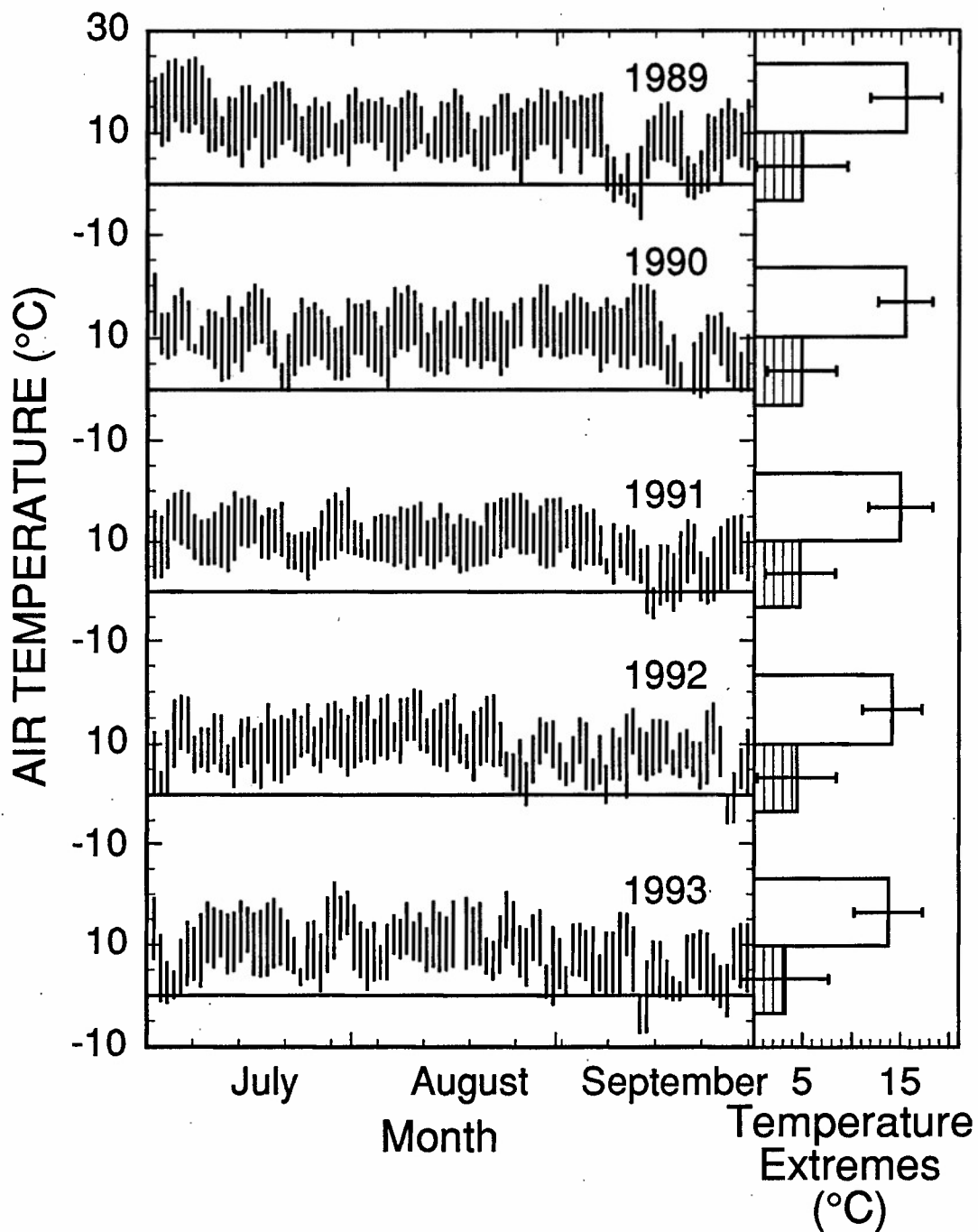


Figure 3.8: Daily growing season T_{air} extremes for 5 years from a U. S. Forest Service 10 m meteorological tower (1989-1993). Horizontal bars to the right of each series indicate seasonal mean T_{air} maxima (open bars) and minima (striped bars). Horizontal error bars indicate \pm one standard deviation.

data set was used to test if the 8 cm data were typical. No significant annual differences were evident in the 1989-1993 data at 10 m (Fig. 3.8).

Discussion

Frequency, duration and intensity of freezing temperatures

It is well known that nighttime air temperatures near the ground often approach minima just before sunrise, after the atmosphere has cooled throughout the night and cold air settling has generated temperature inversions. However, leaves in exposed locations not within topographic depressions can be influenced strongly by radiative cooling and can approach temperature minima at different times than T_{air} . The singular importance of radiative cooling to leaf temperature minima is demonstrated by our observation that greater than 40% of nights during June-Sept. of 1993 had leaf temperature and air temperature minima occurring at different times. Compared to T_{air} minima, T_{leaf} minima were more evenly distributed over time. Some subfreezing leaf temperatures did occur after sunrise, when frozen photosynthetic tissues were also exposed to direct light. It may be noteworthy that radiation frosts occur because of clear skies at night; these nights are also associated with clear skies and high sunlight levels the following morning. This simultaneous occurrence of low tissue temperatures with high incident sunlight has been shown to have a particularly severe effect on photosynthetic properties (Long et al. 1983; Powles et al. 1983; Ögren et al. 1984; Strand and Öquist 1985; Steffen and Palta 1989; see Baker and Bowyer 1994 for review).

The growing season for agricultural crops is often defined in terms of frost-free days, or the number of consecutive days with T_{air} remaining above some threshold value (Suckling 1989). Roughly one-third of the total nights during the summer of 1993 produced leaf frost. Using a "frost-free days" definition of $T_{\text{leaf}} > 0^{\circ}\text{C}$ would have limited the 1993 growing season for some plants to about 5 days. In the high elevation and high latitude environment, this definition may lack precision because the meadow

vegetation close to the ground can experience radiation-driven frost throughout the growth season. Radiational cooling may be particularly important to broadleaf species in exposed habitats. The differences between frost frequencies at the clearing center in *E. peregrinus* and *A. lasiocarpa* were most likely due to a combination of boundary layer factors. Conifer needle temperatures tended to track air temperature more closely and, thus, experienced less frequent radiative frost. The aerodynamic leaf dimension of *E. peregrinus* was an order of magnitude larger, creating a larger leaf boundary layer. Individual measured leaves of *E. peregrinus* were also located closer to the ground within the low wind environment of the air boundary layer next to the soil surface. Shelter by the forest overstory dramatically reduced both the frequency and duration of radiative frost events for both broadleaves and conifers.

During conditions of radiative frost (low wind and $R_{l,\downarrow}$), flowers of both *E. peregrinus* and *P. bistortoides* remained warmer than the leaves. The height of plant parts above the ground may affect temperatures in three ways: vertical profiles in air temperature, wind speed, and radiative cooling. Oke (1970) reported a vertical temperature gradient, with coldest air closest to the ground early in the morning, that he attributed to both radiational cooling and vertical wind profile. We observed similar conditions during radiative frost episodes. Increased radiative cooling of flowers raised on a stalk may be offset by greater convective warming due to increased wind speeds at the greater height. Raupach and Thorn (1981) and Miller et al. (1991) showed a rapid increase in mean horizontal wind speed just above the ground in alpine forest clearings. The combination of warmer T_{air} and a higher wind environment may reduce frost frequency and severity for flowers. This observation may point to an adaptive advantage for flowers being higher above the ground in order to reduce frost frequency, duration and intensity for reproductive structures.

Nocturnal microclimate and leaf temperatures

The timing and severity of frost events appeared to be strongly linked to $R_{l,\downarrow}$. When $R_{l,\downarrow}$ is low ($< 260 \text{ W m}^{-2}$), and wind speeds are below 0.75 m s^{-1} , radiative cooling is predicted to dominate over convective heat exchange, resulting in leaf temperatures well below air temperatures and the potential for freezing episodes (Jordan and Smith 1994). These results are supported by our field observations of T_{leaf} minima coinciding with $R_{l,\downarrow}$ minima on a number of nights. When $R_{l,\downarrow}$ was moderate ($\approx 290 \text{ W m}^{-2}$), ΔT ($T_{\text{air}} - T_{\text{leaf}}$) was small; values of $R_{l,\downarrow}$ greater than 310 W m^{-2} corresponded with negative values of ΔT .

Combinations of low wind and low $R_{l,\downarrow}$ contribute to the development of air temperature inversions (Oke 1970), which enhances the convective cooling of leaves. However, the greatest ΔT corresponded with extremely clear sky conditions, even though these conditions also generate air temperature inversions. Leaf temperature depressions based on air temperatures further removed from surfaces cooled by radiation exchange with the sky (i.e., 2 m weather box), would result in substantially greater calculated temperature depressions. Approximately 30% of frost nights in 1993 were strongly influenced ($\Delta T > 3 \text{ }^{\circ}\text{C}$) by radiative cooling. This provides an initial estimate of the number of frost episodes which might be influenced purely by radiative effects of the clear sky versus the more indirect effects of cold air drainage and settling near the soil surface.

Long-term air temperature records

Air temperature observations from a 10 m tower should be relatively insensitive to changes in $R_{l,\downarrow}$. This is supported by the reduced diurnal range of temperatures from the 10 m sensor compared to plant-height T_{air} measurements. During the day, wind shear and buoyancy-induced vertical mixing maintain good agreement between T_{air} measurements at various heights. However, with the low wind speeds typical at night,

the correlation is poorer, particularly in conjunction with clear, high-elevation night skies. The T_{air} data taken at 10 m suggest that, although 1992 and 1993 were not unusual growing seasons from an air temperature perspective, they may have been a bit cooler than the previous years. To the authors' knowledge, no comparable data sets are available for $R_{\text{l},\downarrow}$, and any trends in this parameter are presently unknown.

Conclusions

Leaves of both broadleaf and conifer species in the subalpine environment experienced frost throughout the growing season. The frequency of frost appears strongly linked to microsite sky exposure (net R_{l} flux), nighttime wind and leaf size, as well as vertical position within T_{air} gradients on calm nights. Because of the influence of radiative cooling, T_{leaf} minima are more closely linked to atmospheric $R_{\text{l},\downarrow}$ than ambient T_{air} minima. Increases in $R_{\text{l},\downarrow}$ due to the direct effects of atmospheric warming, or indirectly via increased cloud cover would have a strong impact on frost frequency, duration and intensity. Arguably, these impacts could be greater than those attributable to changes in air temperature. The availability of a longer-term $R_{\text{l},\downarrow}$ dataset could have important implications for understanding the interaction of climate and microclimate and the effects on growth season length.

Chapter 4: Simulated influence of leaf geometry on sunlight interception and photosynthesis in conifer needles

Introduction

At the level of the individual leaf, a thin laminar leaf oriented perpendicular to the sun's direct beam will intercept sunlight at maximum efficiency per unit leaf volume or mass. This efficiency would be expected to decline if the leaf thickens, unless photosynthesis per unit leaf surface area increases. Sequential losses in efficiency would also be expected at the shoot, branch, crown, and canopy levels of structural organization because of the addition of non-photosynthetic supportive tissues and an increase in shading (Oker-Blom 1986; Oker-Blom and Kellomaki 1983). Losses in efficiency at each of these structural levels must be quantified before a comprehensive understanding of the adaptive significance of whole-plant architecture will be possible. A logical place to begin an evaluation of this leaf-to-crown hierarchy is at the individual leaf level. There are no studies that have systematically investigated the efficiency of sunlight interception for non-laminar leaf shapes such as those found commonly in coniferous species and species with stem photosynthesis, except for some studies on cacti (Geller and Nobel 1984). A few studies have alluded to the potential importance of individual leaf geometry to the efficiency of sunlight interception in conifer tree species (Leverenz and Jarvis 1980; Carter and Smith 1985; Wang and Jarvis 1990).

The purpose of this study was to evaluate quantitatively the influence of leaf geometry in conifer tree species on the efficiency of sunlight interception per leaf. Comparisons of efficiency were based on simulated differences in sunlight interception and corresponding estimates of photosynthetic carbon gain. Here I report on a quantitative evaluation of the singular effect of leaf geometry on light interception and predicted photosynthesis of an individual leaf.

Methods and materials

The general methodology employed in this study began with a selection of representative leaf types in conifer tree species based on their cross-sectional shapes (Fig. 4.1). The five conifer species selected were: *Abies nordmanniana* (Spach), *Picea asperata* (Master), *Pinus cembra* (L.), *P. monophylla* (Torr & Fre'm.), and *P. sylvestris* (L.). The five leaf cross-sectional views of the conifer species selected for the simulations were considered representative of the broad range of cross-sections within conifer tree species and were taken from van Gelderen and van Hoey Smith (1986). A 300 μm thick leaf section representing 1 mm^2 of a broadleaf was included for comparison with the needle leaves of the conifers (Figure 4.1, Table 4.1). A computer program was developed to calculate incident sunlight at any location along the circumference of the cross-section of a leaf based on incident light direction and full-sun irradiance. Leaf surfaces were mathematically described by high order (4-10) polynomial functions. Photosynthetic carbon gain was computed from an idealized photosynthetic response to sunlight. Leaf absorptance to sunlight was considered to be unity. Simulations of light interception and carbon gain were performed at 10° increments in the angle of incidence ranging from directly overhead (90°) to horizontal (0°). Detailed simulations were performed in which the percent of the leaf surface receiving a specific light irradiance was computed for four solar positions: 10°, 30°, 60°, and 90° above the horizon. All leaves were considered to be oriented horizontally along the north-south azimuth. The rotational position of each leaf about its center axis is shown schematically in Figure 4.1. The upper and lower surfaces of the flat leaf section were modelled as if exposed. The edges depicted in Figures 4.1 and 4.4 were assumed to be shaded by adjoining leaf sections and, therefore, were not factored into leaf area calculations for the laminar leaf.

A photosynthetic response to sunlight level was used to estimate photosynthetic carbon gain in all simulations (Fig. 4.2). This curve is an idealized response curve

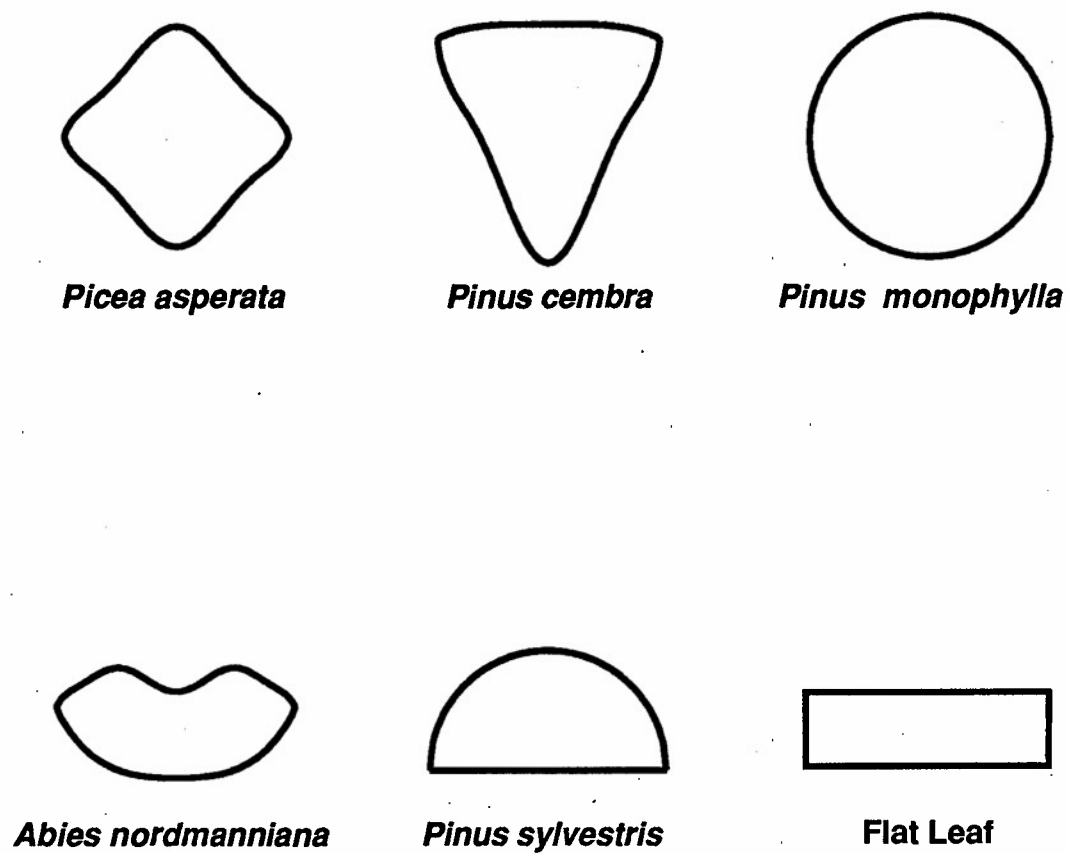


Figure 4.1: Cross sections of modelled leaves used in computing light interception and photosynthetic CO₂ assimilation.

Leaf	Surface Area/Volume (mm ⁻² /mm ⁻³)	Mean PFD (μmol m ⁻² s ⁻¹)	CO ₂ uptake per unit Area/Volume (μmol CO ₂ m ⁻² s ⁻¹ / mmol CO ₂ m ⁻³ s ⁻¹)
<i>Pinus monophylla</i>	3.14/0.79=4.0	566	9.9/39.7
<i>Pinus sylvestris</i>	2.57/0.39=6.6	565	9.4/61.7
<i>Pinus cembra</i>	3.07/0.56=5.5	567	10.4/56.4
<i>Abies nordmanniana</i>	2.39/0.34=7.0	552	9.5/67.9
<i>Picea asperata</i>	2.70/0.50=5.4	572	10.0/54.3
Flat Leaf Section	2.00/0.30=6.7	560	9.5/63.5

Table 4.1: The surface area and volume and surface:volume ratio for a unit length of simulated leaf, along with the corresponding mean photosynthetic photon flux density (PFD) and estimated integrated photosynthetic carbon gain expressed on a surface and volume basis.

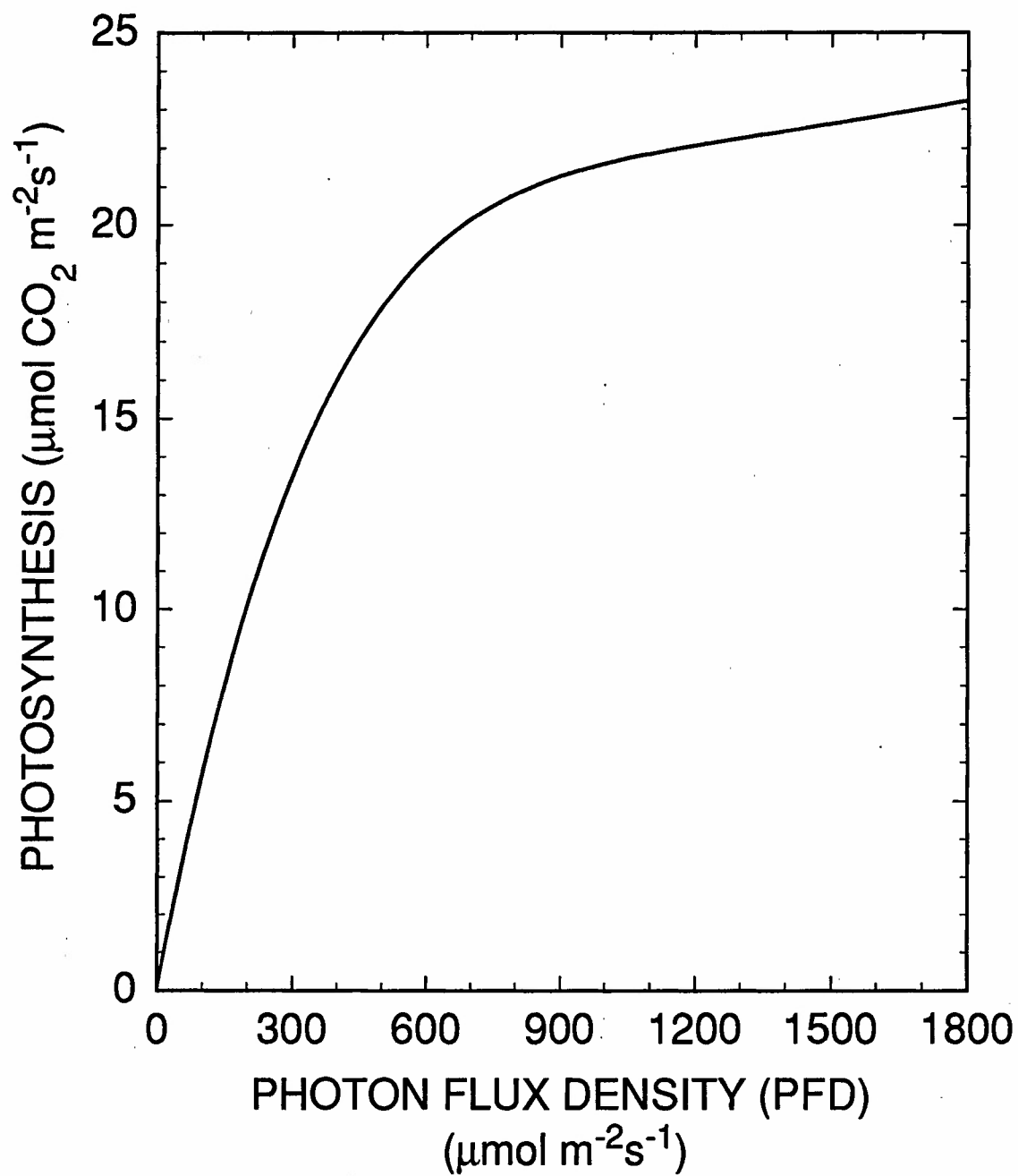


Figure 4.2: Idealized photosynthetic response to light of conifer leaves that was used to estimate carbon gain based on intercepted light

generated for western conifer tree species from data presented in Lassoie et al. (1985) and Smith (1985). The same response curve was assumed for all leaves to permit comparisons due only to leaf geometry effects on light interception and not differences in a species' photosynthetic physiology. A discussion of the limitations of this approach is provided in the Discussion. All computations of intercepted light and resulting carbon uptake were expressed on a unit area and volume basis using the leaf cross-sectional circumference and unit length of each species (Table 4.1). The incident light at each location along the leaf circumference was calculated as the cosine of the angle of incidence (Lambert's Cosine Law). Total and mean incident light and corresponding CO₂ uptake were determined by integrating over the entire leaf cross-sectional circumference. An example of how incident sunlight and CO₂ uptake were computed over the surface of a leaf cross-section of *A. nordmanniana* is illustrated in Figure 4.3. In all simulations, the portion of a leaf not intercepting direct sunlight would, realistically, be receiving diffuse irradiance from the surroundings. Moreover, this diffuse light could result in photosynthetic carbon gain which was not incorporated in these simulations. The possibility of mutual shading among adjacent needles on a shoot also was not considered here, only carbon gain from intercepted direct light was computed.

Results

Light interception

The total percent of leaf surface area receiving direct sunlight (photosynthetic photon flux density, PFD) did not deviate from 50% for the circular cross-section represented by *P. monophylla* or for the laminar leaf section (Fig. 4.4). In contrast, the amount of sunlit area varied from a low of near 35% in *P. sylvestris* to a high of 63% in *P. cembra*. There was a greater diversity of irradiances across the leaf surface for all of the conifer species represented in Figure 4.4 than for the laminar leaf section. Somewhat less than half of the sunlit area of the more circular cross-sections (*P. monophylla* and *P.*

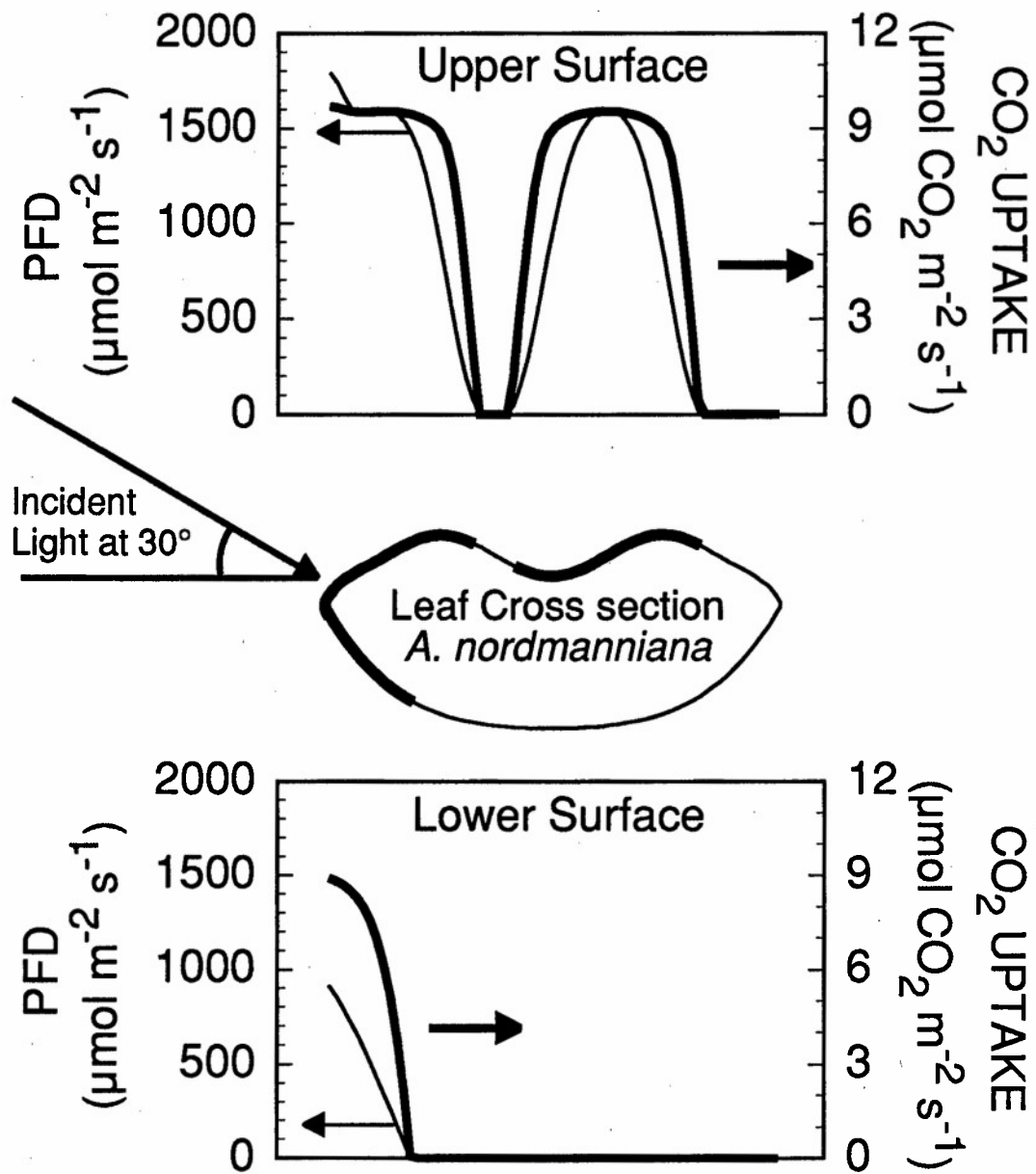


Figure 4.3: Graphical representation of the computation of light interception and CO₂ uptake on an *Abies nordmanniana* needle with incident light at 30°.

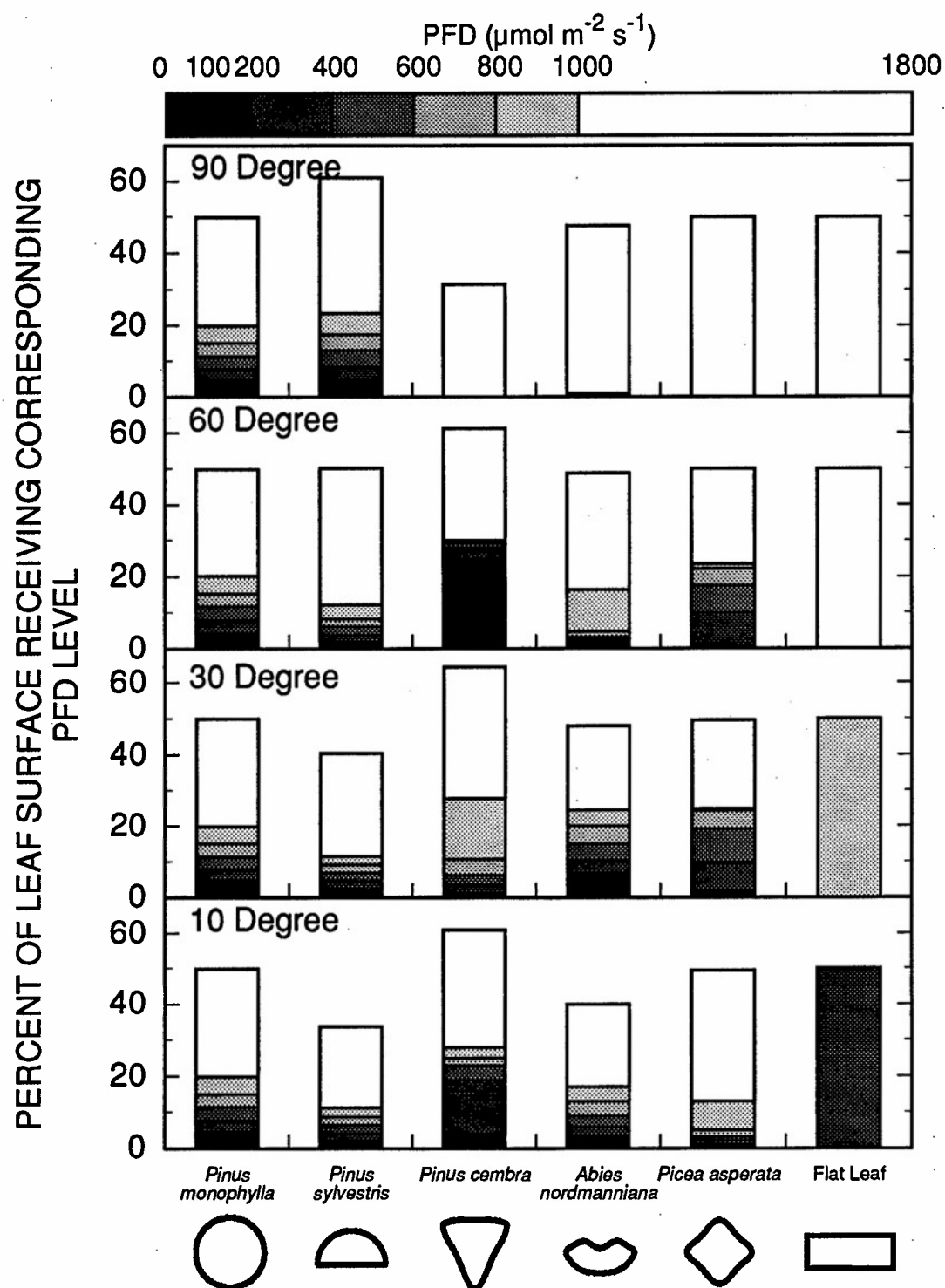


Figure 4.4: Distribution of PFD ($\mu\text{mol m}^{-2} \text{s}^{-1}$) on modelled leaves at selected angles of incident light.

sylvestris) was divided into relatively equal portions of the lower PFD. At solar elevations of less than 30°, all conifer species had at least 30% of the total leaf surface area intercepting PFDs of at least 1000 $\mu\text{mol m}^{-2} \text{s}^{-1}$. However, no portion of the laminar leaf section received more than 1000 $\mu\text{mol m}^{-2} \text{s}^{-1}$ at these low angles of incidence (Fig. 4.4). *Pinus cembra* was the only species that had an increase in the total proportion of sunlit surface area at lower solar elevations compared with 90° incident light.

The mean incident PFD over the leaf varied substantially among the species according to incident light angle (Fig. 4.5). For all of the conifer species, mean incident PFD remained above 300 $\mu\text{mol m}^{-2} \text{s}^{-1}$ at all incident light angles. In contrast, incident PFD simulated for the laminar leaf varied from 0 to 900 $\mu\text{mol m}^{-2} \text{s}^{-1}$ (Fig. 4.2). The thicker cross-sectional shapes (lower surface:volume ratios, Table 4.1) resulted in the most consistent values of mean incident PFD across all light angles, i.e., *P. monophylla*, *P. cembra*, and *Picea asperata* (Fig. 4.5). No angular-dependent change was predicted for the circular cross-section of *P. monophylla*.

Simulated carbon gain

Photosynthetic carbon gain expressed per unit leaf surface area varied from 6.0 to 13.5 $\mu\text{mol m}^{-2} \text{s}^{-1}$ among the simulated species depending on incident light angle (Fig. 4.6). Both *P. sylvestris* and *A. nordmanniana* had relatively linear increases in carbon gain with increasing angle of incidence compared to a strong curvilinear increase for the simulated laminar leaf. In contrast, *P. cembra* and *Picea asperata* had less consistent changes in predicted carbon gain that resulted in maxima and minima at intermediate angles of incidence (Fig. 4.6). Mean incident PFD on the *Picea asperata* needle varied from a low of near 490 $\mu\text{mol m}^{-2} \text{s}^{-1}$ to a high of about 660 $\mu\text{mol m}^{-2} \text{s}^{-1}$ with a corresponding change in photosynthesis per unit area from about 65 to 95% of the maximum for the laminar leaf section oriented perpendicular to incident sunlight. *Pinus cembra* exhibited a range in simulated photosynthesis per unit area between 60 and 115% of the maximum for such a

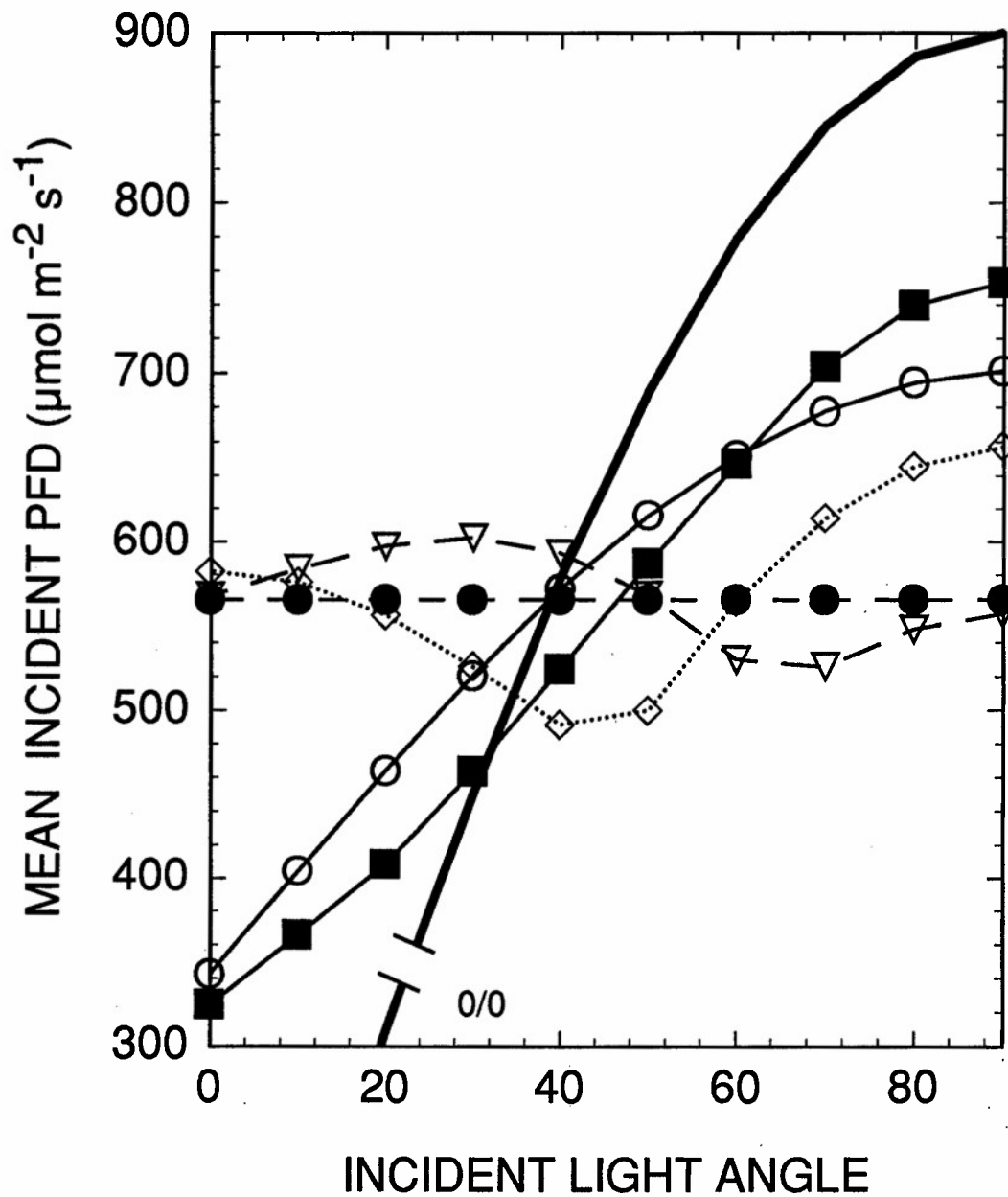


Figure 4.5: Calculated mean PFD intercepted per unit surface area as a function of incident light angle and leaf shape (●: *Pinus monophylla*; ○: *Pinus sylvestris*; ▽: *Pinus cembra*; ■: *Abies nordmanniana*; ◇: *Picea asperata*; —: Flat leaf section).

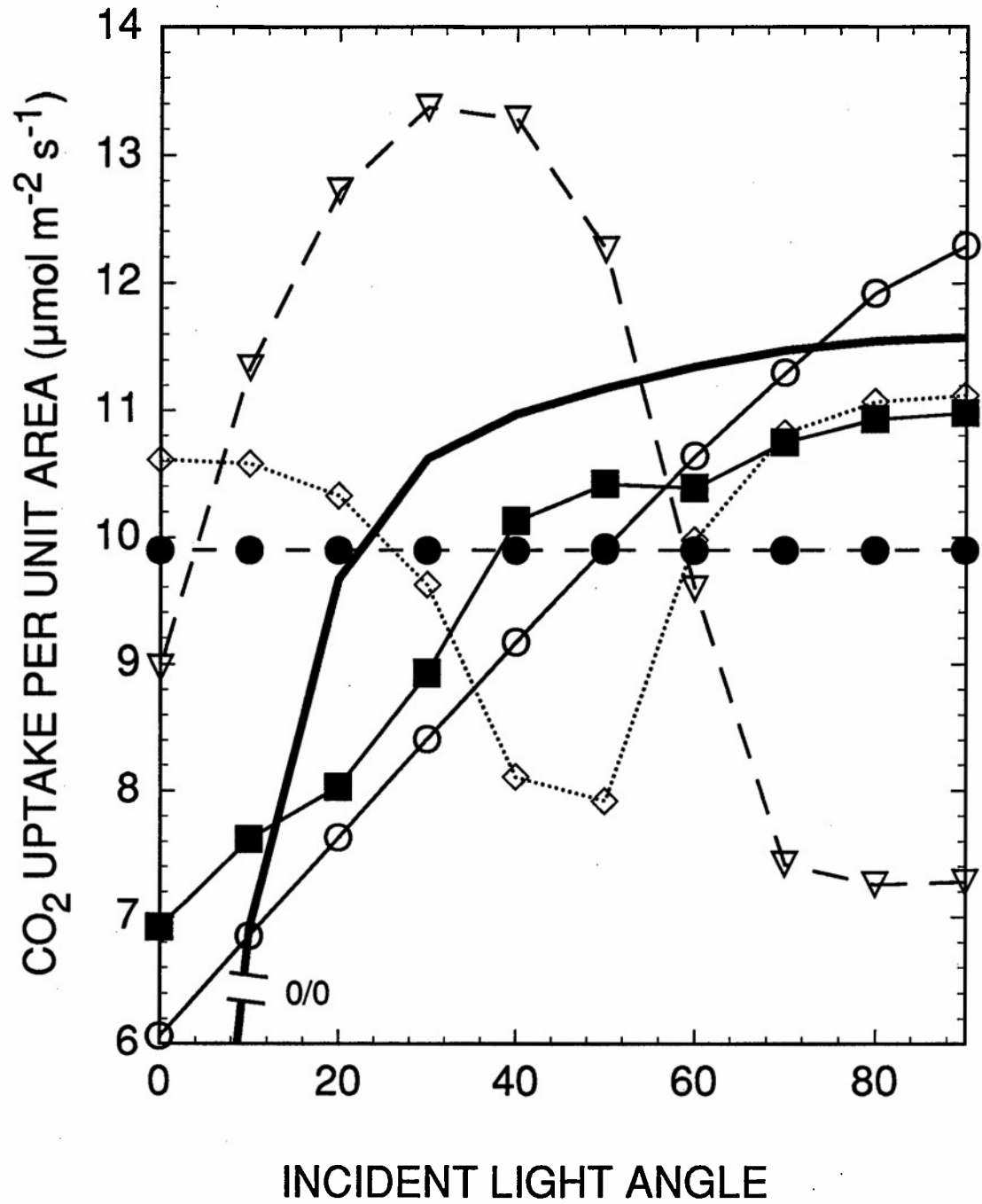


Figure 4.6: Calculated mean CO₂ uptake per unit surface area as a function of incident light angle and leaf shape (Symbols are consistent with Figure 4.5).

surface. All species except *P. cembra* had maximum photosynthesis at incident light angles of greater than 70°. Although all species had carbon gain greater than the simulated laminar leaf at angles less than about 10°, only *P. sylvestris* and *P. cembra* had maximum carbon gain per unit area of incident light that was greater than the maximum predicted for the laminar leaf (Fig. 4.6).

The amount of carbon gain expressed per unit volume varied in a manner similar to the values computed on an area basis, except that all species had significantly lower values compared to the simulated laminar leaf (Fig. 4.7). All species had estimated carbon gain per unit volume greater than the laminar leaf only at very low angles of incidence (<10°). Also, *P. monophylla*, the least flattened cross-section, had the lowest estimated carbon gain per unit volume at all angles of incidence.

Integration of PFD and carbon gain values across the leaf surface showed a certain consistency among the species (Table 4.1). Very little difference between species occurred in the amount of total integrated PFD intercepted (552 to 571 $\mu\text{mol m}^{-2} \text{s}^{-1}$). Only an 11% difference occurred between the minimum and maximum values of estimated carbon gain per unit area (9.4 versus 10.4 $\mu\text{mol m}^{-2} \text{s}^{-1}$) among the species. A much greater difference between species occurred in the integrated amount of carbon gained per unit volume. *Abies nordmanniana* had the maximum estimated carbon gain (67.9 $\text{mmol m}^{-3} \text{s}^{-1}$) compared to the minimum value that occurred (*P. monophylla*, 39.7 $\text{mmol m}^{-3} \text{s}^{-1}$), a difference of 42% (Table 4.1).

Discussion

There is little information about the influence of leaf cross-sectional shape on the interception of direct sunlight. However, it is intuitive that as a leaf thickens and becomes more cylindrical, incident sunlight is spread over a greater surface area regardless of incident light angle. In addition, a thick leaf will become more efficient at intercepting light from sources more tangential to its upper surface (lateral incident light) than a thin leaf,

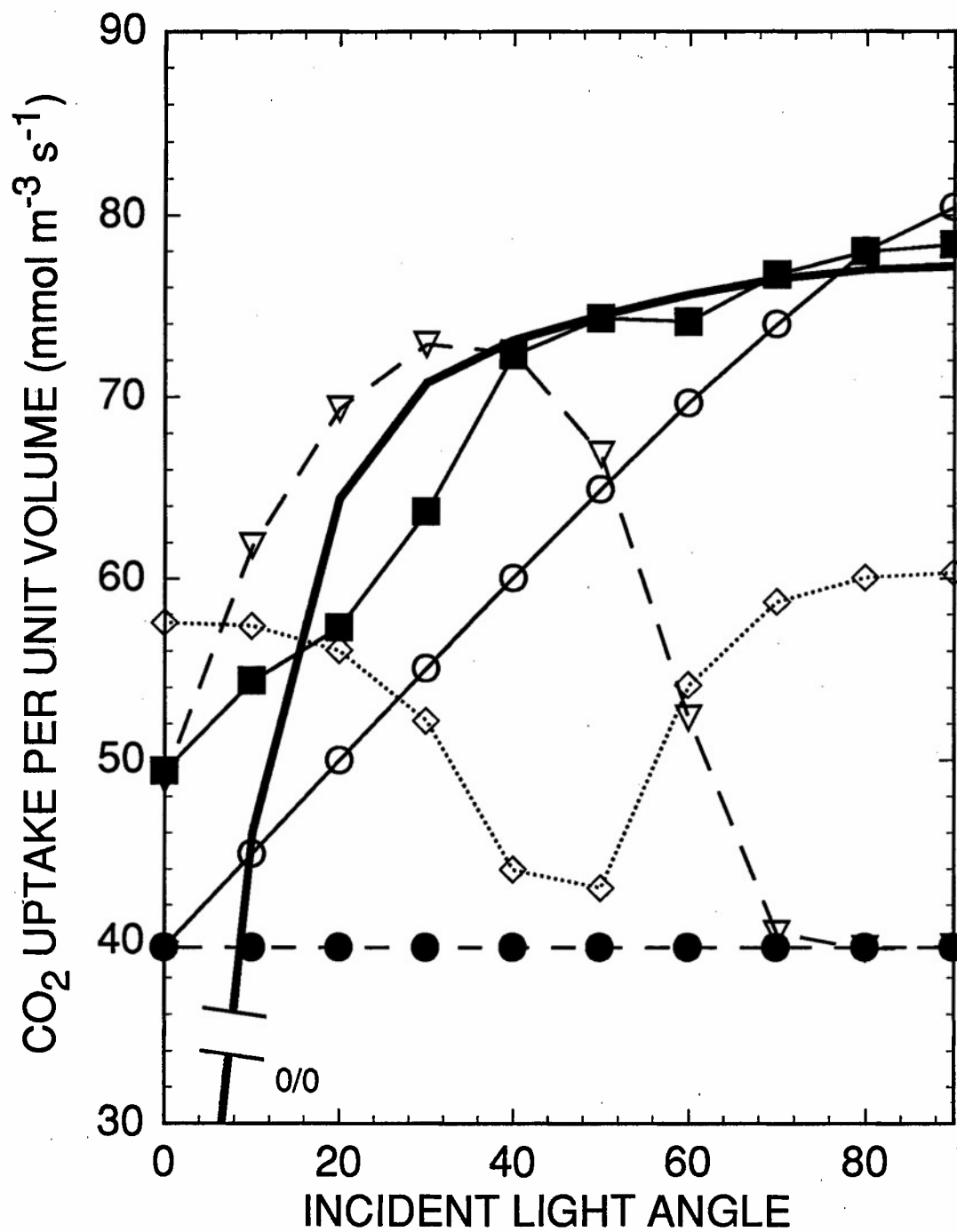


Figure 4.7: Calculated mean CO₂ uptake per unit volume as a function of incident light angle and leaf shape (Symbols are consistent with Figure 4.5).

although the lateral direction becomes less defined as the leaf thickens and approaches a cylindrical cross-section. The photosynthetic stems of many species and the needle-like structure of conifer leaves represent a widespread example of this structural category. The most obvious effect of a more curved leaf surface is that incident sunlight is diminished per unit leaf area so that a cylindrical leaf with its axis perpendicular to the direct beam will not receive full sunlight over all of its surface area. Compared to a laminar leaf, a much more variable PFD will exist over the leaf surface. However, mean incident light across a cylindrical leaf can still be regulated by orienting the leaf axis away from the perpendicular, although not by rotation about the axis (as is the case for a laminar leaf). Also, some cross-sectional shapes (e.g., *P. sylvestris* and *P. cembra* in Fig. 4.4) can result in greater than 50% of the total leaf surface area being sunlit at certain incident light angles, in contrast to a laminar leaf that receives homogeneous PFD on the exposed surface. It is also noteworthy that portions of individual conifer leaves simulated here were above, whereas others were below light saturation of photosynthesis, regardless of the incident light angle (Fig. 4.4).

In general, the conifer leaves were more efficient at intercepting sunlight and photosynthesizing at low angles of incidence than a laminar leaf, but less so at higher angles of incidence (Figs. 4.5, 4.6). This was especially true when photosynthesis was expressed on a unit volume basis. However, two of the species with thin cross-sections (*P. sylvestris* and *A. nordmanniana*) had maximum rates that were similar to the maximum values predicted for the laminar leaf (Fig. 4.7). It may also be significant that the integrated amount of incident sunlight and CO₂ uptake per unit leaf area varied little among the species compared to the variation in CO₂ uptake per unit leaf volume (Table 4.1). Expressing light interception efficiency according to the amount of CO₂ uptake generated per unit volume (or mass) is probably the most meaningful measure of this efficiency, because this volume represents living tissue that must be supported metabolically.

Although there are recent reports of intra- and inter-specific differences in leaf arrangements along shoots in conifers (Carter and Smith 1985; Leverenz and Hinckley 1990; Smith et al. 1991), there is little information about the possible variation in the cross-sectional shapes of individual needles. Leverenz and Jarvis (1980) reported that the sun needles of Sitka spruce *Picea sitchensis* (Bong.) Carr. were more flattened than shade needles of the same tree. However, this is in direct contrast with observations of numerous broadleaf species as well as my measurements on *Abies lasiocarpa*. In this species, sun leaves sampled randomly from three trees averaged $0.86 \text{ mm} \pm 0.12$ (s.d.) in maximum thickness, whereas shade leaves also sampled randomly from three trees averaged $0.50 \text{ mm} \pm 0.12$ (s.d., $n=40$, $F_{1,38} = 85.6$, $p < 0.0001$). The ratio of needle height to width was also significantly greater for sun-exposed leaves ($F_{1,38} = 78.6$, $p < 0.0001$). However, no significant ($p < 0.05$) differences attributable to sun exposure were observed in similar observations of the needle dimensions of *Picea pungens* Engelm. The advantage for broadleaf species of having thick leaves may be an increase in internal CO_2 absorption within the mesophyll because of a greater mesophyll cell surface area per unit leaf surface area (Nobel 1991). If photosynthesis is greater for thicker needles because of increased rates of CO_2 absorption per unit surface area, then an increase in light interception efficiency will modify the values simulated here, which were based on an identical photosynthetic response to light. Of course, individual species may also be expected to have different light response curves based on other physiological differences, a likelihood that was also not included in the present study.

Using an idealized photosynthetic response to light is not a wholly palatable approach for estimating carbon fixation on an individual leaf level. However, light response curves do not appear to exist for individual conifer needles of any species, much less for subsections of them. Leverenz and Jarvis (1979) found significant differences in the photosynthetic responses of *Picea sitchensis* needles illuminated on the adaxial surface,

abaxial surface, and on both surfaces. The shoot light response curves that exist for conifers may be confounded by self-shading or scattering by neighboring needles due to branch architecture (Jarvis and Leverenz 1983; Carter and Smith 1985), and by varying irradiances across the leaf due to the convoluted or curved surfaces. A single photosynthetic response function was selected in order to focus on differences caused by leaf geometry without the confounding effects of different photosynthetic physiologies. Leverenz and Jarvis (1980) examined effects of shoot architecture on Sitka spruce photosynthesis and found that needle orientation on the branch produced substantial effects on shoot photosynthesis. Shade shoots were also found to have needle arrangements that resulted in less self-shading of light incident from directly above.

Although total incident PFD (Table 4.1) integrated over all solar angles was similar among the species, differences in intercepted PFD and estimated carbon gain according to solar angle could reflect preferential periods for carbon gain over a day or season, or a latitudinal preference based on the potential for carbon gain. For example, *P. sylvestris* and *A. nordmanniana* had maximum PFD interception and predicted carbon gain at high solar angles characteristic of midday values and lower latitudes. In contrast, *P. cembra* had maximum values at low solar angles that are characteristic of early morning, late afternoon, and higher latitudes. Considering that greater leaf temperatures usually correspond to higher solar angles, avoiding a high incident PFD at higher solar angles could result in a reduction in transpirational water loss. Then again, if water is not limiting but cold temperatures are, it could be an advantage to maximize PFD interception at higher incident light angles (Smith and Carter 1988).

A major limitation to any interpretation of the adaptive significance of leaf geometry is the lack of information regarding the orientation of individual leaves from the horizontal, as well as their rotational orientation about the leaf axis and along the shoot. Recent studies have begun to evaluate the importance of these orientational effects and mutual shading

among leaves to the light interception capabilities of individual conifer shoots (Carter and Smith 1985, Smith et al. 1991). Comparisons of the silhouette (cast shadow) area to total leaf area (silhouette-to-total area ratio, STAR) showed that significant differences existed between species, within a species, and on the same tree. STAR values varied from near 0.10 for sun shoots with over 25 needles per centimeter of stem length to almost 0.40 for shade shoots that had less than 12 needles per centimeter (Carter and Smith 1985).

For the cross-sections in Figure 4.1, STAR values were constant at 0.32 in *P. monophylla* and ranged from 0.26 to 0.35 (*Picea asperata*), 0.31 to 0.35 (*P. cembra*), 0.19 to 0.42 (*A. nordmanniana*), and 0.19 to 0.39 (*P. sylvestris*) depending on the angle of irradiance. Thus, much of the variation in STAR reported in Carter and Smith (1985) could be due to cross-sectional differences in leaf geometry, except for the minimum of near 0.20 reported for sun shoots with the greatest number of needles per unit stem length. These lower minima for shoots could only result from orientational and/or mutual shading effects.

In conclusion, significant differences in conifer needle geometry could generate similar differences in direct sunlight interception and carbon gain at the leaf level, especially when carbon gain is expressed on a volume basis. In general, thick needle-like leaves are more efficient than thin, laminar leaves at capturing light at lower solar angles, but the incident light is highly variable across the leaf surface. Also, adding thickness generally reduces light interception and carbon gain efficiencies expressed on a tissue volume basis. More information is needed about orientational and rotational configurations of individual leaves and within crowns before any interpretations regarding functional or adaptive significance may be drawn.

Chapter 5: Changes in chlorophyll fluorescence and photosynthetic gas exchange following summertime frost in the field and laboratory

Introduction

Chlorophyll fluorescence has become an important tool for investigations evaluating the effect of chilling or freezing stress on green plants (Krause and Weis 1991). A vast majority of chilling stress studies have focused on crop plants of tropical or subtropical origin (Öquist and Wass 1988; Peeler and Naylor 1988; Hetherington et al. 1989; Larcher and Neuner 1989; Somersalo and Krause 1989, 1990a, b; Burke 1990; Greer 1990; Walker et al. 1990; Ferguson and Burke 1991; Greer et al. 1991; Brüggemann et al. 1992a, b; Feierabend et al. 1992; Greer and Laing 1992; Huner et al. 1992; Burke and Oliver 1993; Lurie et al. 1994), but few have examined the conifer tree *Pinus sylvestris* (Öquist and Wass 1988; Strand and Öquist 1985, 1988; Sundblad et al. 1990). Several others have examined native plants including herbs, shrubs, mosses, and aquatics (Ögren and Öquist 1984; Yakir et al. 1986; Demmig et al. 1987; Schulteis and Santarius 1989; Oberhuber and Bauer 1991; Rütten and Santarius 1992). While some studies have involved evergreen plants which experience frost during the winter, none have examined the effects on species that may be adapted to the frequent occurrence of growing season frosts (e.g., subalpine/alpine species). There are some data that have recently been reported for crustose lichens in the Antarctic (Schroeter et al. 1992).

The use of room temperature chlorophyll fluorescence enables examination of photosystem II (PSII) with an endogenous probe that does not physically disturb leaves (Papageorgiou 1975; Krause and Weis 1991). Certain fluorescence parameters such as photochemical quenching have been shown to be strongly correlated with O₂ evolution, a measure of photosynthetic potential (Schreiber et al. 1988). Although there were numerous investigations on reduced rates of CO₂ uptake following chilling or freezing

exposures (Pharis et al 1970; Long et al. 1983; Ögren et al. 1984; Bauer et al. 1985; DeLucia 1987; DeLucia and Smith 1987; Steffen and Palta 1989), very few have considered natural field conditions and the influence of light exposure the following morning.

In the current study, we addressed the issue of plant physiological responses to freezing from two perspectives. In the field, we measured naturally frozen leaves over time as they recovered from a frost event. A pulse amplitude modulated (PAM) fluorometer, infrared gas analyzer (IRGA) and pressure bomb were used concurrently in the hours following a growing season frost on native subalpine vegetation. In the more controlled conditions of a growth chamber, potted plants of both a native subalpine perennial and domestic tomato were grown and subjected to freezing stress. The responses of photosynthetic parameters to the freezing were analyzed. The two species were selected because of hypothesized differences in freezing tolerance and physiological responses to freezing.

Methods and materials

Many previous studies reported fluorescence parameters as dark-adapted after periods in darkness of between 20 min and 2 h (Strand and Öquist 1989; Genty et al. 1989, 1990; Schulteis and Santarius 1989; Greer 1990; van Wijk and van Hasselt 1990; Greer et al. 1991; Oberhuber and Bauer 1991; Bauer et al. 1992; Maciejewska and Bauer 1992; Rütten and Santarius 1992; Bauer et al. 1994; Lurie et al. 1994). Havaux et al. (1991) indicated that inactive PSII centers ("capable of active water oxidation but ineffective in electron flow to plastoquinone") alter the base fluorescence, and suggest that a more appropriate initial fluorescence can be obtained with low light in order to close these reaction centers. In the context of photoinhibitory damage, where an interaction between leaf temperature, light and time is indicated, light-adapted parameters should provide measurements less subject to difficulties of interpretation caused by leaf

warming in darkness and recovery of the photosystem during the dark-adaption period. Light-adapted fluorescence parameters (no dark-adaption, or dark adaption < 10 min) have also been reported (Demmig et al. 1987; Hetherington et al. 1989; Somersalo and Krause 1989, 1990a; Le Gouallec et al. 1991; Scheuermann et al. 1991; Schroeter et al. 1992; Ting and Owens 1992). For obvious reasons in the field study, and for comparison and practicality purposes in the lab, our fluorescence measurements were light-adapted, with < 5 min interval between full illumination and measurement of initial fluorescence.

Arnica cordifolia Hook. and *Rumex densiflorus* Osterh. were selected for study because they are native high-elevation broadleaf species found in forest clearings. *Arnica cordifolia* also grows in forest understory environments, and therefore experiences varying frequencies and intensities of both sunlight and frost during the growing season (Jordan and Smith, in review). Leaves experiencing frost during the growing season are not able to protect photosynthetic tissues via hardening as conifers do during the winter months (Strand and Öquist 1988; Sundblad et al. 1990). As such, it is possible that in subalpine native flora, different mechanisms exist for protecting active photosynthetic tissues from cold stress than those observed in less frost-prone environments. Tomato (*Lycopersicon esculentum* Mill.) is considered a freezing-sensitive species which has already been investigated in some capacities (Smillie and Nott 1979; Martin et al. 1981; Yakir et al. 1986; Sassenrath and Ort 1990; Walker et al. 1990; Brüggemann et al. 1992a, b), and was included in our study to contrast its response to that of *A. cordifolia*.

Mature plants of *A. cordifolia* and *L. esculentum*, bearing flower buds or flowers, were chilled or frozen in darkness just prior to dawn in order to avoid a simultaneous combination of high light and frozen tissues. The simultaneous combination of freezing stress and high light has been found to be highly photoinhibitory, but is relatively uncommon during the growing season compared with freezing stress followed by high light intensity.

Growth chamber experiment

Root systems of *A. cordifolia* were obtained in September from a clonal patch under a *Pinus contorta* Dougl. ex Loud. canopy. Dormant roots were placed in 15 cm diameter pots in a mixture of vermiculite, peat and sand, and with the apical bud at soil surface level. The pots were stored outside in Laramie, WY, USA until January, when the pots were moved to a greenhouse for germination. Within one week of germination, pots were moved from the greenhouse to growth chambers. Seeds of *L. esculentum* were germinated in flats. Seven days after germination, vigorous seedlings were transplanted to 15 cm diameter pots containing a vermiculite-peat-sand mixture (3 seedlings per pot) and relocated to the growth chambers. Pots were randomly allocated to high- and low-light chambers, and pots were randomly relocated within the chambers twice weekly. After approximately 1 week, pots were thinned to 1 vigorous seedling per pot.

Growing conditions were adapted from field observations of mid-summer conditions in the Medicine Bow Mountains, WY at an elevation of approximately 3000 m, where *R. densiflorus* and *A. cordifolia* are native, and summertime frosts are common (Jordan and Smith, in review). Two growth chambers (CMP 3244, Conviron Products of America, Pembina, ND) were used to grow plants under different environmental conditions. One chamber was designated as a high light chamber, and provided 1000 $\mu\text{mol m}^{-2} \text{s}^{-1}$ of PAR supplied by a combination of fluorescent and incandescent bulbs. The second chamber was set to produce 500 $\mu\text{mol m}^{-2} \text{s}^{-1}$ of PAR. Both chambers were programmed to provide 12 h days, with the first and last 30 min (0700 to 0730 and 1830 to 1900) at less than maximum light intensity to provide a dawn/dusk transition. The light and temperature conditions of the high-light chamber are shown in Figure 5.1. The low-light chamber had one-half the light intensity but the same air temperature regime.

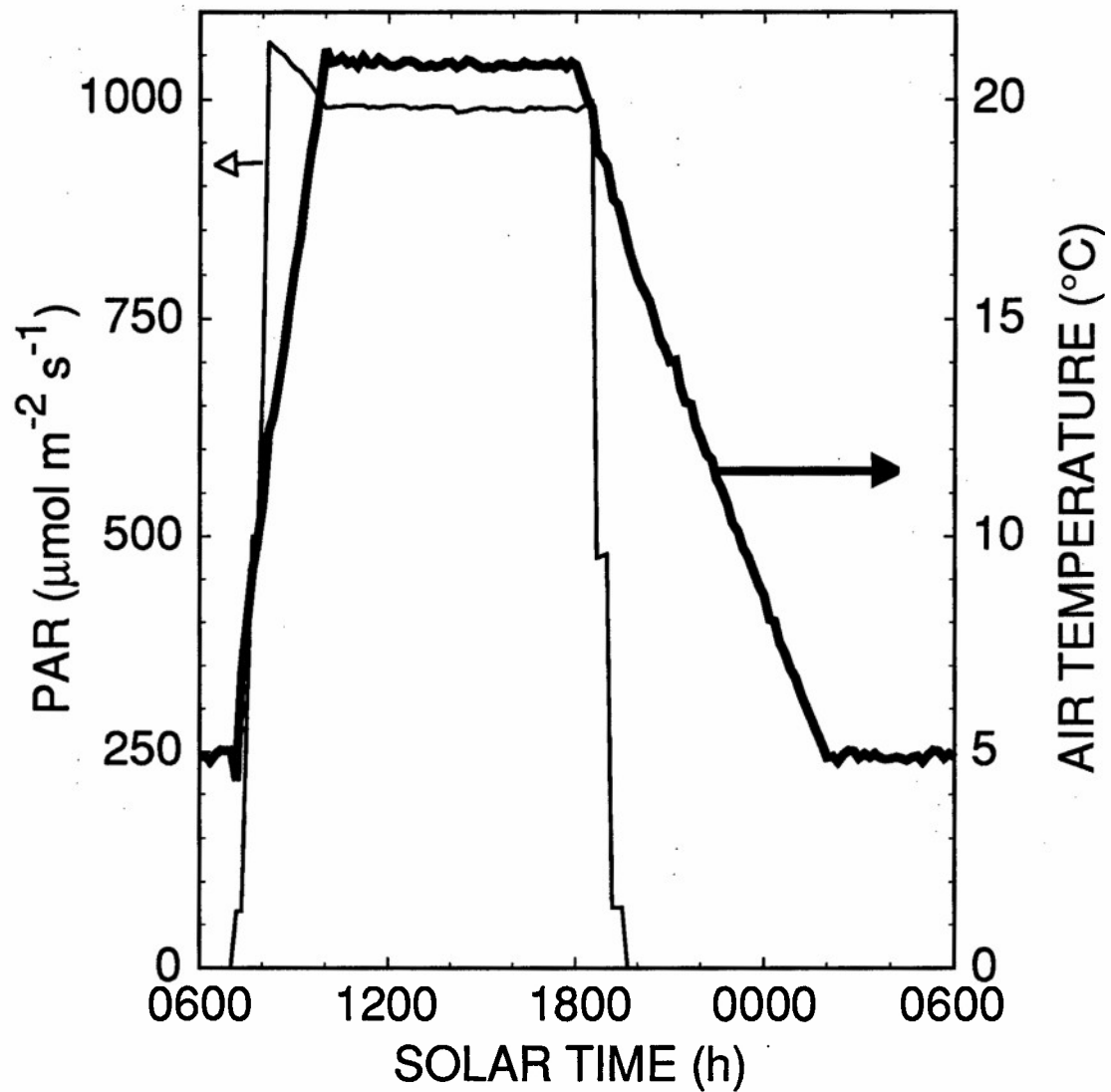


Figure 5.1: Light (left axis) and air temperature (right axis) in the high-light growth chamber. The lines represent observations made by a 21X datalogger (Campbell Scientific) with a LI-190SB quantum sensor (LI-COR Inc.) and a 0.2 mm copper-constantan thermocouple (Omega Engineering Inc.) at 1 min intervals over 24 h. The low-light chamber temperature conditions were similar but the light intensity was reduced by half.

Freezing treatments were accomplished by placing plants in a commercial refrigerator which, due to the characteristics of its thermostat and compressor, would attain temperatures as cold as -5.5°C before cycling of the thermostat within an approximate 3.0°C range (Fig. 5.2). Temperatures in the field fluctuate over a comparable range. Treated plants were returned to 5°C in the growth chamber between 30 and 15 min prior to dawn. Four plants (2 high- & 2 low-light) were used in each freezing treatment. Replication was achieved by repeating the freezing treatments (using separate plants) on 14 different days.

During the mid-morning hours on the day prior to freezing, fluorescence parameters were measured on mature leaves with the PAM fluorometer. The parameters recorded were: F_0 , F_m , F_v/F_m , qP , qN and quantum yield. Individually, the plants were removed from the growth chambers when the chambers attained mid-day equilibrium (20°C & full light @ 1000). Within 1 min after removal, room temperature PAM analysis was initiated, thus the F_v/F_m value measured was light-adapted as in the field study, rather than the frequently-reported dark-adapted state. The sensor was located approximately 1 cm above the adaxial surface of the leaf, perpendicular to the leaf surface, so as to uniformly illuminate the leaf surface. The distance was adjusted so that the PSII fluorescence would produce a signal within the linear portion of the instrument amplifier range at both F_0 and F_m . A weak measuring light was applied to produce state 1 F_0 fluorescence (van Kooten and Snel 1990). Saturating pulses of actinic light (duration 800 μs , dark interval 20 s) were applied, with continuous application of a measuring light. The analysis was allowed to run for 5 min until an equilibrium had been obtained and the final parameter values were recorded. As fluorescence quenching parameter measurements are strongly affected by the incident actinic light, each set of measurements was repeated at light intensities approximating the ambient light levels in the low light chamber ($250 \mu\text{mol m}^{-2} \text{s}^{-1}$), the high light chamber ($800 \mu\text{mol m}^{-2} \text{s}^{-1}$), as

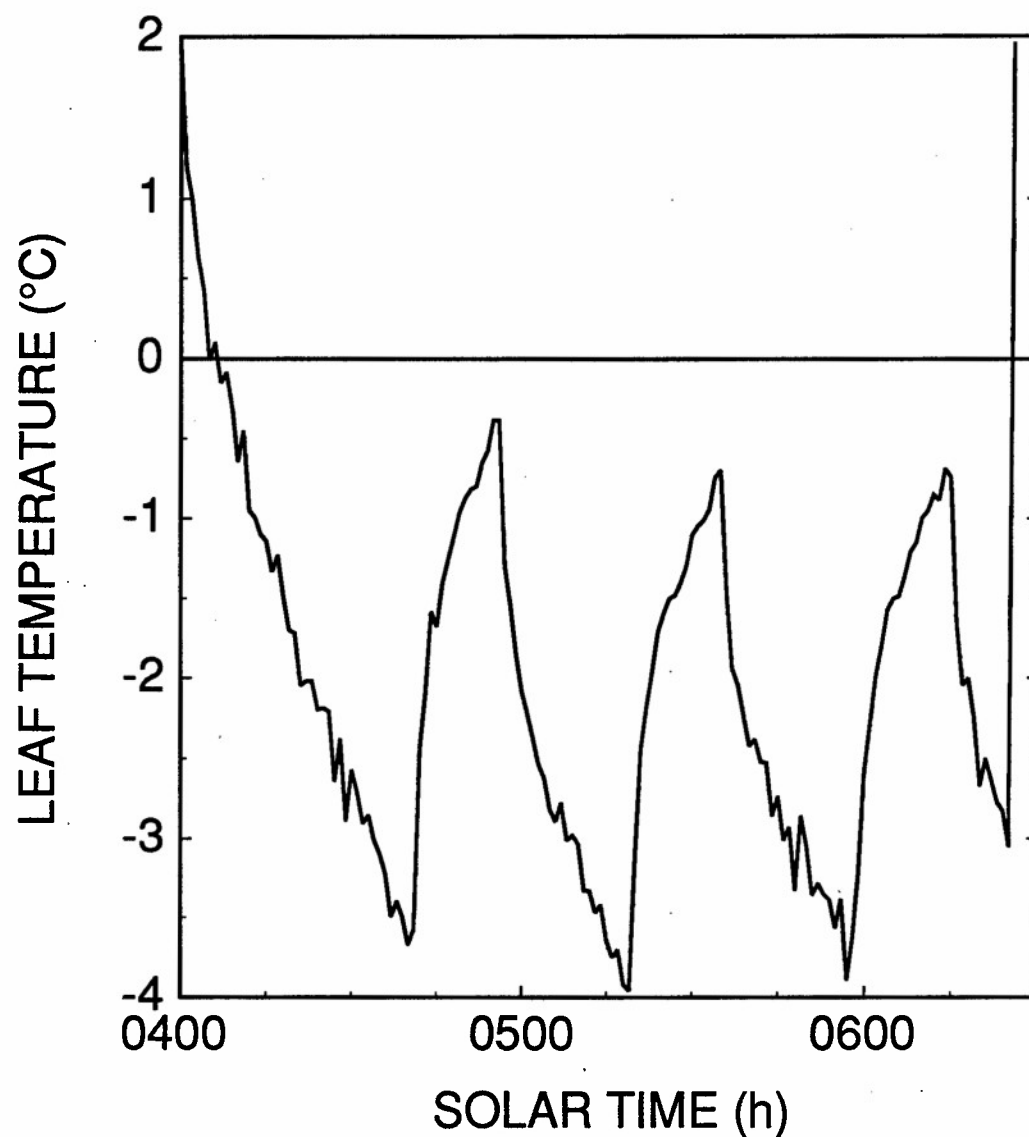


Figure 5.2: Typical freezing treatment of *Arnica cordifolia* leaves measured with a 0.2 mm copper-constantan thermocouple (Omega Engineering Inc.). Pots were moved from the growth chambers during the dark period at 5 °C to the refrigerator on a cart under an inverted cooler. The transport time from chamber to refrigerator was approximately 1 min and leaf temperatures were not monitored during this interval.

well as full sun ($2000 \mu\text{mol m}^{-2} \text{s}^{-1}$). Plants were returned to the growth chambers for approximately 20 min between measurements. All measurements were repeated on the same area of the leaf at the same time on the following morning after freezing treatments. Paired 2-tailed Student's *t* tests were used to analyze changes in leaves as a result of freezing in the high- and low-light chambers separately.

Field experiment

Leaf temperatures of a population of *R. densiflorus* were monitored throughout the night of an anticipated radiational frost (clear sky conditions, Fig. 5.3). Leaves on four exposed and four sheltered plants of *R. densiflorus* were measured every 15 min using 0.2 mm copper-constantan thermocouples (Omega Engineering Inc.), stitched along the midvein, near the center of each leaf. Shelters consisted of inverted cardboard boxes that contained several chemical hand-warmers to provide additional protection from freezing. Shelters were removed prior to sunrise (0615 to 0630).

Commencing prior to first direct light (0715), measurements were made on leaves of plants from both treatments. Leaf temperature increased rapidly after sunrise and reached a plateau by 0830, while photosynthetically active radiation (PAR) rapidly reached saturating levels and increased throughout the morning (Fig. 5.4). Four complete sets of measurements were made throughout the morning hours until PAR became limiting due to cloud-cover. For each fluorescence measurement, a freshly detached (light-adapted) leaf was removed from a plant and sheltered from sunlight for 2 min while being exposed to a low-intensity modulated red light, thus permitting PSII reaction centers to open. Leaves were also sheltered from direct sun during the observation period, and both saturating pulses and actinic light were provided by a portable PAM-2000 fluorometer and DA-2000 software (Heinz Walz GmbH, Effeltrich, Germany). The parameters recorded were: initial fluorescence (all reaction centers open: F_0), maximum fluorescence (all reaction centers closed: F_m), variable fluorescence ($F_v = F_m - F_0$), the ratio of the two

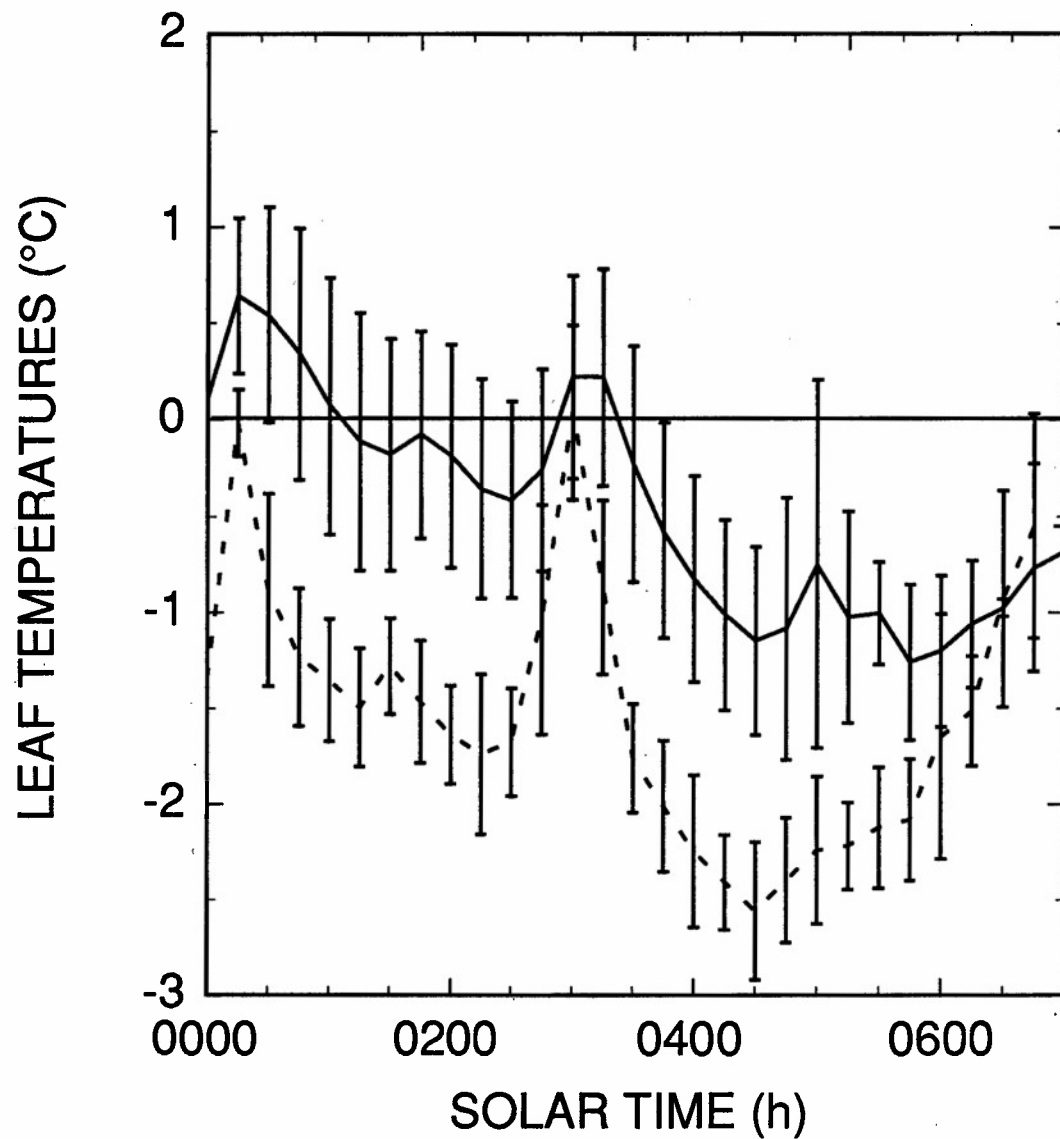


Figure 5.3: Nighttime leaf temperatures of *Rumex densiflorus* in four sheltered (solid line) and four exposed (dashed line) plants. The temperature record extends from midnight to after the shelters were removed at 0600. The vertical error bars represent \pm one standard deviation.

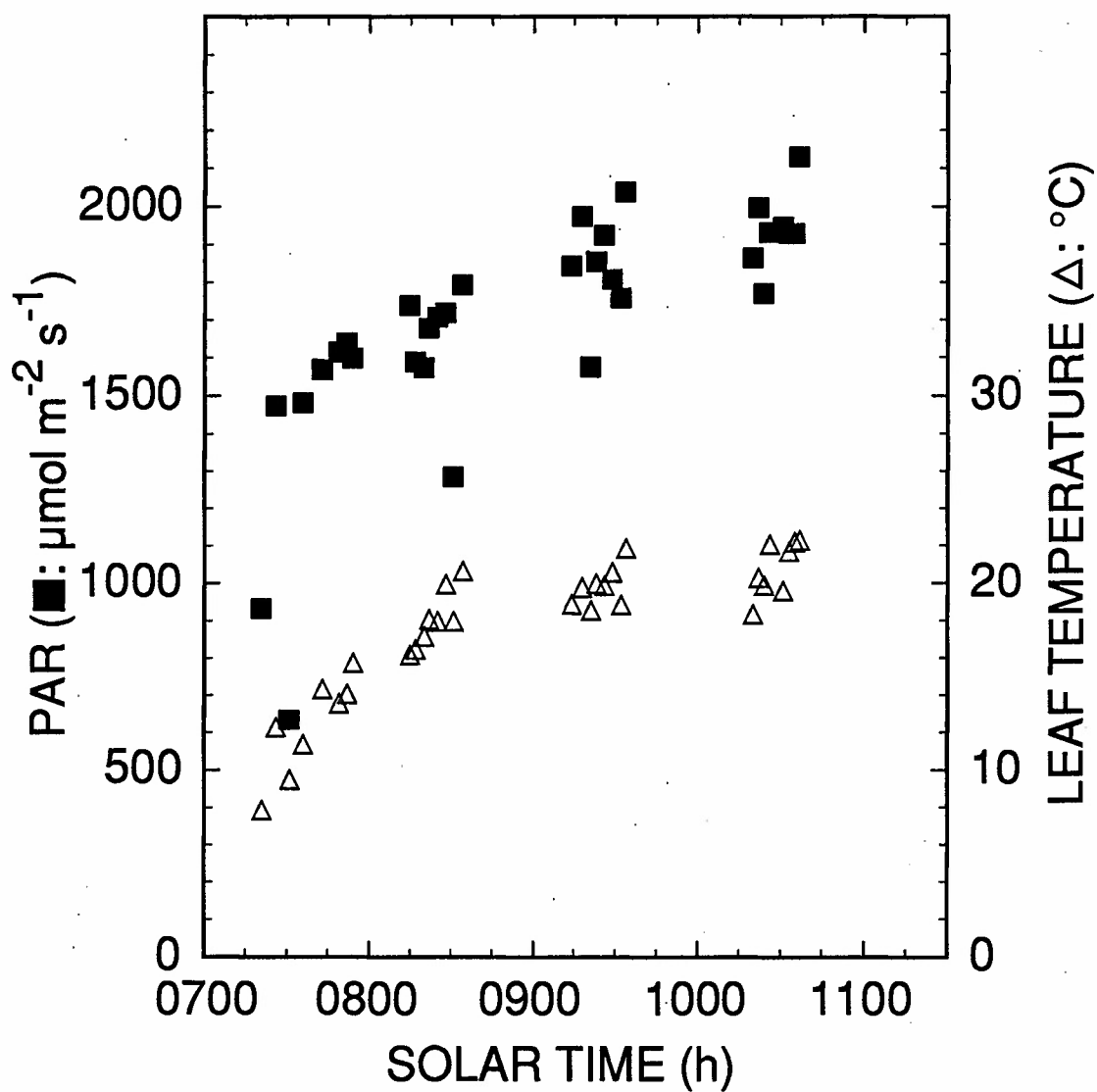


Figure 5.4: Photosynthetically active radiation (■) and *Rumex densiflorus* leaf temperatures (Δ) measured during gas exchange observations beginning at first direct sun following a frost event.

(F_v/F_m) , quantum yield [$Y \equiv (F'_m - F_t)/F'_m$], photochemical quenching [$qP \equiv (F'_m - F_t)/(F'_m - F_o)$], and non-photochemical quenching [$qN \equiv (F_m - F'_m)/(F_m - F_o)$] (see van Kooten and Snel 1990).

Concurrently with the fluorometric observations, gas exchange parameters were recorded on attached leaves of the same plants with a LI-6200 IRGA (LI-COR, Inc., Lincoln, NE, USA). Measurements of PAR, leaf temperature, net carbon assimilation (A_n), stomatal conductance (C_s) and transpiration rate (dE/dt) were made on south-facing leaves in direct sunlight. Leaf water potential (Ψ_L) was monitored on adjacent leaves with a Scholander pressure bomb (PMS Instrument Co., Corvallis, OR, USA). Differences in *R. densiflorus* photosynthetic parameters were analyzed with treatment and time (both first- and second-order polynomial terms) as independent variables using the general linear models procedure (PROC GLM) of SAS (SAS Institute, Cary, NC).

Results

Growth chamber experiment

Paired Student's *t* tests were applied to observations from leaves before and after freezing in each light environment. A highly significant decrease in F_v/F_m attributable to the freezing treatment was observed in both species (Table 5.1). Photochemical quenching was highly significantly increased by freezing in both *A. cordifolia* and *L. esculentum* in the high light chamber, increased significantly in *A. cordifolia* in low-light, and remained unchanged for low-light *L. esculentum* (Table 5.1). Non-photochemical quenching was unchanged in both species in both light-environments (Table 5.1). Quantum yield was unaffected in *A. cordifolia* and the high-light *L. esculentum*, but highly significantly reduced by freezing in the low-light *L. esculentum* (Table 5.1). Significant differences also occurred between chambers and species (statistics not reported).

<i>A. cordifolia</i>					
	Light	Yield	qP	qN	F _v /F _m
Paired 2-tailed t-test	high-	0.2419	0.0040	0.7413	<0.0001
	low-	0.9155	0.0402	0.5148	0.0036
Pre-freeze mean	high-	0.3933	0.6709	0.5191	0.7570
	low-	0.4069	0.7487	0.5905	0.7681
Change due to freezing	high-	0.0075	0.0453**	0.0067	-0.0176**
	low-	-0.0009	0.0357*	0.0115	-0.0129**
<i>L. esculentum</i>					
Paired 2-tailed t-test	high-	0.8679	0.0004	0.7592	<0.0001
	low-	0.0004	0.8536	0.0798	<0.0001
Pre-freeze mean	high-	0.4613	0.8643	0.5103	0.7122
	low-	0.3847	0.8988	0.7436	0.7219
Change due to freezing	high-	-0.0012	0.0486**	-0.0050	-0.0256**
	low-	-0.0405**	-0.0030	0.0178	-0.0155**

Table 5.1: Statistical tests of freezing effects on fluorescence parameters of *Arnica cordifolia* in high- and low-light chambers (high-light n = 37, low-light n = 41), and *Lycopersicon esculentum* (high-light n = 51, low-light n = 52). The mean parameter values prior to freezing and the change resulting from the freeze are reported. Significant changes ($p < 0.05$) in parameters are indicated by * and highly significant changes ($p < 0.01$) are indicated by **.

Field experiment

The light-adapted variable fluorescence (F_v/F_m) was significantly reduced ($p = 0.0035$) in the unsheltered plants. There was no trend during the morning hours of F_v/F_m for either population (Fig. 5.5). There was a significant ($p < 0.0001$) curvilinear change of both qP and qN over time (Fig. 5.6A, B). There was no mean difference between populations in qN , but the response over time of the sheltered population tended to be greater (Fig. 5.6A). Photochemical quenching was reduced ($p = 0.0198$) in the exposed plants compared to the sheltered plants (Fig. 5.6B), but was nearly fully recovered by mid-morning. Quantum yield, as measured with the fluorometer, was also reduced in exposed leaves ($p < 0.0001$), but did not show the recovery seen in qP (Fig. 5.7).

There were no significant differences between freezing treatments in gas exchange parameters (Fig. 5.8). Stomatal conductance and carbon uptake increased in a logarithmic manner over time (Fig. 8A, C), while transpiration exhibited a linear increase with time (Fig. 5.8B).

Following the freeze, most of the exposed plants were visibly wilted, with normally upright leaves falling to a nearly horizontal posture. This was accompanied by ice formation on the leaves and extremely negative Ψ_L related to visible ice formation within leaf petioles. Normal leaf orientation, appearance, and Ψ_L was restored by 30 min after sunrise as leaf melting and rapid warming commenced. No perceptible changes were detectable throughout the remainder of the morning other than gradual leaf drying following the ice melt (data not shown).

Discussion

Net photosynthetic rates, as measured by gas-exchange systems indicate the short-term ability of a leaf to acquire carbon. These measurements have frequently been used to evaluate plant stress, but gas-exchange measurements may be influenced by variation due to stomatal limitations, temperature and water stress.

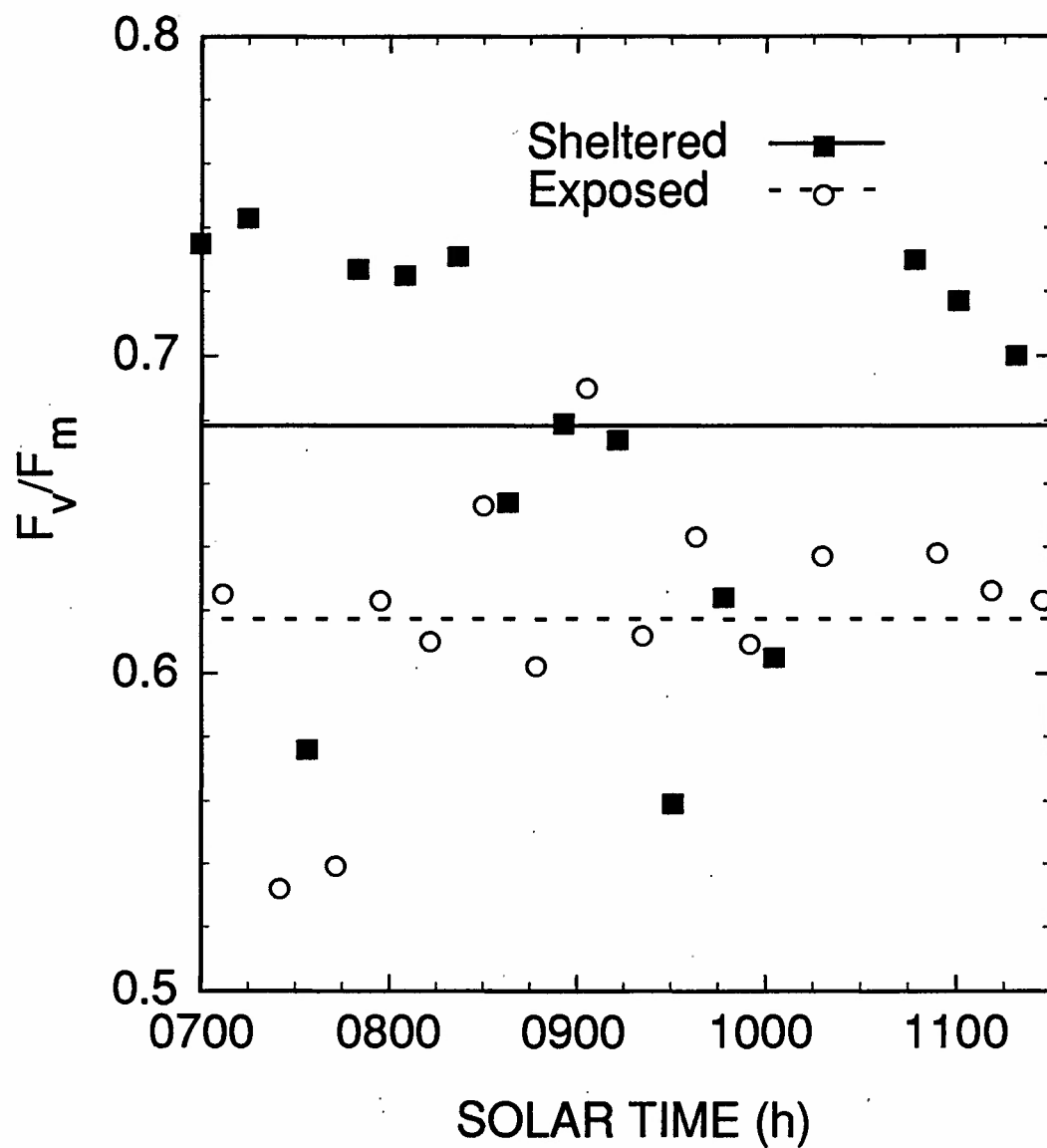


Figure 5.5: Ratio of light-adapted variable fluorescence to maximal fluorescence (F_v/F_m) in *Rumex densiflorus* over the hours following a frost event. The dashed and solid lines represent the linear regression versus time of leaves from sheltered (■) and exposed (○) plants.

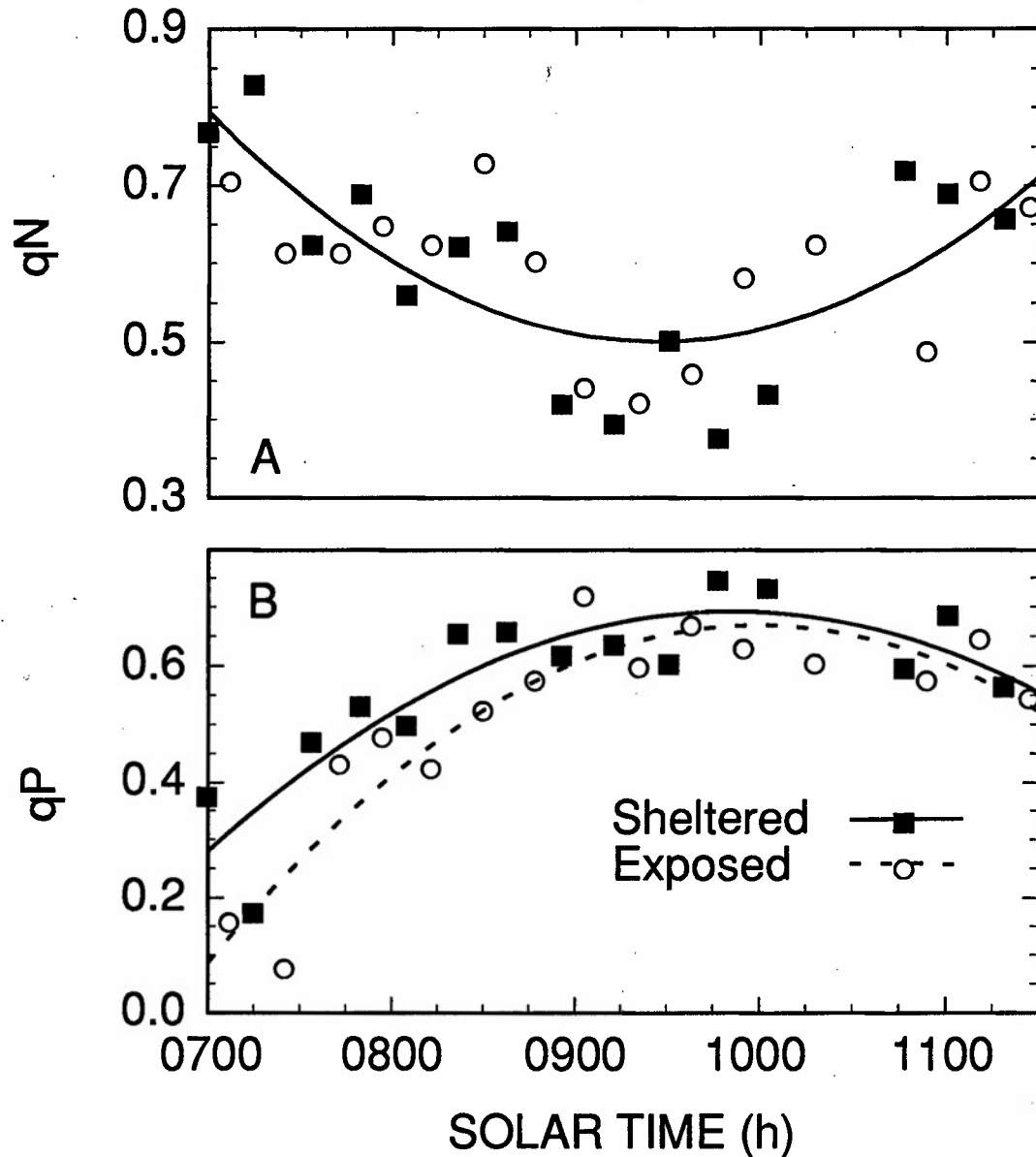


Figure 5.6: A: Trend in non-photochemical quenching over time following a frost event in *Rumex densiflorus*. The two populations were best represented by a single quadratic equation. B: Trend in photochemical quenching in the same *R. densiflorus* leaves. Two separate quadratic equations were used to describe the observations. The dashed and solid lines represent the means of leaves from sheltered (■) and exposed (○) plants.

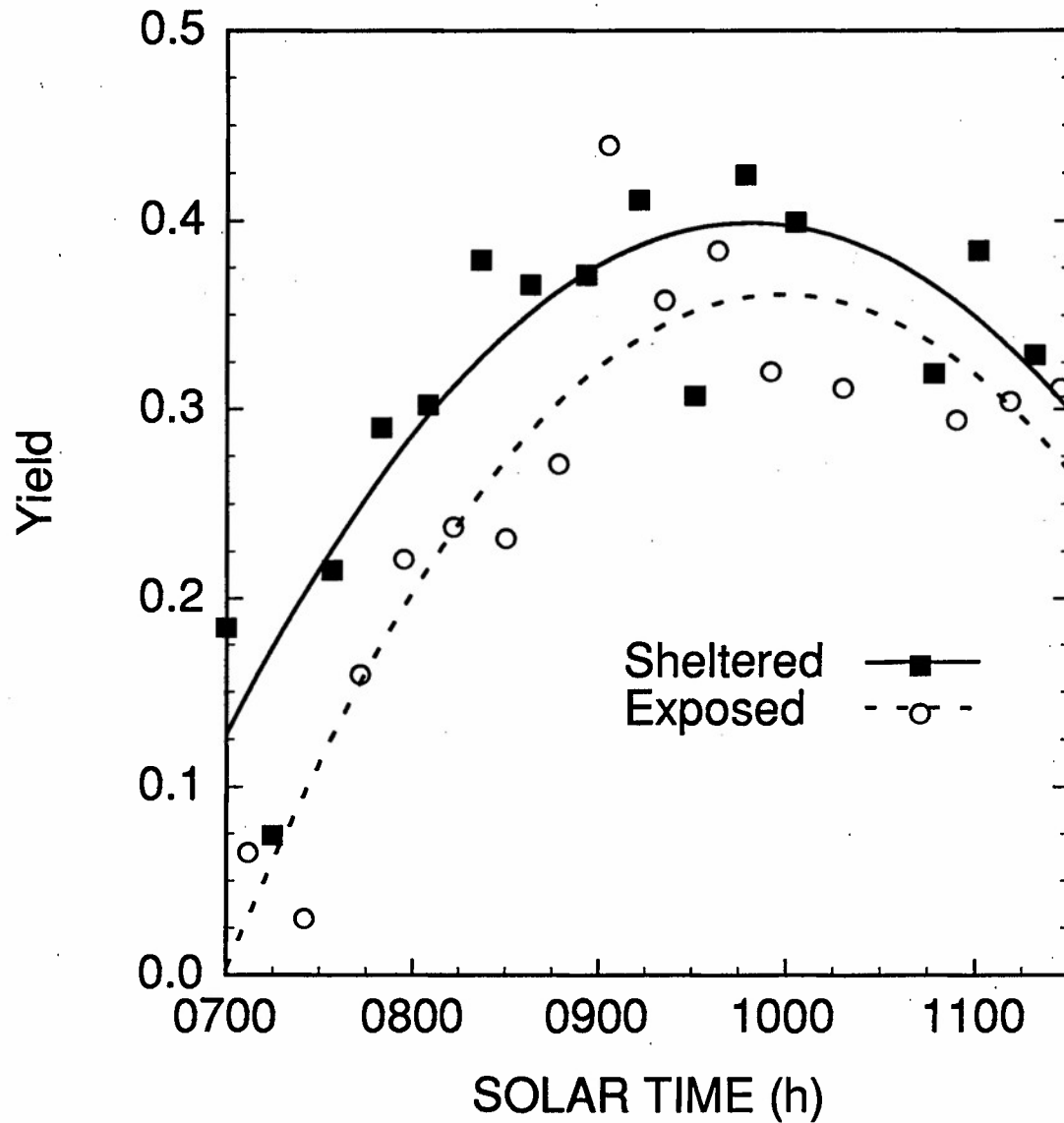


Figure 5.7: Quantum yield of *Rumex densiflorus* following a freeze event. The dashed and solid lines represent the means of leaves from sheltered (■) and exposed (○) plants.

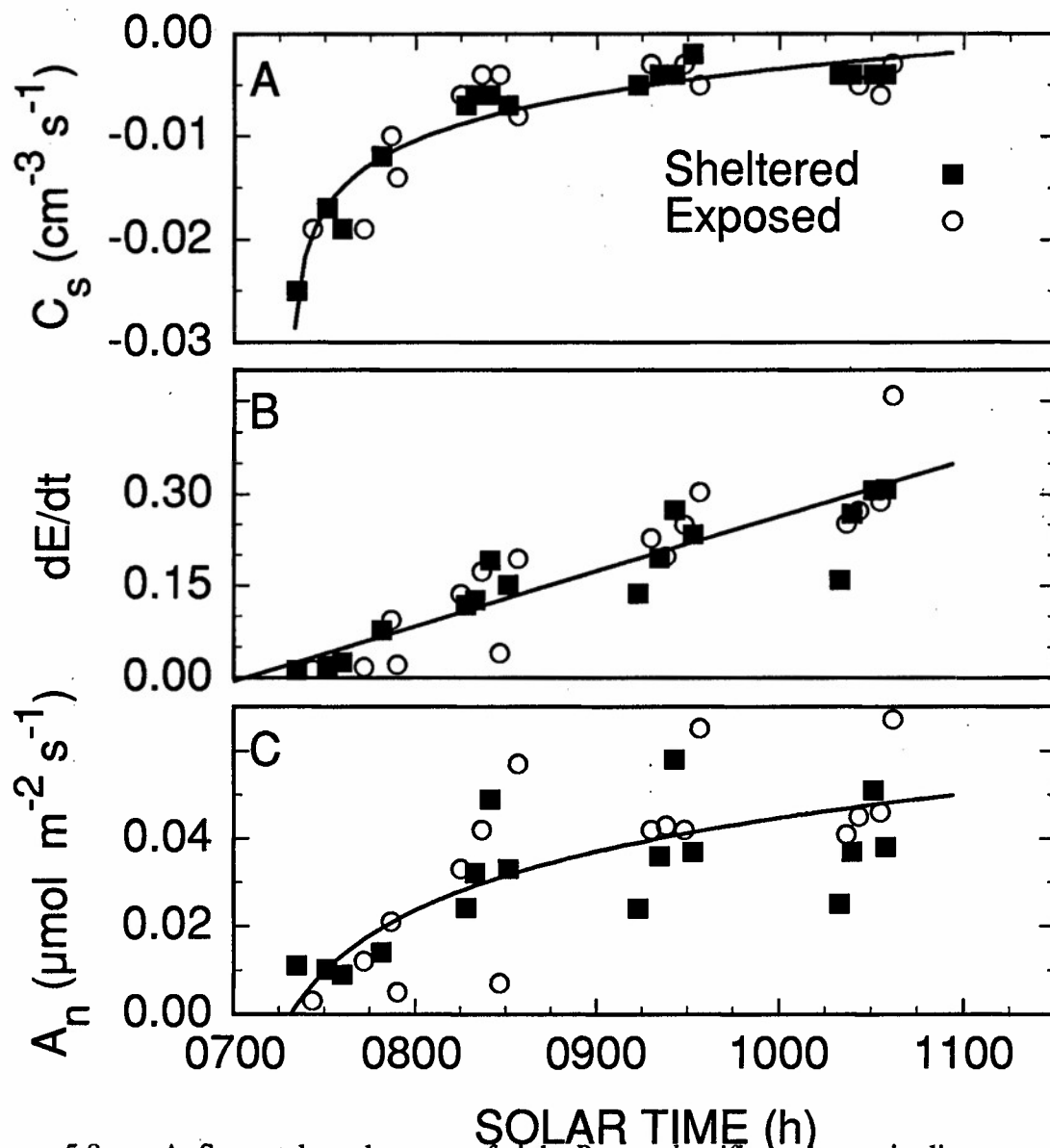


Figure 5.8: A: Stomatal conductance of eight *Rumex densiflorus* leaves in direct sunlight following a frost event. The line through the data is a least squares fit of a natural log function. B: Rate of vapor loss by leaves. A linear regression was fit to the data. C: Rate of net carbon assimilation. The curve fit is a natural log function. Each graph is the summary of individual leaves from 8 different clones of *R. densiflorus* measured repeatedly over time.

Chlorophyll fluorescence provides an endogenous probe of the health of PSII. Both q_N and q_P are regarded as mechanisms which can help prevent photoinhibitory damage to PSII by dissipating excess energy (Genty et al. 1989). Photochemical quenching is thought to indicate the redox state of the quinone A pool, while non-photochemical quenching appears to relate to the ability to establish a pH gradient across thylakoid membranes (Hurry and Huner 1991). However, q_N is more typically interpreted as a dissipation of excess energy by thermal means. Havaux et al. (1991) stated that both photochemical and non-photochemical quenching parameters are deceptive terms, as they are simultaneously affected by changes in various rate constants, and are best used as qualitative indicators of quenching rates. Havaux et al. (1991) concluded that quantum yield of PSII is regulated by rates of non-photochemical energy dissipation. Quantum yield of PSII is considered to be a good indicator of the overall efficiency of the photosynthetic system (DA-2000 manual).

Terashima et al. (1994) determined that chilling damage (below 10 °C) in *Cucumis* occurs on the acceptor side of PSI (not PSII) at low light and in the presence of O_2 . Photoinhibitory damage to PSII is thought to require high levels of light. This may indicate a difference in response between chilling sensitive genera (*Cucumis*, *Lycopersicon*) and genera native to the subalpine environment. At room temperature, PSI fluorescence is negligible. If Terashima et al. (1994) are correct in the site of chilling damage, 77K fluorescence may be required to resolve its extent.

Growth chamber experiment

The significant increase in q_P in the growth chamber experiments does not coincide with theory, as an increase in photochemical efficiency can hardly be expected following a stress event. Photochemical quenching is a computed parameter, so one or more of its components $[(F'_m - F_t)/(F'_m - F'_o)]$ must have changed in such a way as to cause an increase in the term. Figure 5.9 shows that the F_t of frozen populations of A.

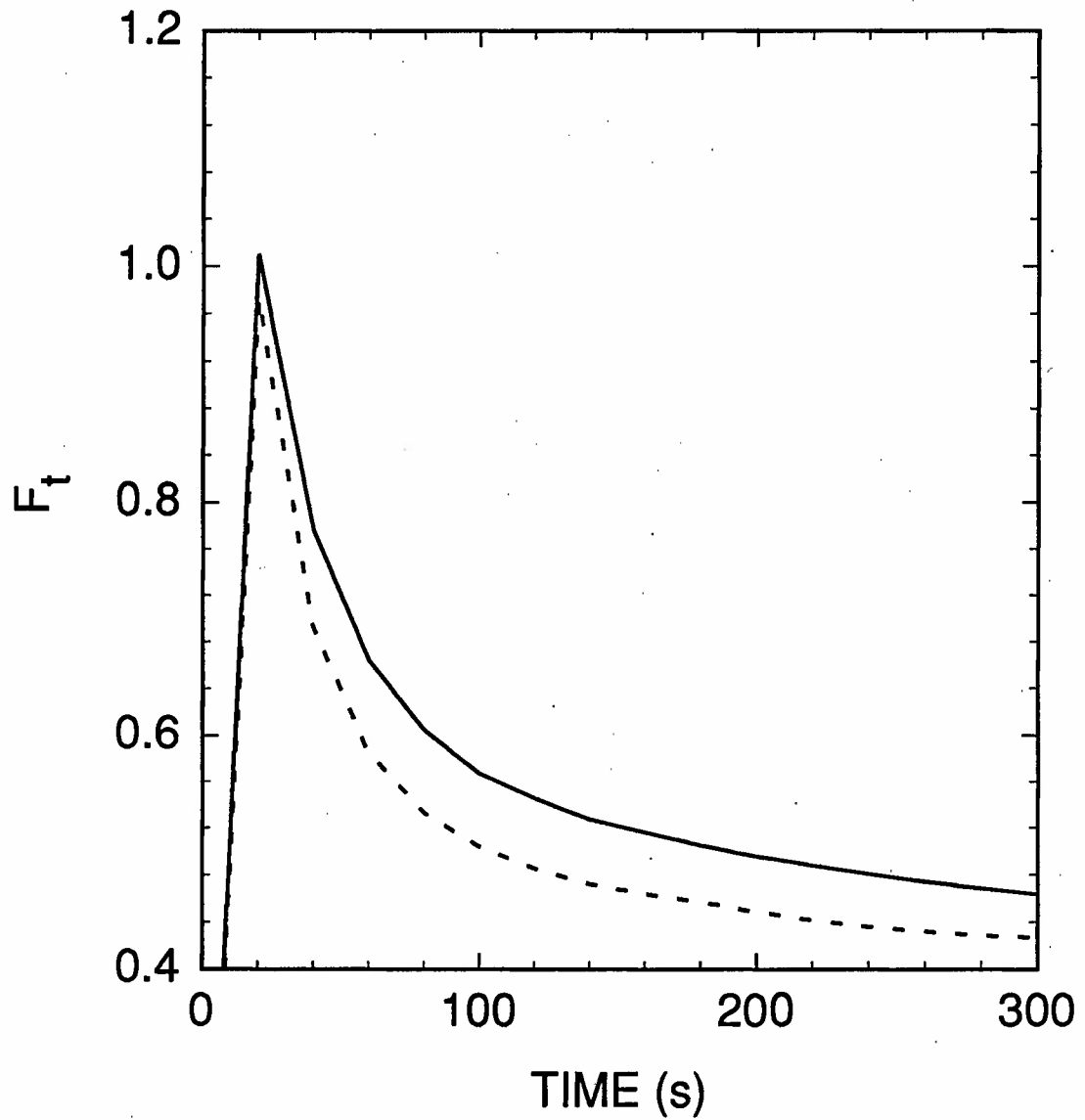


Figure 5.9: Mean instantaneous fluorescence (F_t) measured at 20 s intervals in *Arnica cordifolia* averaged across all treatments except freezing. Solid line: Unfrozen (—), Frozen (---). All observations after 20 s were highly significantly different ($p < 0.01$).

cordifolia decreased more rapidly following the initial peak, and was significantly lower at the termination of the measurement. No significant changes occurred in either F_m' or F_o' . This is consistent with the lack of change in qN , which shares a common denominator with qP . Consequently, while an increase in photochemical quenching in stressed plants is difficult to explain directly, it can be attributed to decreased steady-state fluorescence emission, and not a change in initial or pulse-related fluorescence peak heights. Interpretation of a freezing stress-related decrease in F_t will require additional experimentation. Griffith et al. (1994) reported fluorescence returning to F_o after a saturating pulse more quickly in cold-stressed plants, results consistent with those observed here. Hurry and Huner (1991) reported similar drops in fluorescence in cold-hardened plants relative to unhardened plants, as well as a more rapid rise in qP in these plants. Both results are consistent with our observations, but neither Griffith et al. (1994) nor Hurry and Huner (1991) speculated on the physiological significance of these findings. At present, the interpretation remains equivocal.

Variable fluorescence consistently decreased in both high- and low-light chambers following freezing. Variable fluorescence has been found to be an early indicator of damage to PSII, decreasing even before visible damage symptoms occur (Lurie et al. 1994). In the case of high light stress, this is usually interpreted as photoinhibitory damage, particularly in combination with cold temperature exposure.

Quantum yield, as a measure of the ability of the photosystem to use absorbed light energy, is an extremely useful parameter for analysis of the impact of stresses on plants. In the growth chamber experiment, only the low-light *L. esculentum* treatment showed a decrease in yield following chilling. This may indicate that *A. cordifolia*, as a freezing-tolerant species, was unaffected by the levels of freezing stress applied, or that recovery had been completed by the time the measurements were made. The lack of response in the high-light *L. esculentum* may indicate some physiological adaptation in

high-light (an environment which correlates strongly with colder nocturnal temperatures) conferring some resistance to freezing damage.

Field experiment

The shelter treatment did not prevent leaf temperatures from dropping below 0 °C. However, sheltered leaves did remain significantly warmer than exposed leaves, resulting in a treatment with greater cold exposure than the control. All leaves were exposed to direct sunlight combined with low temperatures (from a photosynthetic perspective) beginning at approximately 0715 (DeLucia and Smith 1987). Full, saturating sunlight and temperatures appropriate for photosynthesis were attained by 0800.

Presumably, both populations of *R. densiflorus* leaves exhibited depressed light-adapted F_v/F_m as a result of the nocturnal temperature regime, but the exposed plants exhibited a greater depression in variable fluorescence. Lack of a decrease in q_N indicates that the chilled plants remain capable of dissipating excess energy, helping to prevent damage to PSII (Havaux et al. 1991). In fact, in the *R. densiflorus* experiment, q_N appears to change over time in such a way as to compensate for fluctuations in q_P which, in turn, are likely related to diurnal trends in ambient light and leaf temperature, as well as recovery from the freezing stress. Photochemical quenching was depressed early in the morning following the frost. It recovered over time and decreased slightly as ambient light intensity reached its daily maximum. Non-photochemical quenching was likely responsible for dissipating excess energy not accounted for by q_P . Non-photochemical quenching decreased as q_P increased, and then increased again as incident sunlight approached a maxima and q_P was reduced. The photochemical quenching parameter responded differently in *R. densiflorus* than in both of the growth chamber experiment species. The timing of the experimental measurements may help account for this discrepancy, as the *R. densiflorus* population would not have exhibited a significant

change in qP if observations were taken only at mid-morning (i.e., 1000 to 1200), as in the growth chamber experiments.

Significant decreases in yield as a result of freezing occurred in *R. densiflorus* following the freeze, indicating a decrease in photosystem efficiency. The time course in yield implies that in the early morning following the frost, leaves were not operating at peak efficiency but recovered strongly by mid-morning. Efficiency in the late morning dropped off in all leaves as light intensity increased to levels well above saturation. However, while carbon fixation rates increased concurrently with increases in yield, no treatment differences were apparent in the gas exchange measurements, as they were in the fluorescence observations.

Conclusions

The decreases in F_v/F_m in all 3 species as a result of freezing imply a reduction in the ability of PSII to quench excitation. Non-photochemical quenching was uniformly unaffected by freezing treatment, while qP presented a response that is more difficult to interpret, with increases in 3 of 4 light-species combinations in the growth chambers, but a decrease in the native population of *R. densiflorus*.

While some photosynthetic parameters (both chlorophyll fluorescence and gas-exchange) were not significantly altered by the freezing treatment, all showed significant changes over time during the morning following a freeze. To some extent, these changes probably represent responses to increasing light intensity and increasing leaf temperature, but a component of recovery from the freeze most likely accounts for some of the rate increase. Plants native to the subalpine environment must be able to recover rapidly (within hours) from frost events, or risk losing a substantial portion of an already short growing season. The lack of treatment differences in gas exchange of *R. densiflorus* suggests that these plants are well-adapted to the summertime frosts observed in this area. Even though early wilting and freezing of xylem sap was observed in exposed leaves,

rapid recovery coincided with melting and no differences due to treatment were apparent. In addition, clear morning skies are frequently associated with nocturnal radiation frosts, and the ability to utilize light efficiently on these mornings should be an adaptive advantage in this environment.

Summary

Frost is a frequent stress event in the subalpine environment throughout the growth season, and radiative cooling often enhances both the frequency and intensity of frost events in locations exposed to the night sky. The impact of radiative cooling is regulated by the thickness of the leaf boundary layer, leaf exposure to the sky and the atmospheric infrared environment. Larger leaves are more susceptible to radiational cooling because the balance between radiative exchange and convective exchange is tipped towards the radiative due to the thicker leaf boundary layer. Radiative cooling influences not only leaf temperature, but also the temperature of the air near the leaves via convective cooling, thus reducing the rate of convective warming on calm, clear nights, as colder air collects near the ground, particularly in topographic depressions. An energy balance analysis using field conditions indicated a relatively equal contribution of radiational cooling of the leaf itself and the independent effects of air cooling next to the ground.

Coniferous forest trees typically have needle-like leaves with a smaller characteristic dimension than herbaceous plants of the subalpine zone, or elsewhere. The small leaf dimension is somewhat counteracted by the clumping of needles which acts to increase the thickness of the boundary layer beyond that of an isolated needle. Regardless, the larger, horizontal leaves of herbaceous meadow vegetation were found to be colder on radiation frost nights than nearby conifer needles. The exposed herbaceous vegetation experienced frost throughout the growing season, with a maximum frost-free period for broadleaves in 1993 of only 5 consecutive days, which was much shorter than the air temperature frost-free interval. Thus, radiational frosts may particularly impact large, broadleaf species with high microsite sky exposure. The smaller leaf dimension observed in more exposed sites appears to match changes expected in high-light

adaptations to reduce daytime heat stress, but this could also represent an adaptation for avoidance of radiative frosts.

The needle leaves of conifers are effective at reducing the intensity of direct sunlight due to their cross-sectional geometry. Thus, they are most likely less susceptible to photoinhibitory effects of low temperatures followed by, or in combination with, high light. In contrast, broadleaf plants may experience the coldest leaf temperatures due to radiational frost effects, as well as almost simultaneous exposure to full sunlight in the early morning hours. Radiative frosts were strongly associated with cloudless conditions, and were frequently observed to coincide with clear skies and full sunlight the following morning. In addition, minimum nightly temperatures frequently occurred just before sunrise. Significant impairment of photosynthetic capacity by frost would be highly detrimental in this environment, given the frequency of frost events. Coupled with high sun exposure the following morning, nighttime frost could lead to a particularly severe combination of low temperature/high light stress. The ability of selected native species to photosynthetically fix CO_2 in full sunlight was not impaired by a freezing event, but fluorescence parameters did demonstrate significant short-term changes. Similar responses of fluorescence parameters were observed under more-controlled conditions in growth chamber experiments in both high- and low-light environments. The plants studied exhibited more tolerance of cold temperatures than has been reported for vascular plants during the growing season in the literature.

Literature Cited

- Aase JK and Idso SB 1978. A comparison of two formula types for calculating longwave radiation from the atmosphere. *Water Resour Res* 14:623-625
- André JC and Mahrt L 1982. The nocturnal surface inversion and influence of clear-air radiative cooling. *J Atmos Sci* 39:864-878
- Ångström A 1915. A study of the radiation of the atmosphere. *Smithsonian Misc Coll* 65: pp 159
- Arny DC and Upper CD 1973. Example of the effects of early season frost damage on yield of corn. *Crop Sci* 13:760-761
- Baker NR and Bowyer JR 1994. Photoinhibition of photosynthesis from molecular mechanisms to the field. BIOS Scientific Publishers, Oxford, UK. 494 pp
- Ball FK 1956. The theory of strong katabatic winds. *Aust J Phys* 9:373-386
- Bauer H, Nagele M, Comploj M, Galler V, Mair M and Unterpertinger E 1992. Photosynthesis after freezing stress in plants with various degrees of freezing tolerance. *Photosynthetica* 27:627-635
- Bauer H, Nagele M, Comploj M, Galler V, Mair M and Unterpertinger E 1994. Photosynthesis in cold acclimated leaves of plants with various degrees of freezing tolerance. *Physiol Plant* 91:403-412
- Bauer H, Wierer R, Hatheway WH and Larcher W 1985. Photosynthesis of *Coffea arabica* after chilling. *Physiol Plant* 64:449-454
- Bergen JD 1971. An inexpensive heated thermistor anemometer. *Agric For Meteorol* 8:395-405
- Billings WD 1969. Vegetational pattern near timberline as affected by fire-snowdrift interactions. *Vegetatio* 19:192-207

- Brüggemann W, van der Kooij TAW and van Hasselt PR 1992a. Long-term chilling of young tomato plants under low light and subsequent recovery. I. Growth, development and photosynthesis. *Planta* 186:172-178
- Brüggemann W, van der Kooij TAW and van Hasselt PR 1992b. Long-term chilling of young tomato plants under low light and subsequent recovery. II. Chlorophyll fluorescence, carbon metabolism and activity of ribulose-1,5bisphosphate carboxylase/oxygenase. *Planta* 186:179-187
- Brunt D 1932. Notes on radiation in the atmosphere. *Q J R Meteorol Soc* 58:389-418
- Brutsaert W 1975. On a derivable formula for long-wave radiation from clear skies. *Water Resour Res* 11:742-744
- Burke JJ 1990. Variation among species in the temperature dependence of the reappearance of variable fluorescence following illumination. *Plant Physiol* 93:652-656
- Burke JJ and Oliver MJ 1993. Optimal thermal environments for plant metabolic processes (*Cucumis sativus* L.). *Plant Physiol* 102:295-302
- Campbell GS 1977. An Introduction to Environmental Biophysics. Springer-Verlag, New York. 159 pp
- Carter GA and Smith WK 1985. Influence of shoot structure on light interception and photosynthesis in conifers. *Plant Physiol* 79:1038-1043
- Chazdon RL and Field CB 1987. Photographic estimation of photosynthetically active radiation: evaluation of a computerized technique. *Oecologia* 73:525-532
- Dang QL, Lieffers VJ and Rothwell R 1992. Effects of summer frosts and subsequent shade on foliage gas exchange in peatland tamarack and black spruce. *Can J For Res* 22:973-979
- Deacon EL 1970. The derivation of Swinbank's long-wave radiation formula. *Q J R Meteorol Sci* 96:313-319

- DeLucia EH 1987. The effect of freezing nights on photosynthesis, stomatal conductance, and internal CO₂ concentration in seedlings of Engelmann spruce (*Picea engelmannii* Parry). Plant, Cell Environ 10:333-338
- DeLucia EH and Smith WK 1987. Air and soil temperature limitations on photosynthesis in Engelmann spruce during summer. Can J For Res 17:527-533
- Demmig B, Winter K, Krüger A and Czygan FC 1987. Photoinhibition and zeaxanthin formation in intact leaves. A possible role of the xanthophyll cycle in the dissipation of excess light energy. Plant Physiol 84:218-224
- Eastham J and Rose CW 1988. Pasture evapotranspiration under varying tree planting density in an agroforestry experiment. Agric Water Manage 15:87-105
- Feierabend J, Schann C and Hertwig B 1992. Photoinactivation of catalase occurs under both high- and low-temperature stress conditions and accompanies photoinhibition of photosystem II. Plant Physiol 100:1554-1561
- Ferguson DL and Burke JJ 1991. Influence of water and temperature stress on the temperature dependence of the reappearance of variable fluorescence following illumination. Plant Physiol 97:188-192
- Floor C 1989. Estimating grass minimum temperature and probability of ground frost at Eelde (Netherlands). Meteorological Magazine 118:261-265
- Foster JR and Smith WK 1986. Influence of stomatal distribution on transpiration in low-wind environments. Plant, Cell Environ 9:751-759
- Freeburg RS 1972. Thermal environment of orchards as influenced by tree spacing. Transactions of the ASAE. Am Soc Ag Eng 15:615-619
- Gardner WK, McDonald GK, Ellis SE, Platt M and Flood RG 1991. A review of factors affecting minimum temperature reached on clear, windless nights. Aust J Agric Res 42:191-203
- Gates DM 1980. Biophysical Ecology. Springer-Verlag, New York 611 pp

- Gates DM and Papian LE 1971. Atlas of energy budgets of plant leaves. Academic Press, New York, 277 pp
- Geller GN and Nobel PS 1984. Cactus ribs: influence on PAR interception and CO₂ uptake. *Photosynthetica* 18:482-494
- Genty B, Griantis JM and Baker NR 1989. The relationship between the quantum yield of photosynthetic electron transport and quenching of chlorophyll fluorescence. *Biochim Biophys Acta* 990:87-92
- Genty B, Harbinson J, Briantais J-M and Baker NR 1990. The relationship between non-photochemical quenching of chlorophyll fluorescence and the rate of photosystem 2 photochemistry in leaves. *Photosyn Res* 25:249-257
- Grace J 1978. The turbulent boundary layer over a flapping *Populus* leaf. *Plant, Cell Environ* 1:35-8
- Greer D 1990. The combined effects of chilling and light stress on photoinhibition of photosynthesis and its subsequent recovery. *Plant Physiol Biochem* 28:447-455
- Greer DH and Laing WA 1992. Photoinhibition of photosynthesis in intact kiwifruit (*Actinidia deliciosa*) leaves. *Planta* 186:418-425
- Greer DH, Ottander C and Öquist G 1991. Photoinhibition and recovery of photosynthesis in intact barley leaves at 5 and 20 °C. *Physiol Plant* 81:203-210
- Griffith M, Boese SR and Huner NPA 1994. Chilling sensitivity of the frost-tolerant potato *Solanum commersonii*. *Physiologia Plant* 90:319-326
- Hadley JL and Smith WK 1987. Influence of krummholz mat microclimate on needle physiology and survival. *Oecologia* 73:82-90
- Havaux M, Strasses RJ and Greppin H 1991. A theoretical and experimental analysis of the qP and qN coefficients of chlorophyll fluorescence quenching and their relation to photochemical and nonphotochemical events. *Photosyn Res* 27:41-55

- Havranek WM and Tranquillini W 1994. Physiological processes during winter dormancy and their ecological significances. In: (WK Smith and TM Hinckley, eds.) Ecophysiology of coniferous forests. Academic Press, San Diego, CA
- Hetherington SE, He J and Smillie RM 1989. Photoinhibition at low temperature in chilling-sensitive and -resistant plants. *Plant Physiol* 90:1609-1615
- Holopainen JK 1990. The relationship between multiple leaders and mechanical and frost damage to the apical meristem of Scots pine seedlings. *Can J For Res* 20:280-284
- Huner NPA, Öquist G and Sundblad L-G 1992. Low temperature induced artifactual increase in chlorophyll a fluorescence. *Plant Physiol* 98:749-752
- Hurry VM and Huner NPA 1991. Low growth temperature effects a differential inhibition of photosynthesis in spring and winter wheat. *Plant Physiol* 96:491-497
- Idso SB 1972. Systematic deviations of clear sky atmospheric thermal radiation from predictions of empirical formulae. *Q J R Meteorol Soc* 98:399-401
- Idso SB 1981. A set of equations for full spectrum and 8-14 μm and 10.5-12.5 μm thermal radiation from cloudless skies. *Water Resour Res* 17:295-304
- Jarvis PG and Leverenz JW 1983. Productivity of temperate, deciduous, and evergreen forests. 233-280. In: Encyclopedia of Plant Physiology. Physiological Plant Ecology IV: Ecosystem processes: Mineral Cycling, Productivity, and Man's Influence. Eds. OL Lange, PS Nobel, CB Osmond and H Ziegler. Springer-Verlag, Berlin Heidelberg New York 644 pp
- Jordan DN and Smith WK 1994. Energy balance analysis of nighttime leaf temperatures and frost formation in a subalpine environment. *Agric For Meteorol* 71:359-372
- Jordan DN and Smith WK (in review) Microclimate factors influencing the frequency and duration of growth season frost for subalpine plants. *Agric For Meteorol*
- Kimball BA, Idso SB and Aase JK 1982. A model of thermal radiation from partly cloudy and overcast skies. *Water Resour Res* 18:931-936

- Krause GH and Weis E 1991. Chlorophyll fluorescence and photosynthesis: the basics. *Annu. Rev. Plant Physiol. Plant Mol Biol* 42:313-349
- Larcher W and Neuner G 1989. Cold-induced sudden reversible lowering of *in vivo* chlorophyll fluorescence after saturating light pulses. *Plant Physiol* 89:740-742
- Lassoie JP, Hinckley TM and Grier CC 1985. Coniferous forests of the Pacific Northwest. *In: Physiological ecology of North American plant communities*. Eds. BF Chabot and HA Mooney. Chapman and Hall, New York pp. 127-161
- Le Gouallec J-L, Cornic G and Briantais J-M 1991. Chlorophyll fluorescence and photoinhibition in a tropical rainforest understory plant. *Photosyn Res* 27:135-142
- Leuning R 1988. Leaf temperatures during radiation frost. Part II. A steady state theory. *Agric For Meteorol* 42:135-155
- Leuning R and Cremer KW 1988. Leaf temperatures during radiation frost. Part I. Observations. *Agric For Meteorol* 42:121-133
- Leverenz JW and Hinckley TM 1990. Shoot structure, leaf area index and productivity of evergreen conifer stands. *Tree Physiol* 6:135-149
- Leverenz JW and Jarvis PG 1979. Photosynthesis in Sitka spruce. VII. The effects of light flux density and direction on the rate of net photosynthesis and the stomatal conductance of needles. *J Appl Ecol* 16:919-932
- Leverenz JW and Jarvis PG 1980. Photosynthesis in Sitka spruce (*Picea sitchensis* (Bong.) Carr.) IX. The relative contribution made by needles at various positions on the shoot. *J Appl Ecol* 17:59-68
- Long SP, East TM and Baker NR 1983. Chilling damage to photosynthesis in young *Zea mays*. I. Effects of light and temperature variation on photosynthetic CO₂ assimilation. *J Exp Bot* 34:177-188
- Lu SL, Rieger M and Duemmel MJ 1992. Flower orientation influences ovary temperature during frost in peach. *Agric For Meteorol* 60:181-191

- Lundmark T and Hällgren JE 1987. Effects of frost on shaded and exposed spruce and pine seedlings planted in the field. *Can J For Res* 17:1197-1201
- Lundmark T, Hällgren JE and Degermark C 1988. Effects of summer frost on the gas exchange of field-grown *Pinus sylvestris* L. seedlings. *Scand J For Res* 3:441-448
- Lundmark T, Hällgren JE and Heden J 1988. Recovery from winter depression of photosynthesis in pine and spruce. *Trees* 2:110-114
- Lurie S, Ronen R and Meier S 1994. Determining chilling injury induction in green peppers using nondestructive pulse amplitude modulated (PAM) fluorometry. *J Amer Soc Hort Sci* 119:59-62
- Maciejewska U and Bauer H 1992. Effects of cold acclimation on chlorophyll fluorescence in winter rape leaves. *Photosynthetica* 27:559-562
- Martin B, Ort DR and Boyer JS 1981. Impairment of photosynthesis by chilling-temperatures in tomato. *Plant Physiol* 68:329-334
- Miller DR, Lin JD and Lu ZN 1991. Air flow across an alpine forest clearing: A model and field measurements. *Agric For Meteorol* 56:209-225
- Nelson BE 1984. Vascular plants of the Medicine Bow Mountains. Jelm Mountain Press, Laramie, Wyoming. 357 pp
- Nobel PS 1991. Physiochemical and Environmental Plant Physiology. Academic Press, San Diego, CA. 635 pp
- Nobel PS 1983. Biophysical Plant Physiology and Ecology. WH Freeman and Company. New York. 608 pp
- Nowak H 1989. The sky temperature in net radiant heat loss calculations from low-sloped roofs. *Infrared Phys* 29:231-232
- Nunez M and Bowman DMJS 1988. Nocturnal cooling in a high altitude stand of *Eucalyptus delegatensis* as related to stand density. *Scan J For Res* 16:185-197

- Oberhuber W and Bauer H 1991. Photoinhibition of photosynthesis under natural conditions in ivy (*Hedera helix* L.) growing in an understory of deciduous trees. *Planta* 185:545-553
- Ögren E and Öquist G 1984. Photoinhibition of photosynthesis in *Lemna gibba* as induced by the interaction between light and temperature. II. Photosynthetic electron transport. *Physiol Plant* 62:187-192
- Ögren E, Öquist G and Hällgren J-E 1984. Photoinhibition of photosynthesis in *Lemna gibba* as induced by the interaction between light and temperature. I. Photosynthesis *in vivo*. *Physiol Plant* 62:181-186
- Oke TR and Fuggle RF 1972. Comparison of urban/rural counter and net radiation at night. *Bound Layer Meteorol* 2:290-308
- Oke TR 1970. The temperature profile near the ground on calm clear nights. *Q J R Meteorol Soc* 96:14-23
- Oker-Blom P 1986. Photosynthetic radiation regime and canopy structure in modeled forest stands. *Acta For Fenn* 197:1-44
- Oker-Blom P and Kellomaki S 1983. Effect of grouping of foliage on the within-stand and within-crown light regime: comparison of random and grouping models. *Agric Meteorol* 28:143-155
- Öquist G and Wass R 1988. A portable, microprocessor operated instrument for measuring chlorophyll fluorescence kinetics in stress physiology. *Physiol Plant* 73:211-217
- Papageorgiou G 1975. Chlorophyll fluorescence: an intrinsic probe of photosynthesis. In: Govindjee (ed.) *Bioenergetics of photosynthesis*. Academic Press, New York. pp. 319-371
- Paton DM 1988. Genesis of an inverted treeline associated with a frost hollow in South-eastern Australia. *Aust J Bot* 36:655-663

- Peeler TT and Naylor AW 1988. The influence of dark adaptation temperature on the reappearance of variable fluorescence following illumination. *Plant Physiol* 86:152-154
- Percival NS, Hawke MF and Andrew BL 1984. Preliminary report on climate measurements under radiata pine planted on farmland. In: Bilbrough GW (ed), *Proc Tech Workshop Agroforestry*, Dunedin, N. Z. Ministry of Agriculture and Fisheries, pp 57-60
- Pharis P, Hellmers H and Schuurmans E 1970. Effects of sub-freezing temperatures on photosynthesis of evergreen conifers under controlled environment conditions. *Photosynthetica* 4:273-279
- Powles SB, Berry JA and Björkman O 1983. Interaction between light and chilling temperature on the inhibition of photosynthesis in chilling-sensitive plants. *Plant, Cell Environ* 6:117-123
- Raitio H 1987. Site elevation differences in frost damage to Scots pine (*Pinus sylvestris*). *For Ecol Manage* 20:299-306
- Ramanathan V, Cess RD, Harrison EF, Minnis P, Barkstrom BR, Ahmad E and Hartman D 1989. Cloud-radiative forcing and climate: Results from the Earth Radiation Budget Experiment. *Science* 243:57-63
- Raupach MR and Thom AS 1981. Turbulence in and above plant canopies. *Ann Rev Fluid Mech* 13:97-129
- Rejman A 1977. Frost damage on highbush blueberries in central Poland during the years 1971-1975. *Acta Horticulturae* 61:163-173
- Robberecht R and Junttila O 1992. The freezing response of an Arctic cushion plant, *Saxifraga caespitosa* L. -- Acclimation, freezing tolerance and ice nucleation. *Annals of Bot* 70:129-135

- Rütten D and Santarius KA 1992. Age-related differences in frost sensitivity of the photosynthetic apparatus of two *Plagomnium* species. *Planta* 187:224-229
- Sakai A and Larcher W 1987. Frost survival of plants. Springer-Verlag, New York, 321 pp
- Sassenrath GF and Ort DR 1990. The relationship between inhibition of photosynthesis at low temperature and the inhibition of photosynthesis after rewarming in chill-sensitive tomato. *Plant Physiol Biochem* 28:457-465
- Scheuermann R, Biehler K, Stuhlfauth T and Fock HP 1991. Simultaneous gas exchange and fluorescence measurements indicate differences in the response of sunflower, bean and maize to water stress. *Photosyn Res* 27:189-197
- Schreiber U, Neubauer C and Klughammer C 1988. New ways of assessing photosynthetic activity with a pulse modulation fluorometer. In: Applications of chlorophyll fluorescence in photosynthesis research, stress physiology, hydrobiology and remote sensing. Lichtenthaller, HK (Ed.), Kluwer Academic Publishers, Dordrecht, The Netherlands, 366 pp
- Schroeter B, Green TGA, Seppelt RD and Kappen L 1992. Monitoring photosynthetic activity of crustose lichens using a PAM-2000 fluorescence system. *Oecologia* 92:457-462
- Schulzeis C and Santarius KA 1989. Effects of prolonged freezing stress on the photosynthetic apparatus of moderately hardy leaves as assayed by chlorophyll fluorescence kinetics. *Plant, Cell Environ* 12:819-823
- Silberbauer-Gottsberger I, Morawetz W and Gottsberger G 1977. Frost damage of cerrado plants in Botucatu, Brazil, as related to the geographical distribution of the species. *Biotropica*, 9:253-261
- Smillie RM and Nott R 1979. Assay of chilling injury in wild and domestic tomatoes based on photosystem activity of the chilled leaves. *Plant Physiol* 63:796-801

- Smith WK 1978. Leaf temperatures of desert plants: Another perspective on the adaptability of leaf size. *Science* 201:614-616
- Smith WK 1985. Environmental limitations on leaf conductance in Central Rocky Mountain conifers, USA. Eds. H Turner and W Tranquillini. *Proc. 3rd IUFRO Workshop 1984*. Eidg Anst forstl Versuchswes, Ber. 270. pp. 95-101
- Smith WK and Carter GA 1988. Shoot structural effects on needle temperatures and photosynthesis in conifers. *Amer J Bot* 75:496-500
- Smith WK, Schoettle AW and Cui M 1991. Importance of the method of leaf area measurement to the interpretation of gas exchange of complex shoots. *Tree Physiol* 8:121-127
- Smith WK and McClean TM 1989. Adaptive relationship between leaf water repellancy, stomatal distribution, and gas exchange. *Amer J Bot* 76:465-469
- Somersalo S and Krause GH 1989. Photoinhibition at chilling temperature. Fluorescence characteristics of unhardened and cold acclimated spinach leaves. *Planta* 177:409-416
- Somersalo S and Krause GH 1990a. Effects of freezing and subsequent light stress on photosynthesis of spinach leaves. *Plant Physiol Biochem* 28:467-475
- Somersalo S and Krause GH 1990b. Photoinhibition at chilling temperatures and effects of freezing stress on cold acclimated spinach leaves in the field. A fluorescence study. *Physiol Plant* 79:617-622
- Steffen KL and Palta JP 1989. Light stress following a frost episode influences the frost tolerance of a wild potato species. *J Amer Soc Hort Sci* 114:656-661
- Strand M and Öquist G 1985a. Inhibition of photosynthesis by freezing temperature and high light levels in cold-acclimated seedlings of Scots pine (*Pinus sylvestris*). I: Effects on the light-limited and light saturated rates of CO₂ assimilation. *Physiol Plant* 64:425-430

- Strand M and Öquist G 1985b. Inhibition of photosynthesis by freezing temperature and high light levels in cold-acclimated seedlings of Scots pine (*Pinus sylvestris*). II: Effects on chlorophyll fluorescence at room temperature and 77 K. *Physiol Plant* 65:117-123
- Strand M and Öquist G 1988. Effects of frost hardening, dehardening and freezing stress on *in vivo* chlorophyll fluorescence of seedlings of Scots pine (*Pinus sylvestris* L.). *Plant, Cell Environ* 11:231-238
- Suckling PW 1989. Application of a climate departure index to the study of freeze dates and growing season length in the South-Eastern United States. *Int J Climatol* 9:383-394
- Sundblad L-G, Sjöström M, Mamlberg G and Öquist G 1990. Prediction of frost hardiness of Scots pine (*Pinus sylvestris*) using multivariate analysis of chlorophyll a fluorescence and luminescence kinetics. *Can J For Res* 20:592-597
- Swinbank WC 1963. Long-wave radiation from clear skies. *Q J R Meteorol Soc* 89:339-348
- Taylor SE 1975. Optimal leaf form. In: Gates DM and Schmerl RB (eds) Perspectives of biophysical ecology. Springer-Verlag, New York. 609 pp
- Terashima I, Funayama S and Sonoike K 1994. The site of photoinhibition in leaves of *Cucumis sativus* L. at low temperatures is photosystem I, not photosystem II. *Planta* 193:300-306
- Thorpe MR and Butler DR 1977. Heat transfer coefficients for leaves on orchard apple trees. *Bound Layer Meteorol* 12:61-73
- Ting CS and Owens TG 1992. Limitations of the pulse-modulated technique for measuring the fluorescence characteristics of algae. *Plant Physiol* 100:367-373
- Unsworth MH 1975. Long-wave radiation at the ground. II. Geometry of interception by slopes, solids, and obstructed planes. *Q J R Met Soc* 101:25-34

- van Gelderen DM and van Hoey Smith JRP 1986. Conifers. Timber Press, Portland, OR
375 pp
- van Kooten O and Snel JFH 1990. The use of chlorophyll fluorescence in plant stress physiology. *Photosyn Res* 25:147-150
- van Wijk KJ and van Hasselt PR 1990. The quantum efficiency of photosystem II and its relation to non-photochemical quenching of chlorophyll fluorescence; the effect of measuring-and growth temperature. *Photosyn Res* 25:233-240
- Walker MA, Smith DA, Pauls KP and McKersie BD 1990. A chlorophyll fluorescence screening test to evaluate chilling tolerance in tomato. *HortScience* 25:334-339
- Wang YP and Jarvis PG 1990. Influence of crown structural properties on PAR absorption, photosynthesis, and transpiration in Sitka spruce: application of a model (MAESTRO). *Tree Physiol* 7:297-316
- Yakir D, Rudich J and Bravado BA 1986. Adaption to chilling: photosynthetic characteristics of the cultivated tomato and a high altitude wild species. *Plant, Cell Environ* 9:477-484
- Ye ZJ, Segal M, Garratt JR and Pielke RA 1989. On the impact of cloudiness on the characteristics of nocturnal downslope flows. *Bound Layer Meteorol* 49:23-51

M97053790



Report Number (14) DOE/OR/00033--T758

Publ. Date (11) 199505

Sponsor Code (18) DOE/ER, XF

UC Category (19) UC-480, DOE/ER

DOE